MODELLING PERMAFROST HYDROLOGY USING LIMITED DATA

bY

ZHAO-JUN XIA, B.E., M.Sc.

A Thesis

Submitted to the School of Graduate Studies

in Partial Fulfilment of the Requirements

for the Degree

Doctor of Philosophy

McMaster University

February 1993

MODELLING PERMAFROST HYDROLOGY USING LIMITED DATA

DOCTOR OF PHILOSOPHY (1993)

McMASTER UNIVERSITY
Hamilton, Ontario

TITLE: Modelling Permafrost Hydrology Using Limited Data

AUTHOR: Zhao-jun Xia, B.E. (Dalian University of Science and Technology)
M.Sc. (Chinese Academy of Sciences)

SUPERVISOR: Dr. M.K. Woo

NUMBER OF PAGES: xxiv, 228

ABSTRACT

The hydrological processes of the active layer in continuous permafrost areas are governed by water and energy fluxes, with most hydrological activities concentrated in the thawed seasons. This study was focused on the modelling of hydrological processes in the active layer, emphasizing the fluctuations of the frost table and the moisture status in the thawed zone. Emphases were placed on the calibration of a one-dimensional hydrological model and the development of a two-dimensional model to simulate frost table descent during the summer time. Woo and Drake (1988) developed a model to simulate the daily hydrological and thermal processes of a vertical column in continuous permafrost areas. It combines freeze-thaw processes with water balance to enable daily updating of the status of the frost table, water table, soil moisture, snowmelt and evaporation. Input data include only precipitation, global solar radiation, and air temperature. This model has not been calibrated for the High Arctic and only limited field testing has been performed. This study used field measurements from Resolute,

Northwest Territories, to calibrate the model. Independently by obtained data sets were used to test the model outputs and compared with field measurements. The model performed well. The model was then applied to simulate the hydrological responses to climatic variability. The sensitivity of the model was analyzed and discussed.

The frost table represents the dynamic lower boundary of the thawed zone. The horizontal variation in frost table depth was modeled, applying the Green theorem to solve the heat flow equation for the active layer zone where the 0^0C isotherm is the limit of thaw. This model incorporates the effect of ground ice content in the retardation of thawing front descent, and the moisture status in the calculation of thermal conductivity. The frost table computed for a transect comprising two distinct soil segments compared favourably with field measured values. The model was used to assess frost table responses to varying degrees of soil saturation, ice content and air temperatures. This model was also coupled to the outputs from the one-dimensional model to allow horizontal extension of the frost table simulations. Coupling of these two models enable hydrological simulation of continuous permafrost terrain using limited input data that can be obtained from Arctic Weather Stations.

ACKNOWLEDGEMENTS

I wish to thank my supervisor Dr. M. K. Woo for his supervision, friendship, and encouragement throughout this study, I am grateful to other members of my supervisory committee, Dr. S. B. McCann and Dr. Lam, for their useful discussions and comments. Funding for this study was provided by the Natural Sciences and Engineering Research Council of Canada, the Presidential Committee on Northern Studies of McMaster University and the Northern Training grant from the Department of Indian and Northern Affairs of Canada. Generous logistical support was provided by the Polar Continental Shelf Project, Department of Energy, Mines and Resources.

Many thanks go to Drs. Albert Lincoln Washburn, Philip Marsh, Richard Heron and Hongming Yin, Professor Kai Wu and fellow graduate students who provided advice and assistance in the field, Kathy Young, Mary Ferguson, Philip Giles, Kelly Thompson, Suyun Chen and Changsheng Chen; and all those who made my stay at McMaster so enjoyable. Special thanks must go to Dr. George Hobson and Mr. Frank Hunt of Polar Continental Shelf Project and their staff at Resolute, Jim, Barry, Sue, Fred, Bill, Emile, George, Lief and Frank, for their assistance and support.

TABLE OF CONTENTS

	Page
CHAPTER 1 INTRODUCTION	1
1.1 Permafrost hydrology	1
1.2 Permafrost-hydrologic modeling	3
1.2.1 Model review and selection	5
1.2.1.1 Outcalt model	5
1.2.1.2 Bonan model	8
1.2.1.3 Kane and Hinzman model	13
1.2.1.4 Fox model	14
1.2.1.5 Woo and Drake model	18
1.2.1.6 Model selection for this study	22
1.3 Objectives of this study	24
CHAPTER 2 STUDY AREA AND METHODS	26
2.1 Research area	26
2.1.1 Landform and soil	26
2.1.2 Climate	30
2.1.3 Hydrologic conditions	31
2.1.4 Permafrost environment	34
2.2 Experimental site	37
2.2.1 Slope characteristics	37
2.2.2 Soil properties	40
2.3 Instrumentation and methods	43
2.3.1 Weather station data	43
2.3.2 Meteorological data from experimental site	44

2.3.2.1 Precipitation 46
2.3.2.2 Radiation 46
2.3.2.3 Air temperature and humidity 47

2.3.3 Hydrological data and soil parameters 48

2.3.3.1 Hydraulic conductivity 48
2.3.3.2 Bulk density and porosity 49
2.3.3.3 Specific yield and retention 51
2.3.3.4 Soil moisture and water table 52
2.3.3.5 Soil structure and composition 54
2.3.3.6 Ground temperature and frost table 55

CHAPTER 3 ONE DIMENSIONAL MODEL FOR CONTINUOUS PERMAFROST 58

3.1 Woo and Drake (WAD) model 58

3.1.1 Physical background 59

3.1.1.1 The winter season 59
3.1.1.2 The summer season 60

3.1.2 Flow diagram for the model 61

3.2 Model description 64

3.2.1 Snow accumulation and melt submodel 64

3.2.1.1 Snow accumulation 64
3.2.1.2 Snow melt processes 65

3.2.1.2.1 Snow melt computation 65
3.2.1.2.2 Melting front advance 67
3.2.1.2.3 Basal ice formation 69

3.2.2 Ground temperature and frost table model 70

3.2.2.1 Heat conduction and finite difference approach 71
3.2.2.2 Boundary conditions 73

3.2.2.2.1 Bottom temperature 73
3.2.2.2.2 Surface temperature 73

3.2.2.3 Initial temperature profile 75
3.2.2.4 Thermal conductivity and heat capacity 77
4.2.2.5 Apparent thermal capacity 78
3.2.2.6 Frost table and active layer 79

3.2.3 Evaporation submodel 80

3.2.3.1 Priestley and Taylor model 80
3.2.3.2 Ground heat flux 81
3.2.3.3 Empirical coefficient α 82

3.2.4 Soil moisture, water table and runoff submodel 83

3.2.4.1 Water balance 83
3.2.4.2 Apparent water balance 84
3.2.4.3 Soil moisture profile 86
3.2.4.4 Storage change and outflow 88

3.3 Input and output of WAD model 89

3.3.1 Input 89

3.3.1.1 Description of data file 89
3.3.1.2 Interactive input 90

3.3.2 output 91

3.4 Model testing 93

3.4.1 Parameter and variables 93

3.4.1.1 Premelt snow parameter 93
3.4.1.2 Coefficients for calculate net radiation 95
3.4.1.3 Coefficients for estimate turbulent fluxes 98
3.4.1.4 Parameters for soil moisture Estimation 99
3.4.1.5 List of parameters used in WAD model 101

3.4.2 Model calibration 104

3.4.2.1 Error estimation 104
3.4.2.2 Model structure and parameter calibration 106
3.4.2.3 Inflow calibration in peaty soil site 111
3.4.2.4 Warm-up period 112
3.4.2.5 Field measurements calibration 113

3.4.3 Model testing 118
3.4.4 Model application 122

3.4.4.1 Simulation with historical data 123
3.4.4.2 Hydrological modeling results 125
3.4.4.3 The output test with field measurements 132
3.4.4.4 Simulated active layer water balance 134

CHAPTER 4 TWO DIMENSIONAL MODEL FOR ACTIVE LAYER THAW 136

4.1 Background of the study 136
4.2 Development of the model 137

4.2.1 Active layer heat transfer processes 138

4.2.1.1 Heat transfer equations 139
4.2.1.2 Heat transfer processes 144

4.2.2 Green's theorem 145

4.2.2.1 General Description 146
4.2.2.2 The Green's identities 148
4.2.2.3 Green's representation 150

4.2.3 Models of heat transfer without phase change 155

4.2.3.1 Domain and boundary conditions 155
4.2.3.2 Steady state heat transfer model 158
4.2.3.3 Unsteady state heat transfer model 161

4.2.4 Model of heat transfer with phase change 164

4.2.4.1 General expression 164
4.2.4.2 Apparent temperature 165
4.2.4.3 The equivalent solution 168

4.3 Input and output of the model 170

4.3.1 Input 170

4.3.1.1 Thermal and soil data 171
4.3.1.2 Hydrological input data 176

4.3.2 Output 178

4.3.2.1 Thawing front profile 178
4.3.2.2 Maximum or minimum thawing depth 180

4.4 Model testing 187

4.4.1 Modeling procedures 188
4.4.2 Modeling results 190

4.5 Theoretical analysis of model application 193

4.5.1 Thawing depth at geometrical characteristic points 196
4.5.2 Thawing front profile under the middle soil segment 200
4.5.3 Thawing beneath trenches 203

4.5.3.1 Open trench 204
4.5.3.2 Trench with water 209

4.6 Joint application of WAD and Xia models 211

4.6.1 Joint application 212
4.6.2 Discussion 214

CHAPTER 5 CONCLUSIONS 216

REFERENCES 220

LIST OF FIGURES

Figure		Page
1.1	Permafrost distribution in Canada.	2
2.1	Location of the study site at Resolute in the Canadian High Arctic.	27
2.2	The study site in McMaster River basin near Resolute.	28
2.3	Mean monthly and extreme air temperatures for Resolute.	31
2.4	Annual variation in rain received at Resolute Weather Station	33
2.6	Ground temperature regime for Resolute.	36
2.7	Surface condition of part of the study area shown in aerial photographs.	38
2.8	Aerial photograph of the study slope.	39
2.9	Grain size distribution of soil samples obtained from the experimental slope.	41
2.10	Location of instruments and measurements on the study slope.	45
2.11	Using Gamma Probe to determine soil moisture changes in the active layer. The measurement was started at the beginning of the melt season.	53
2.12	The water table fluctuation at No. 8 observation well.	54

2.13	The stratigraphy of soil structures of the study site	56
3.1	Major physical processes represented by the model.	58
3.2	Flow-chart of Woo and Drake model	62
3.3	Snow accumulation and melt processes	68
3.4	Boundary conditions for the ground temperature submodel.	72
3.5	Hypothetical temperature profiles.	74
3.6	The seasonal water table and frost table development patterns.	85
3.7	The various cases of vertical soil moisture profile changes.	87
3.8	The regression of Q^t to $K\downarrow$ at gravelly soil site, in 1988.	95
3.9	The regression of Q^t to $K\downarrow$ at gravelly soil site in 1989.	96
3.10	The regression of Q^t to $K\downarrow$ at Peaty soil site in 1989.	96
3.11	Regression of snow melt with turbulent heat flux to air temperature.	99
3.12	The regression of soil moisture to water table in gravelly soil site.	100
3.13	List of parameters used in WAD model	101
3.14	The calibration of WAD model with gravelly soil site data.	107
3.15	The calibration of WAD model with peaty soil site data.	108
3.16	The evaporation calibration of WAD model with peaty soil site data.	108
3.17	Comparison of frost table depth simulation with field measurements at gravel soil.	109

3.18	Comparison of water table depth simulation with field measurements at gravel soil.	109
3.19	Comparison of modeled evaporation with Priestley and Taylor model.	110
3.20	The regression of air temperature measured in weather station to our measurements	113
3.21	Ultimate compressive strength of frozen soils.	115
3.22	The steel rods and hammers used for the frost table measurement calibration.	116
3.23	The soil profile and the error comparison measured with different steel rod.	117
3.24	Precipitation distribution in the thawing season of the year 1989.	118
3.25	Radiation distribution in the model testing period.	119
3.26	Air temperature variation in the model testing period.	119
3.27	The testing results of WAD model with gravelly soil site data.	120
3.28	The testing results of WAD model with peaty soil site data.	120
3.29	The input data of six year hydrologic modeling.	124
3.30	The output of Six year hydrological modeling in gravelly soil site, Resolute.	126
3.31	The output of six year hydrological modeling in peaty soil site, Resolute.	127
3.32	The simulated evaporation variation.	129
4.1	The coordinates and the domain of the basic Green's theorem.	146
4.2	Plane surface with different temperature and its coordinates.	156

4.3	Temperature distribution crossing thawing front.	167
4.4	Regression of air temperature and surface temperature for gravelly soil.	172
4.5	The correlation of the surface temperature in gravelly soil area with the surface temperature in peaty soil area.	174
4.6	Assumed moisture content profile.	177
4.7	Calculated and measured frost table positions along the transect, 1988 and 1989	189
4.8	The sensitivity of ground thaw to temperature and soil moisture.	194
4.9	The sensitivity of ground thaw to temperature and ice content.	195
4.10	Thawing depth at building characteristic points.	196
4.11	Thawing front profile and its maximum thawing depth.	201
4.12	The coordinate system and the assumed temperature distribution for open trench.	204
4.13	The coordinate system and the assumed temperatures distribution for trench with water.	210
4.14	Simulated frost table position using a combination of WAD and XIA models.	213

LIST OF TABLES

Table		Page
1.1	The characteristics of Outcalt model and WAD model.	19
1.2	The Characteristics of Bonan's models.	20
1.3	The characteristics of Kane & Hinzman model and Fox model.	21
2.1	Soil bulk densities of the study site.	50
2.2	Soil compositions in gravelly and peaty soils.	55
3.1	Snow densities and depths.	94
3.2	Parameters for the empirical equation.	97
3.3	Surface type-dependent parameters.	102
3.4	Miscellaneous parameters.	103
3.5	The calculated RMSE values for model proper initiation calibration.	112
3.6	The accuracy of the model simulation.	122
3.7	The total amount evaporation simulated from 1976 to 1981.	130
3.8	The estimated error for frost table and water table modeling.	133
3.9	Summary of modeled hydrologic events of six historical years.	135

4.1	Relationship between air temperature and ground surface temperature.	173
4.2	Soil structure and grain size distribution.	175
4.3	The input variables of modeled sensitivity.	191
4.4	The output variables in gravelly soil segment.	192
4.5	The output variables in peaty soil segment.	192
4.6	The inputs and parameters used in two-dimensional model, supplied from the one-dimensional model.	214

NOTATION

Symbol	Variable Description	Dimensions
A	area	m^2
A_b	annual amplitude of the temperature at the bottom slab	^0C
A_{min}	the minimum seepage section area	m^2
a	half wide of the middle soil segment	m
a_0	empirical coefficient	dimensionless
a_1	empirical coefficient	dimensionless
$BAL(T_s)$	energy balance on the ground surface	$W\ m^{-2}$
BICE	basal ice	m
$BICE_p$	maximum basal ice	m
b_0	empirical coefficient	dimensionless
b_1	empirical coefficient	dimensionless
C	heat capacity	$J\ kg^{-1}\ ^0C^{-1}$
C_a	heat capacity of air	$J\ kg^{-1}\ ^0C^{-1}$
C_e	atmospheric turbulent exchange coefficient	$kg\ m^{-2}s^{-1}$

C_{app}	apparent heat capacity	J m^{-3} $^{o}C^{-1}$
C_{ice}	volumetric heat capacity of ice	J m^{-3} $^{o}C^{-1}$
c_0	empirical coefficient	dimensionless
DZ	layer thickness	m
E	evaporation computed	m
E_p	potential evaporation	m
F(x)	force along x axial direction	N
F(z)	force along z axial direction	N
M(y)	momentum in xz plane	N m
f_a	fraction of air content	dimensionless
f_i	the fractional volumetric content of each component i	dimensionless
f_{ice}	fractional volumetric ice content	dimensionless
GSNOW	ground snow depth	m
g_0	empirical coefficient	dimensionless
g_1	empirical coefficient	dimensionless
h	thawing front depth	m
h_a	specific humidity for air	dimensionless
h_s	specific humidity for ground surface	dimensionless
h_1	thawing depth in natural state	m
$h_{(0)}$	thawing depth under point of x = 0	m
$h_{(a)}$	thawing depth under point of x = a	m
$h_{(-a)}$	thawing depth under point of x = -a	m
h_{rsf}	surface relative humidity fraction	dimensionless

I_s	surface freezing index, cumulative degree-days	^0C day
K_f	frozen soil thermal conductivity	W m^{-1} $^0C^{-1}$
K_{dry}	dry soil thermal conductivity	W m^{-1} $^0C^{-1}$
K_{sat}	saturated soil thermal conductivity	W m^{-1} $^0C^{-1}$
K_{soil}	unsaturated soil thermal conductivity	W m^{-1} $^0C^{-1}$
k	thermal conductivity	W m^{-1} $^0C^{-1}$
k_s	soil thermal conductivity of surface slab	W m^{-1} $^0C^{-1}$
k_u	unfrozen soil thermal conductivity	W m^{-1} $^0C^{-1}$
k_w	thermal conductivity of water	W m^{-1} $^0C^{-1}$
k_H	hydraulic conductivity	m s^{-1}
L	volumetric latent heat of fusion in soil	J m^{-3}
L_i	latent heat of fusion of the ith soil layer	J m^{-3}
LS_M	soil moisture of previous day	dimensionless
M	amount of daily melt	m
MF	melting front	m
M_p	melting point of snow	^0C
m	1) fractional volumetric water content of a soil layer (eq.1.7); 2) the total mass in soil bulk density calculation (eq.2.2)	dimensionless kg
m_s	the total mass of soil moisture	kg
m_t	the dry weight of a sample soil	kg
N_i	number of required degree-days	^0C day
P_a	1) air pressure (eq.1.5)	p_a

P	2) snowfall recorded at the nearby base station (eq.3.1)	m
P_r	precipitation as rain	m
$P_{s(i)}$	snow cover water equivalent of various terrains	m
Q^*	net all-wave radiation	W m^{-2}
Q_i^*	net radiation at height h_i	W m^{-2}
Q_l^*	net long wave radiation	W m^{-2}
Q_s^*	net short wave radiation	W m^{-2}
Q_c	energy transferred by heat conduction	J
Q_E	latent heat flux	W m^{-2}
Q_{Ei}	latent heat flux at height h_i	W m^{-2}
Q_G	ground heat flux	W m^{-2}
Q_g	energy developed within the system	J
Q_{Gi}	ground heat flux [$Q_{Gi} = 0$ for $i \neq n$]	W m^{-2}
Q_H	sensible heat flux	W m^{-2}
Q_{Hi}	sensible heat flux at height h_i	W m^{-2}
Q_i	heat energy transferred into the system	J
Q_M	energy available for snow melt	W m^{-2}
Q_o	heat energy transferred out of the system	J
Q_r	energy transferred by radiation	J
Q_T	turbulent heat fluxes	W m^{-2}
q	heat flow	W m^{-2}
q_i	heat flux used for increasing soil temperature	W m^{-2}
q_{ii}	heat flux used for soil moisture phase change	W m^{-2}

R	sum of thermal resistances for the overlying layers	$m^2\ ^0C\ h\ kcal^{-1}$
R_i	thermal resistance of the layer	$m^2\ ^0C\ h\ kcal^{-1}$
r	radius of the auger hole for hydraulic conductivity measurement	m
r_h	bulk aerodynamic resistance to convective heat transfer	$s\ m^{-1}$
r_{hr}	combined convective and radiative resistances	$s\ m^{-1}$
r_r	radiative resistance	$s\ m^{-1}$
S	fractional degree of saturation	dimensionless
SM	soil moisture	dimensionless
SM_s	surface soil moisture	dimensionless
S_r	specific retention	dimensionless
S_y	specific yield	dimensionless
T	temperature	^0C
T_A	air temperature	^0C
T_a	ground surface temperature at segment a	^0C
T_n	ground surface temperature in boreal forests	^0C
T_o	boundary temperature	^0C
T_0	1) boundary temperature at the segment $-b < x < b$ (eq. 4.126 -4.136)	^0C
	1) water surface temperature at the segment $-b < x < b$ (eq. 4.138)	^0C
T_b	1) annual mean temperature at the bottom slab (eq. 3.12)	^0C
	2) ground surface temperature at segment b (eq.4.67)	^0C
T_s	ground surface temperature	$^0C^{-1}$

T_1	boundary temperature at the soil segment $-\infty < \xi < -a$	^0C
T_2	boundary temperature at the soil segment $-a < \xi < a$	^0C
T_3	boundary temperature at the soil segment $a < \xi < \infty$	^0C
T_i	ground temperature used for increasing soil energy and develop thawing depth	^0C
T_{ii}	ground temperature used for soil moisture phase change from ice to water	^0C
T^*	apparent ground temperature	^0C
T_0^*	apparent ground surface temperature	^0C
T_a^*	apparent ground surface temperature at segment a	^0C
T_b^*	apparent ground surface temperature at segment b	^0C
T_c^*	apparent ground surface temperature at segment c	^0C
T_f^*	apparent temperature of the fill filled trench at depth h_1	m
$T_{(s-1)}$	ground temperature in the first layer below the surface	^0C
T_{b0}	temperature in water at trench bottom	^0C
$T_{b(t)}$	bottom temperature on day t	^0C
TSNOW	the below-freezing snow temperature	^0C
V	total volume of soil sample	cm^3
V_v	voids volume of soil sample	cm^3
V_{dw}	volume f water drained from the saturated soil sample	cm^3

V_{rw}	the volume of retained water in drained soil sample	cm^3
W_T	water table depth	m
w_t	water released during thawing	cm
Y_l'	the finishing level of hydraulic conductivity measurement	m
Y_0'	starting level of hydraulic conductivity measurement	m
Z	depth of the column vertical profile	m
Z_f	depth of frost table from surface	m
Z_i	depth of thaw in soil layer in the ith month	cm
Z_{i-1}	depth of thaw in previous month	cm
Z_w	water depth	m

GREEK

δ	slope of saturated vapour pressure-temperature curve	dimensionless
α	empirical coefficient	dimensionless
ε	arbitrary temperature range, above or below the freezing point	^0C
λ	1) latent heat of evaporation (eq.1.6) 2) latent heat of fusion from ice to water (eq.4.80)	$J\ m^{-3}$
θ	volumetric moisture content	dimensionless
θ_j	volumetric moisture content of jth soil layer	dimensionless

ρ_a	air density	kg m^{-3}
ρ_d	soil density	kg m^{-3}
ρ_i	ice density	kg m^{-3}
ρ_w	water density	kg m^{-3}
$\rho_{s(i)}$	snow density of certain terrain type	kg m^{-3}
ρ_t	bulk density	kg m^{-3}
γ	psychometric constant	dimensionless
ϕ	soil porosity	dimensionless
ϕ_e	effective porosity	dimensionless
ϕ_s	snow porosity	dimensionless
φ	ice content in soil	dimensionless
ΔQ_s	energy storage change	W m^{-2}
Ω	a closed region in XY-plan	m^2
ξ	coordinate of a point along x direction at the case of z = h	m
ξ_1	coordinate of a point along x direction	m
ξ_2	coordinate of a point along z direction	m
ζ	x coordinate of the maximum or minimum thawing depth	m

CHAPTER 1

INTRODUCTION

1.1. Permafrost Hydrology

Permafrost hydrology studies the distribution, movement and storage of water as it is directly or indirectly influenced by the presence of perennially frozen ground (Woo 1986). Permafrost underlies about half the land area of Canada (Fig. 1.1) and also parts of the shallow offshore in the Canadian Arctic (Brown, 1970). The formation and maintenance of permafrost is due to intense and persistent cold conditions, and therefore the prevalence of coldness permeates the hydrological cycle in the North.

The common hydrological properties under different permafrost environment are as follows: (1) The frozen ground has limited permeability and it acts effectively as an aquiclude (Dingman, 1975). (2) Most hydrological activities are confined to the seasonally-frozen and thawed zone above the permafrost table, known as the active layer. (3) Most surface hydrological processes are inactive during the long, cold winters. (4) Energy and water fluxes are closely linked as water storage and redistribution are modified by freeze-

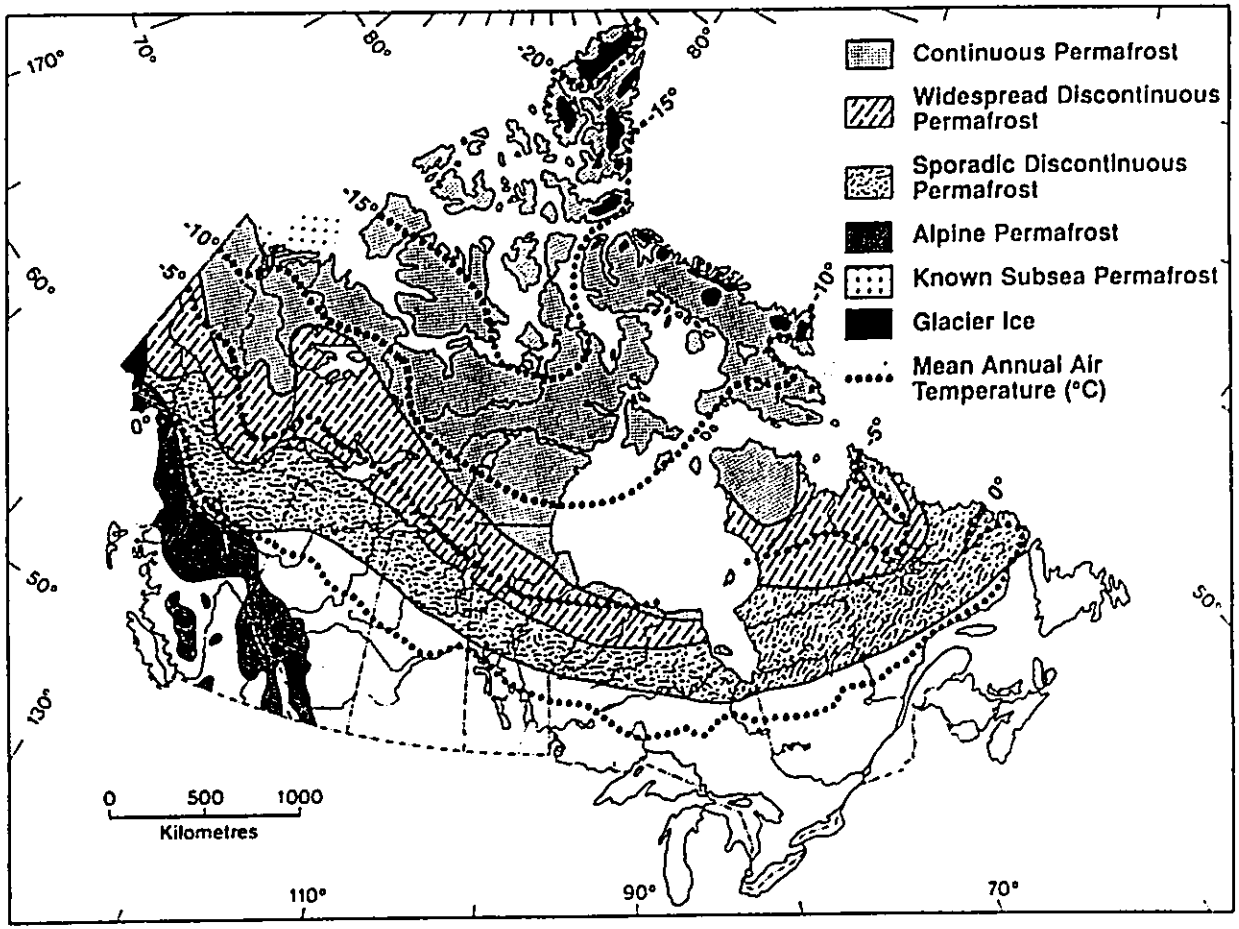

Figure 1.1 Permafrost distribution in Canada *(after Heginbottom, 1989 and Johnston, 1981).*

thaw events. (5) Snow and ice storage on a seasonal or multi-annual basis affects the temporal distribution of water, and the release of meltwater often has pronounced effects on other surface hydrological processes (McCann et al. 1972).

Research in permafrost hydrology has been driven by scientific curiosity as well as by the pressure for applications (Woo 1990). Progress in the past several decades has allowed an improved understanding of the major hydrological processes that are active in the permafrost area. Quantitative hydrological prediction remains inadequate. The push for development, the maintenance of ecological balance in the Arctic and the need to predict man-induced climatic change impacts in polar regions, call for hydrologic modelling of the permafrost environment. Through such modelling effort, we may gain a better quantitative appreciation of the hydrological responds to external forcing. This will allow us to improve our planning for the future and for the preservation of the physical environment of the continuous permafrost regions.

1.2 Permafrost-hydrologic Modeling

The frost table is the lower boundary of the thawed zone of the active layer, and the permafrost table is the annual maximum extent of the frost table. The presence of

this boundary in the hydrological system distinguishes permafrost hydrology from non-permafrost hydrology. It is imperative to determine the day to day variations of the frost table because most hydrological activities occur above it. Many one-dimensional (Outcalt et al. 1975; Smith 1978) ground thermal models have been developed to calculate the position of the frost table, through energy balance and heat flow approaches using finite difference or finite element method (Outcalt 1975; Smith 1978, Goering and Zarling 1985), and the Stefan formula (Bonan 1989; Fox 1992). Since the freeze and thaw processes are strongly influenced by the moisture content of the frozen and the thawed zone of the active layer, thermal modelling has to be coupled with hydrological variables. Numerical models developed for non-permafrost areas do not have this coupled thermal and hydrological component. In recent years, several models have been produced or modified to incorporate the freeze and thaw processes, specifically for the permafrost environment (Woo and Drake 1988; Bonan 1991; Kane and Hinzman 1991; Fox 1992). Following is a brief review of these models and a discussion of how well they perform for a point or for a section of the Arctic terrain.

1.2.1 Model Review and Selection

Models which are applicable to the permafrost area have different degrees of complexity, different degrees of parameter optimization and amount of data input, and are applicable at various time and spatial scales of investigation.

1.2.1.1 Outcalt Model

Outcalt et al. (1975) applied a one-dimensional model to study the thermal regime of a permafrost site. One distinguishing feature is its usage of a finite difference solution of the soil thermal evolution equation and the use of the interval-halving algorithm in the search for the surface equilibrium temperature (Table 1.1).

The equilibrium temperature of the ground surface is back calculated from energy balance equations:

$$Q^* + Q_H + Q_E + Q_G = BAL(T_s) \qquad (1.1)$$

in which Q^* is net all-wave radiation, Q_H is sensible heat flux, Q_E is latent heat flux, and Q_G is ground heat flux.

$$Q^* = Q_S^* + Q_L^* \qquad (1.2)$$

Q_s^* and Q_l^* are short net short wave radiation and net long wave radiation respectively.

$$Q_G = k \frac{T_{(s-1)} - T_s}{DZ} \qquad (1.3)$$

T_s is ground surface equilibrium temperature, and $T_{(s-1)}$ is the ground temperature in the first layer below the surface. Q_H and Q_E are both affected by T_s through the following relationships

$$Q_H = c_e\, c_a\, (T_a - T_s) \qquad (1.4)$$

$$h_s = f(T_s, h_{rsf}, P_a) \qquad (1.5)$$

$$Q_E = c_e\, L\, (h_a - h_s). \qquad (1.6)$$

where c_e is atmospheric turbulent exchange coefficient; L is latent heat of evaporation; h_a and h_s are specific humidities for air and ground surface separately. h_s is a function of ground surface temperature, of surface relative humidity fraction h_{rsf}, and air pressure P.

When BAL(T_s) is sufficiently close to zero, all the energy budget components are correctly specified, and the value of the surface temperature is also correct. The solution for a sufficiently small BAL(T_s) is accomplished by making two initial guesses at the surface temperature using an interval halving algorithm followed by further estimates for solution surface temperatures (T_s) using the secant algorithm (Outcalt 1975).

The major weakness of this model is that it does not deal with the dynamic hydrological behaviours of the soil. The thermal conductivity and heat capacity of soils are invariant with the unknown soil moisture content, and the phase change associated with freeze and thaw of ground ice is not considered.

Smith (1978) provided a variant of the Outcalt model. The Priestley and Taylor equation was used for latent heat flux computation, and limited the parameter requirements for specific humidity of air and ground surface. The computation method is improved. An iterative technique was used to compute the surface equilibrium temperature instead of Outcalt's interval halving algorithm.

The thermal conductivity and heat capacity were determined separately for frozen and unfrozen soils, both phase changes associated with freeze-thaw processes were ignored.

1.2.1.2 Bonan Model

Bonan (1989) produced an ecological model for the forested, discontinuous permafrost environment. He pointed out that the vegetation patterns within the circumpolar boreal forest reflect a complex interrelationship among climate, solar radiation, soil moisture, soil temperature, the forest floor organic layer, forest fires, and insect outbreaks (Bonan 1989). His model was used to explore the environmental subset of this interrelationship, and simulated solar radiation, soil moisture, soil freezing and thawing for specific sites in the boreal forest (Table 1.2). The model solved for various environmental factors on a monthly time step using easily obtainable soil and climatic data as inputs.

The soil profile is treated as a one or two-layered system consisting of a forest floor moss-organic layer, if present, and the underlying mineral soil. For each different layer the monthly soil water content is partitioned between ice and unfrozen water. The water released during thawing of a soil layer is proportional to the depth of thaw in that layer:

$$w_t = \frac{m}{100}(Z_i - Z_{i-1}) \qquad (1.7)$$

where w_t is water released during thawing (cm), m is volumetric water content of soil layer, Z_i is depth of thaw in soil layer in the ith month (cm), and Z_{i-1} is depth of thaw in previous month (cm). Monthly potential water loss is calculated as precipitation minus potential evapor-transpiration.

The depths of seasonal freezing and thawing in the soil profile are solved on a monthly basis using the Stefan formula. The degree-days required to freeze or thaw the ith layer are (Jumikis 1966):

$$N_i = Z_i L_i (R + R_i/2) \; / \; 24 \qquad (1.8)$$

where N_i is number of required degree-days, Z_i is thickness of the ith layer, L_i is latent heat of fusion of the ith layer, R_i is thermal resistance of the layer, and R is the sum of resistances for the overlying layers.

The major weakness in this model is that it does not explicitly deal with snow accumulation and melt, has too coarse a time step (monthly intervals), and views surface temperature as occurring at the mineral soil surface as opposed to the snow or organic matter surface (Fox 1992). Using a degree-day method to model the freezing process means that the simulated freezing front can only descend from

ground surface, and this does not allow for two-sided freezing as autumnal freeze-back may proceed also upward from the permafrost table (Mackay 1973, Black 1974, Washburn 1979). For ground surface temperature estimation, an empirical correction factor over a specified period of time is used to adjust the heat load for surface conditions, and this is a weaker approach than that used by Outcalt and Smith.

A second model was proposed by Bonan in 1991 (Table 1.2). The surface energy budget of a multilayer forest canopy is solved daily to provide estimates of ground surface temperature, evapotranspiration, and snowmelt required to evaluate the soil moisture and soil temperature regimes (Bonan 1991). In this model, the canopy is divided into n layers, and the energy balance of each layer is written as a function of n unknown surface temperatures so that

$$Q_i^*(T_1,\cdots,T_n) + Q_{Hi}(T_1,\cdots,T_n) + Q_{Ei}(T_1,\cdots,T_n) + Q_{Gi}(T_n) = 0 \qquad (1.9)$$

where T_i is surface temperature at height h_i, and T_n is the ground surface temperature. These n equations are solved for the n unknown temperatures. and temperature and moisture in a multilayer soil were updated at the same time (Bonan 1991).

The soil is divided into n_s layers consisting of snow, moss, humus, and mineral soil. With the ground surface temperature T_1 known and zero heat flux at the bottom of the soil profile, an implicit finite difference solution is used to update soil temperatures. The effect of phase change on soil temperature is considerated and included through the apparent heat capacity method outlined by Lunardini (1981). In this method the volumetric latent heat of fusion is added to heat capacity over a temperature range $T_f \pm \Delta T_f$. Outside of this range the heat capacity of a soil layer is either frozen or unfrozen, depending on its thermal state. With the temperature range $T_f \pm \Delta T_f$ the thermal conductivity of the frozen and unfrozen soil are linked as a linear function.

For mineral soil the unfrozen and frozen thermal conductivities are (Kersten, 1949):

$$k_u = (a_1 \log_{10}[\theta_j \frac{\rho_w}{\rho_d}] + a_2)\ a_x^{\rho d} \qquad (1.10)$$

$$k_f = a_4 a_5^{\rho d} + a_6 [\theta_j \frac{\rho_w}{\rho_d}]\ a_7^{\rho d} \qquad (1.11)$$

where the parameters a_1 - a_7 vary with fine-grained and coarse-grained soil (Kersten 1949). θ_j is volumetric moisture

content of jth soil layer. For unfrozen moss and organic matter, a series of measured thermal conductivities corresponding to different bulk density of different material in saturated and dry state are used. For frozen material, 4 times the unfrozen value is used for saturated thermal conductivities in this model.

A simple mass balance method is used to update soil moisture. The water content of each soil layer is the difference between the water entering the soil and the water removed as transpiration and drainage (Bonan 1991). Total transpiration is partitioned into water loss from a certain soil layer based on moisture, temperature, and root abundance. Drainage is the amount of water in excess of field capacity. If the soil profile is frozen at some depth, drainage is set to zero, and water accumulated up to saturation. Excess water is lost as runoff or subsurface flow.

As the model is sensitive to the thermal conductivity of moss, the surface resistance, and the bulk density of mineral soil (Bonan 1991), it may further be improved by linking water balance and heat balance computations. It uses computed thermal conductivity instead of empirical values and field measurements. The thermal conductivity of saturated frozen organic material may not always be 4 times its unfrozen value. It varies with the material composition,

structure, porosity and irreducible air content change.

1.2.1.3 Kane & Hinzman Model

Kane and Hinzman (1991) modified the HBV model developed by Bergström (1986) of the Swedish Meteorological and Hydrological Institute, to simulate the hydrology of a basin completely underlain by permafrost. The goal is to provide hydrologic forecasting for basins with limited data.

The HBV is a conceptual runoff model designed for continuous calculation of runoff using a lumped parameter representation. The model has 41 parameters, of which 26 are used to describe the basin or input data while the rest collectively describe snow accumulation and ablation, soil moisture accounting, and generation or transformation of the hydrograph (Kane et al. 1991). Several of these parameters are empirical values determined by model calibration. Input data include air temperature, precipitation, and monthly estimates of evapotranspiration.

The routine which calculates snowmelt and refreezing is based upon a simple degree day method. A threshold temperature is used to define freezing, melting and snowfall-rainfall separation. Water from rainfall or snowmelt is partitioned into evaporation and infiltration in the soil moisture routine (Table 1.3). The soil moisture routine is

the main component controlling the generation of runoff. This routine is based upon the storage capacity of the soil, evapotranspiration from the soil, and a response function describing the amount of runoff generated from precipitation.

While this model is suitable for basin-scale investigation, the temperature index method does not provide sufficient detail for site studies, and the parameter estimation technique renders the model non-portable from site to site without major re-calibration.

1.2.1.4 Fox Model

Fox (1992) incorporated soil freeze-thaw processes into a water balance model such that frost depth and thaw depth can be calculated over time and their influence on soil water infiltration, storage, evapotranspiration, and drainage can be simulated. This model is designed to be sensitive to snow depth and timing, air temperature, surface organic matter thickness, and soil characteristics and to operate with readily available meteorological data for multiyear simulations.

Like Bonan's (1991) model, the Stefan equation is used for freeze or thaw depth calculation. Assuming sensible heat effects are negligible, frost depth is given by

$$Z_f = [48\ K_f I_s / (L\theta)]^{0.5} \qquad (1.12)$$

where Z_f is the depth of frost table from surface; K_f is frozen soil thermal conductivity; I_s is surface freezing index, cumulative degree-days; L is volumetric latent heat of fusion; θ is volumetric moisture content.

Ground surface temperature is calculated by using a combination of energy balance and bulk aerodynamic approaches. The surface energy balance is written as

$$Q^* = Q_H + Q_E + Q_G \qquad (1.13)$$

where Q_H is heat flux between the surface and the air

$$Q_H = \rho_a C_a (T_s - T_a) / r_h \qquad (1.14)$$

where ρ_a and C_a are the air density and specific heat; T_s and T_a are the surface and air temperature; r_h is the bulk aerodynamic resistance to convective heat transfer. Neglecting Q_G , combining these two equations to solve for T_s yields

$$T_s = T_a + r_h(Q^* - Q_E) / \rho_a C_a \qquad (1.15)$$

The Q^* term assumes knowledge of T_s in calculating long wave radiation emission from the surface. This problem is overcome by substituting isothermal net radiation at T_a for Q^*. The resistance term r_h becomes r_{hr} and is defined as

$$1/r_{hr} = 1/r_h + 1/r_r \qquad (1.16)$$

where r_r is a radiative resistance and r_{hr} is the combined convective and radiative resistances.

$$r_h = [\ln(z - d)/z_0]^2 / k^2 u \qquad (1.17)$$

where z is height above the surface at which average wind speed u and air temperature are measured, z_0 is the aerodynamic surface roughness length, d is the zero-plane displacement length, and k is the von Karman's constant. The radiative resistance is estimated as

$$r_r = \rho_a C_a / 4\sigma T_a^3 \qquad (1.18)$$

where σ is the Stefan-Boltzmann constant (Campbell 1977).

However, the effect of evaporation on surface temperature can be important for wetted surfaces.This model

considered this effect and the final expression for surface temperature is

$$T_s = T_a + r_{hr}\,[Q_i^* - \min(LE_p, L\theta)]/\rho_a C_a \qquad (1.19)$$

where θ is soil moisture content on a volumetric basis, L is the latent heat of vaporization, E_p is the potential evaporation, and Q_i^* is isothermal net radiation.

In this model freeze thaw calculations are linked to the soil water balance: (1) by considering the effect of soil moisture content on soil thermal conductivity and volumetric latent heat of fusion and (2) by including the effect of ice content on infiltration and soil water movement.

$$K_{soil} = (K_{sat} - K_{dry})\,S + K_{dry} \qquad (1.20)$$

where K_{soil} is unsaturated soil thermal conductivity; K_{sat} is saturated soil thermal conductivity; K_{dry} is dry soil thermal conductivity and S is fractional degree of saturation.

Compared with the Bonan's models and Kane & Hinzman's modified HBV model, Fox's model has a stronger physical basis. Freeze-thaw activities are connected to the water balance and the effects of solar radiation and turbulent heat flux are included. However, thawing calculation, through the

degree day method, does not offer a two-sided freezing as freezing can only proceed downward. Another weakness is that daily evaporation and water table fluctuation are not evaluated, and these are also important considerations in permafrost hydrology.

1.2.1.5 Woo and Drake Model

Woo and Drake (1988) proposed a model to simulate the daily hydrological and thermal conditions of a vertical column in continuous permafrost (Table 1.1). The snow on the ground is incremented when air temperature is below freezing on a day with precipitation. Snow-melt is partitioned into radiation melt, rain-on-snow melt and turbulent-flux melt indexed by air temperature (because wind and humidity data are generally unavailable). The penetration of the meltwater front utilizes Colbeck's (1976) equation and basal ice growth and infiltration into frozen soil are also considered, although in a primitive fashion. Evaporation is computed using the Priestley and Taylor (1972) approach. Ground temperatures are calculated using finite difference, and the solution allows the frost-table to be located. Daily water balance is performed and the water-table is updated. When the water-table rises above the ground to exceed the depression storage, lateral run-off is generated from the site.

Table 1.1 The characteristics of Outcal model and Woo and Drake model

MODELS	**OUTCALT** 1975	**WOO & DRAKE** 1988
Inputs	Incoming radiation; Cloudiness; Mean air temperature; Wind speed; Relative humidity; Air pressure; Snowfall	Precipitation; Incoming radiation; Air temperature
Parameters required	31	24
Time scale	Daily	Daily
Spatial scale	Tundra vertical profile	Tundra vertical profile
Application	Snowmelt and soil thermal regimes	Hydrology and Ground Thermal Regimes
Permafrost type	Continuous	Continuous
Ground thaw calculation	Finite difference	Finite difference
Outputs	Radiation fluxes; Energy fluxes; Snow accumulation and melt; Surface and ground temperature	Snow accumlation & melt; Frost table and water table; Evaporation; Soil moisture; Water balance

Table 1.2 The characteristics of two Bonan models

MODELS	**BONAN** 1989	**BONAN** 1991
Inputs	Mean: Air temperature; Rain fall; Mean cloudiness; Daily mean max & min temperature	Mean: Air temperature; Incoming radiation; Relative humidity; Air pressure; Wind speed; Cloudiness. Precipitate
Parameters required	40	74
Time scale	Daily	Daily
Spatial scale	Boreal forest	Boreal forest
Application	Solar radiation; Soil moisture; Ground thermal regimes	Biophysical surface energy budget of soil temperature
Permafrost type	dis-continuous	dis-continuous
Ground thaw calculation	Stefan formula	Finite difference
Outputs	Monthly mean radiation; monthly potential evaporation; Depth of seasonal freeze and thaw	Radiation fluxes; Energy fluxes; Snow accumulation and melt; Active layer processes

Table 1.3 The characteristics of two selected models

MODELS	**KANE & HINZMAN** 1991	**FOX** 1992
Inputs	Mean: Air temperature; Snow fall; Rain fall; Evaporation rate; Basion area and elevation	Mean: Air temperature; Incoming radiation; Rain fall; Snow fall; Wind speed; Surface roughness; Soil composition
Parameters required	41	50
Time scale	Daily	Daily
Spatial scale	Small Arctic basin	Vertical profile in permafrost area
Application	Hydrologic forecast for basins using modified HBV model	Water balance with freeze thaw processes
Permafrost type	Continuous	Continuous and dis-continuous
Ground thaw calculation	Stefan formula	Stefan formula
Outputs	Discharge; Snow ablation; Soil moisture; Soil temperature	Snow accumulation and melt; Frost advance; Thaw advance

This algorithm can be used to generate run-off for different points in the basin or on a slope, but further work is needed to bring the point values into a spatial framework, and to route the flow down the slopes and along the channels. More detailed review of this model is presented in chapter 3.

1.2.1.6 Model Selection for This Study

Scientific hydrological studies have yielded sufficient information to allow an attempt at producing physically-based, deterministic models tailored to the permafrost region. Hydrometeorological data remain limited, however, because of the sparse weather-station network in the Arctic (Woo 1990). To be practical, a model has to make use of readily-obtainable data including air temperature, precipitation and perhaps, radiation. Outcalt model and Smith model are strong at surface energy balance and soil thermal regime modeling, but they have no hydrologic component, and therfore use constant soil moisture and thermal conductivity, which severely limit their model application.

Bonan's (1991) model shows an improvement over the Outcalt model and Smith model. Bonan's model incoporates freeze and thaw processes into a water balance model. Unfortunately, most effort is placed on the canopy above the ground surface and is deficient in the subsurface system.

There is no quantitative modeling for water table fluctuation, which strongly affects soil moisture distribution and this, in turn, affects thermal conductivity. Another problem for Bonan's 1991 model is that it requires several input variables that are not transferable, like wind speed and humidity.

Kane and Hinzman's model involves a large amount of empiricism and requires considerable parameterization. Although applicable for small drainage basins, it cannot provide sufficient detail for point modeling. Fox's model has a stronger physical base, but still is weak at evaporation and does not model water table change.

Woo and Drake's model is a point model, developed specifically for the continuous permafrost environment. Although it simplifies several hydrological processes, there is an adequate physical basis, and the data requirement is not stringent. The outputs, including the water table and the frost table, snow melt and evaporation, are the main features in permafrost terrain. It has not been thoroughly tested by field data and the present thesis proposes to fill in this void. The point models and the basin model presented above do not handle spatial variations of thermal and hydrological variables in permafrost terrain. In this case, a simple model has to be designed to extend the point model but bearing in mind the constraints placed by data limitation in permafrost areas.

1.3 Objectives of This Study

In many permafrost hydrologic investigations, the temporal fluctuation and the horizontal variations of the water table and the frost table are of considerable importance (Woo and Steer 1982). These two boundaries determine the transition to surface flow and define the zone of suprapermafrost ground water occurrence. The positions of these two boundaries are controlled by thermal and hydrological processes which until now cannot be modelled satisfactorily. The objectives of this study are:

(1) Calibrate and test the Woo and Drake model in a continuous permafrost environment, using field collected measurements.

(2) To develop a new model to extend the vertical model results to two-dimensional simulation of the frost table profile and variation along a terrain cross section, with model inputs being easily-obtainable field measurements or being outputs from the Woo and Drake model.

(3) Using the two calibrated models, to simulate the hydrological responses and freeze-thaw variations under natural and man disturbed situations.

To calibrate and test the models, field work was carried out at a continuous permafrost site near Resolute, N.W.T., and Chapter 2 describes the location and the research

methods. The Woo and Drake model will be described in detail in Chapter 3, and the calibration using the 1988 and 1989 field data are also presented. The model was then tested with other data collected previously in the 1970's and early 1980's. Chapter 4 presents the XIA model which extends the one-dimensional results to two-dimensional sections, based on the Green function to be discussed in the Chapter 4. The accuracy of the models' performance are determined by the root mean square method. The applications of these models to the natural and disturbed environment will be presented.

CHAPTER 2

STUDY AREA AND METHODS

2.1 Research Area

This study was carried out in McMaster River basin, about 5 km northeast of Resolute, Cornwallis Island, N.W.T. (Figs. 2.1 and 2.2). The area is underlain by Paleozoic rocks and is in the Cornwallis Fold Belt on the southern edge of the Innuitian Region (Bostock 1972). Continuous permafrost occurs at depths of between 0.25 and 1.0 m below the surface.

2.1.1 Landforms and Soil

The region has been glaciated at least once (Thorsteinsson 1958) but little is known about the detailed glacial history. Deglaciation occurred about 10,000 years B.P. followed by submergence. Emergence commenced approximately 9000 years ago (Washburn and Stuiver 1985). Marine shells are found at elevations of 150 m while the highest strand lines reach 105 m and possibly higher.

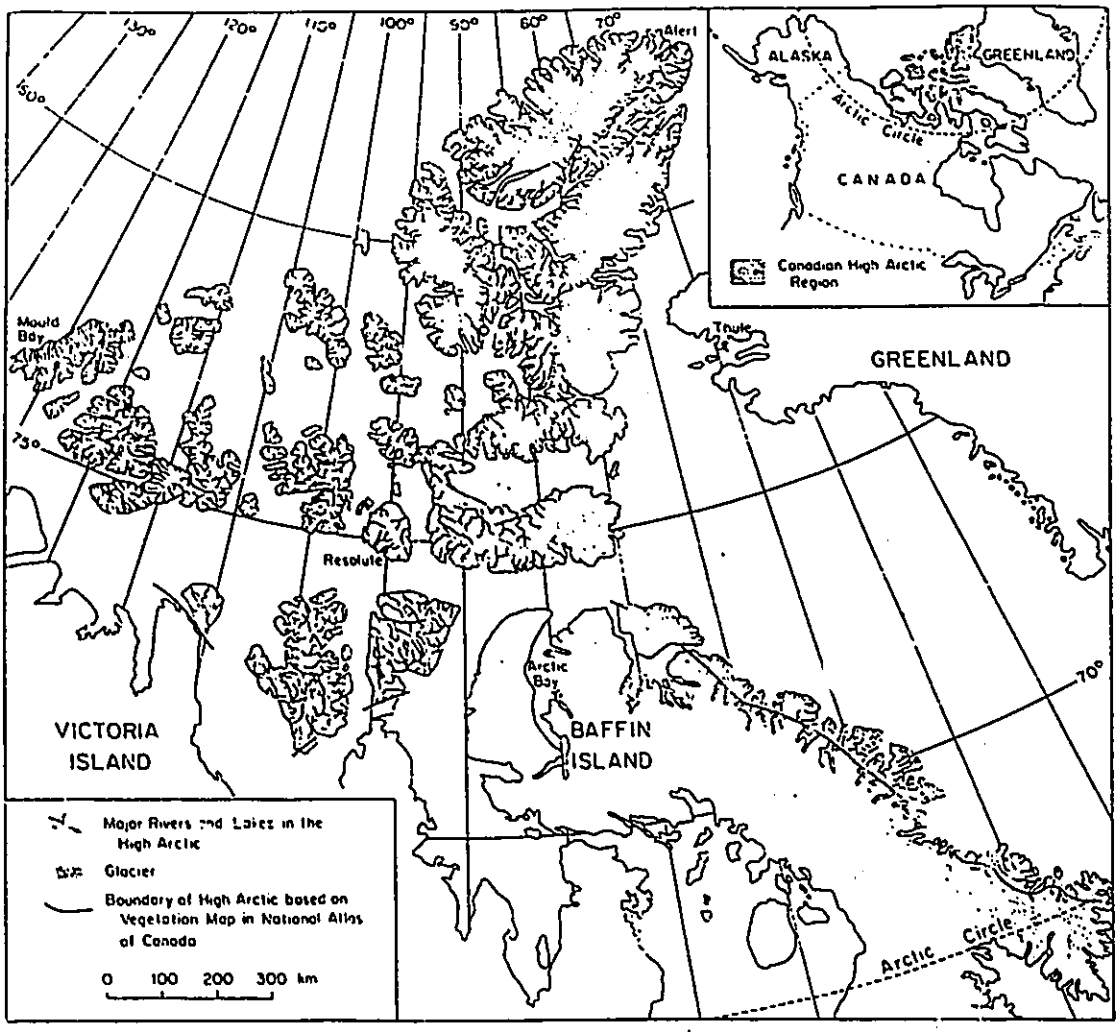

Figure 2.1 Location of the study site at Resolute on Cornwallis Island in the Canadian High Arctic. The southern limit of the High Arctic is determined by the tundra vegetation boundary

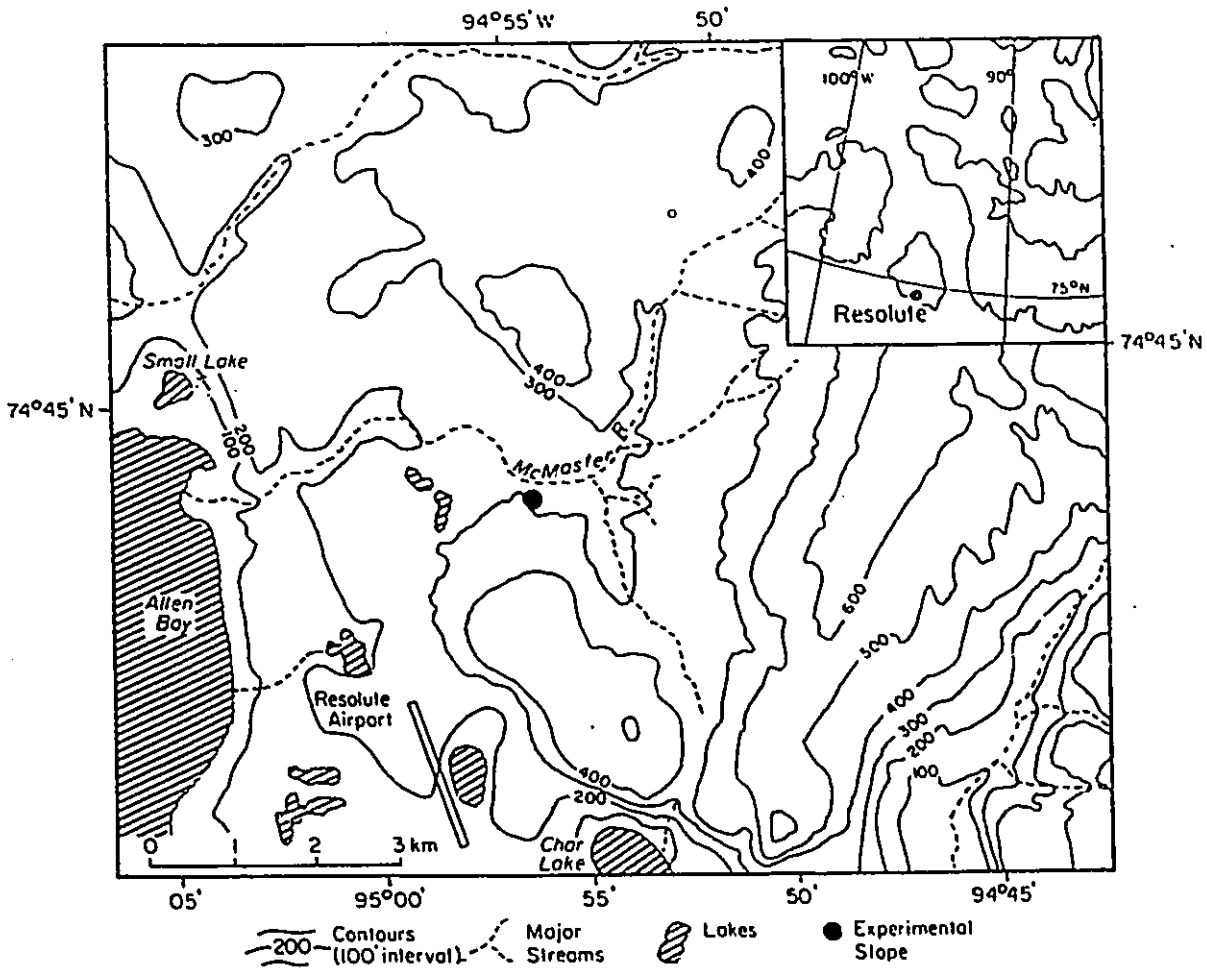

Figure 2.2 The study site in McMaster River basin, near Resolute, Cornwallis Island, Northwest Territories.

The surface material is composed mainly of rock fragments and fine sands and silts. The parent material is till and locally-derived rock fragments but solifluction and cryoturbation have modified their original properties. Cruikshank (1971) classified the soils around Resolute into three groups;

Lithosols are composed of fragmented limestone and dolomite gravels. They are associated with scree slopes, shattered rock or located near the bedrock outcrops on level ground at lower elevations. Lithosols have less than a 10 percent plant cover (Cruickshank 1971).

The polar desert soils are very sparsely vegetated and consist of limestone and dolomite gravels in a sand and silt matrix. This soil is found on elevated level ground, patterned ground, and frost-heaved ground. The small limestone ceasts are weakly sorted or non-sorted. These soils are almost ahumic, well drained and alkaline in reaction. Due to the low temperatures of this environment combined with the scarcity of vascular plants, this soil type has a very low organic content (French 1976).

Bog soils (actually, most of these are in fens) occur where moisture is augmented by lateral drainage or snowmelt. These fine grained tundra gley soils are restricted to slopes and depressions that remain wet most of summer and are completely vegetated with lichens, mosses, sedges and

grasses (Cruickshank 1971). Due to the spatial domination of the polar desert soils and lack of vegetation, Cornwallis Island lies in the High Arctic vegetation zone (Fig. 2.1) (Energy, Mines and resources 1974).

2.1.2 Climate

This study area lies in the northwestern climatic zone of the Canadian Arctic (Maxwell 1980). Polar night with 24 hours of darkness lasts from November 4th to February 5th. By April 30th daylight lasts 24 hours and this continues until August 15th. This extreme radiation regime produces extremely low temperatures in winter.

At Resolute Airport, the mean annual temperature is -13.5 ^{0}C. Peak summer temperatures are generally below 10 ^{0}C while winter temperatures reach -35 ^{0}C. Mean daily temperature rises above 0 ^{0}C on June 10th and falls below zero on August 24th. Fig. 2.3 shows the mean monthly and extreme air temperatures for Resolute. However, temperature can drop below zero on any day in the summer. Such thermal regime produces approximately 300 thawing degree days and more than 6000 freezing degree days annually (Energy, Mines and Resources 1974).

The prevailing wind directions at Resolute are northwesterly and southeasterly, the latter being prevalent

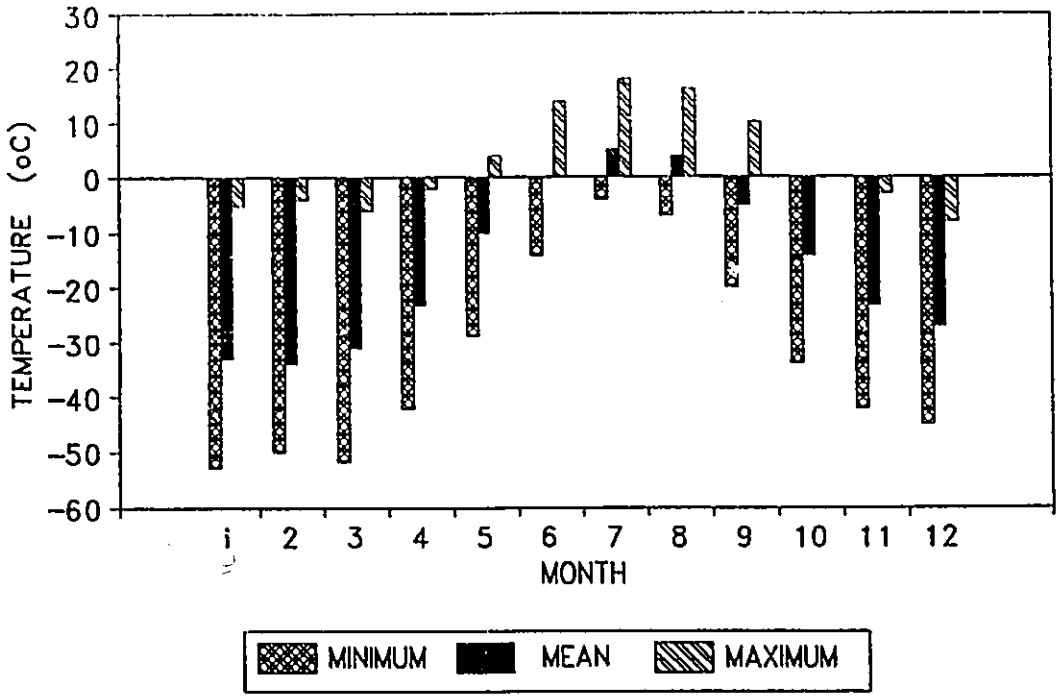

Figure 2.3 Mean Monthly and Extreme Air Temperatures for Resolute, Cornwallis Island, N.W.T.

in the summer months (Heron 1985). The least frequent wind direction is the southwest. The mean summer wind speed is 21 km/h (Maxwell 1980).

2.1.3 Hydrologic Conditions

Resolute has low precipitation, with the weather station recording only 130 mm annually (Maxwell 1980).

However, Woo et al (1983) have shown that the High Arctic weather stations greatly underestimate the snow received in the surrounding catchments due to the many blowing snow and trace precipitation events. A mean annual precipitation total of 180 to 210 mm is a more reasonable value. The monthly variation of precipitation is indicated in Fig. 2.4. The highest snowfall occurs in the spring and fall when atmospheric moisture is available, though snow can fall at any time of the year. Drifting snow is common in the winter, producing an extremely uneven snowcover (Xia and Woo 1992). Hilltops and exposed locations may be bare while the snowpacks of lee slopes and sheltered depressions are many meters thick (Woo et at 1983). The main melt season usually arrives in late June and the abundant quantities of meltwater are released rapidly.

The only limiting factor for soil moisture replenishment is the low infiltration capacity of the frozen soil (Kane and Stein 1983). Any water that cannot infiltrate is refrozen at the base of the snow to form basal ice (Marsh and Woo 1984), or runs off as surface flow from hill slopes.

The peak precipitation period is in the summer with rainfall being dominant, although it accounts for less than 20 percent of the total annual precipitation (Woo and Marsh 1990). Rainfall in the High Arctic is seldom of high intensity. The amount of rain that fell in 1988 and 1989 were

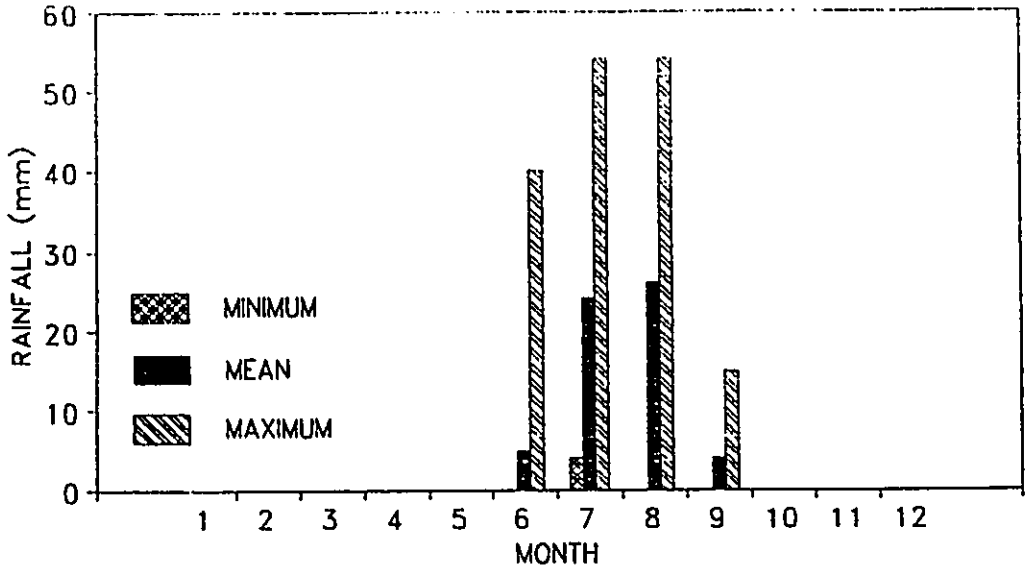

Figure 2.4 Annual Variation in Rain Received at Resolute Weather Station

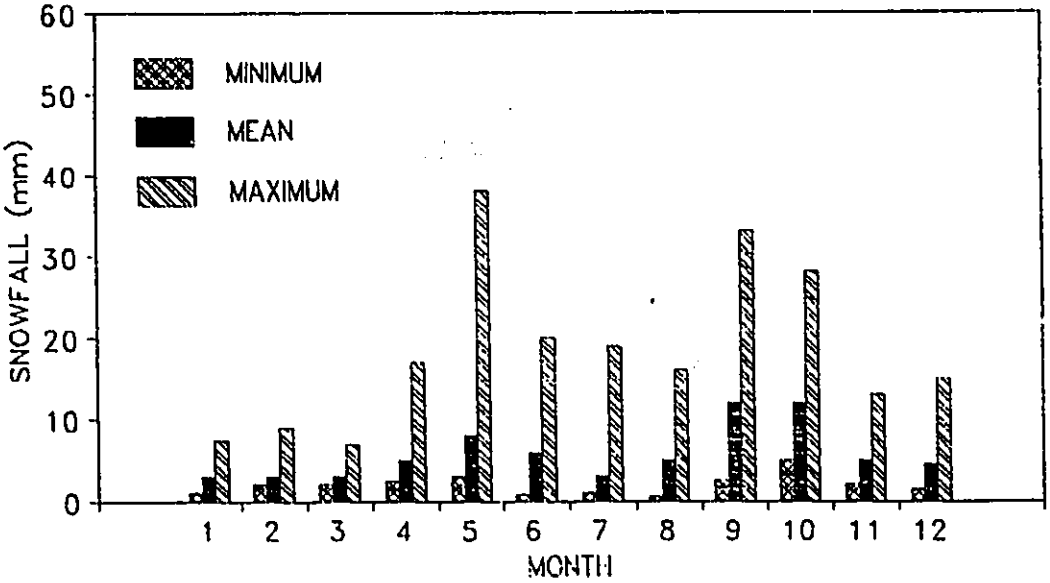

Figure 2.5 Annual Variation in Snow Received at Resolute Weather Station

and 1989 were substantially less than snow accumulation at the study sites. However, rainfall events were often able to increase soil moisture storage and to raise the water table.

Evaporation at this northern latitude is limited by the long duration of snow and ice on the ground and low level of energy available during the thawed season (Woo 1992). But, it accounts for a significant portion of water loss during the thawed season, due to 24 hour sunshine. Evaporation from the three typical soil types is different too. As the water table in the fine grained soils is usually close to the surface, the evaporation rate is the highest. The polar desert soil, with more moisture at the surface than the gravel, has the next highest amount of evaporation (Woo and Marsh 1990).

2.1.4 Permafrost Environment

Permafrost is earth material which remains at or below 0 ^{0}C (cryotic) for at least two consecutive years. Here, cryotic is defined as a temperature $\leq 0^0$C, and is to be distinguished from freezing conditions because water that is impure or under pressure or tension stays unfrozen at 0^0C (van Everdingen, 1987). The top of the permafrost is the permafrost table. The zone which freezes and thaws annually in the permafrost region is the active layer. The cold climate in High Arctic favours the development and maintenance of

permafrost to great thickness. Based on ground temperature measurements down to 195 m, Meisner (1955) estimated the permafrost thickness to be 390 m. Fig. 2.5 shows the monthly temperature profiles for June, July and August along with the annual maximum and minimum ground temperatures. The zero amplitude point is located at 19.2 m where the temperature is -12.6 ^{0}C (Fig. 2.6). The thickness of the Active layer thaw rarely exceeds 0.75 m in polar desert and gravelly soils and 0.5 m in tundra peaty soils (Heron 1985, Marsh and Woo 1993).

Frost cracks and ice-wedge polygons are common at this research area. Frost cracking is fracturing by thermal contraction at subfreezing temperatures (Lachenbruch 1966, Xia 1985). Vegetation is sparse and it is generally concentrated along the furrow and emphasizes the pattern. Permafrost usually has very low hydraulic conductivities which inhibits water movement. Groundwater occurs either in the taliks, or seasonally in the active layer. Active layer storage capacity is limited and is highly variable, depending on the depth of thaw during different times of the year (Woo 1986). In spring when the active layer is largely frozen, meltwater will not penetrate easily and much runs off as overland flow (Woo 1992, McCann et al. 1975).

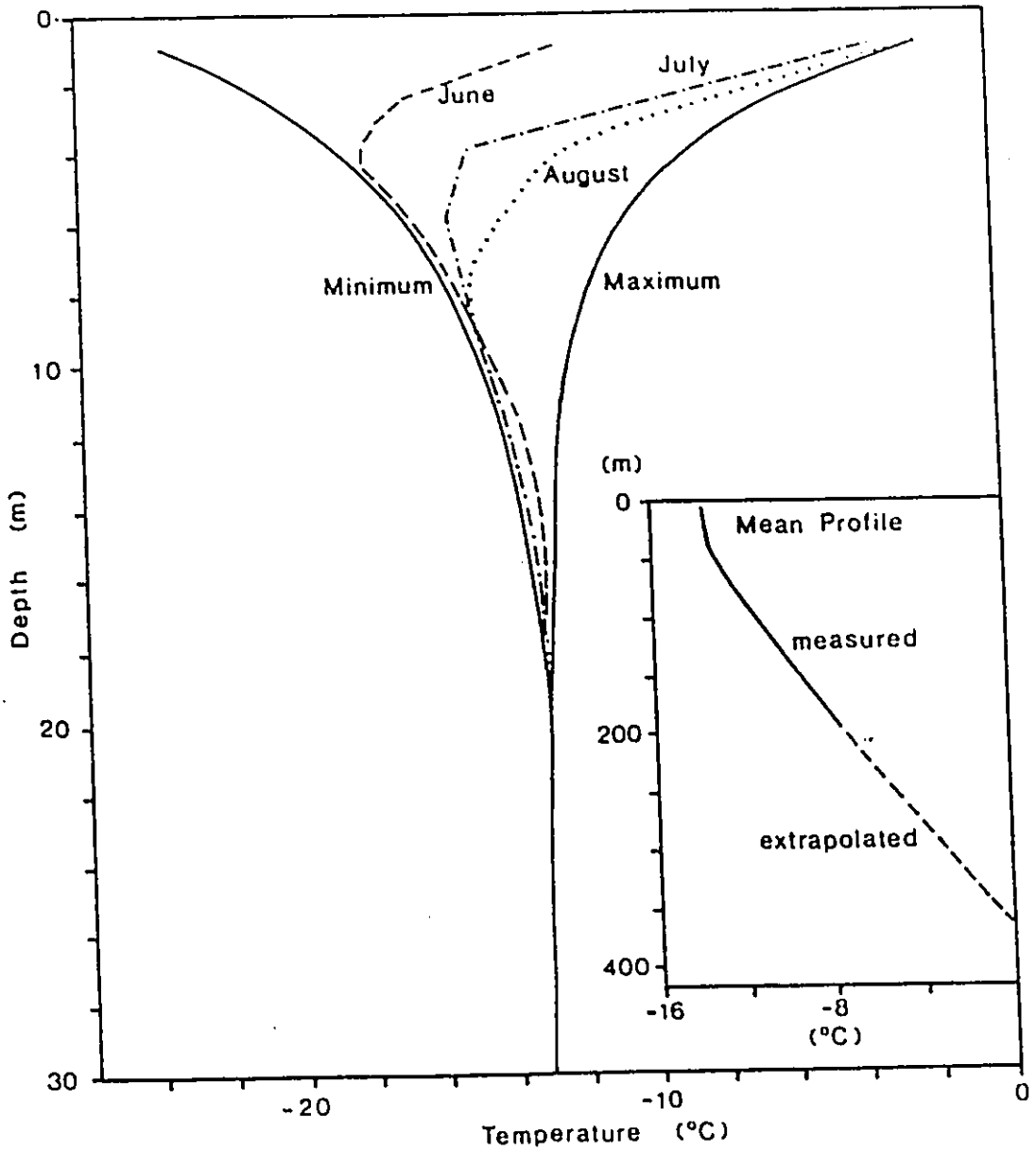

Figure 2.6 Ground Temperature Regime for Resolute. The Monthly Temperature Profiles for June, July, and August are Shown Along With the Annual Maximum and Minimum Ground Temperatures (after Meisener 1955, Cook 1958).

2.2 Experimental Site

One slope within the area was selected as experimental site for intensive study (Fig. 2.7). The site was chosen because previous work in the slope (e.g. Woo, 1976; Marsh, 1978; Heron, 1979; Steer,1982) allows access to a seven year data base.

2.2.1 Slope Characteristics

The experimental slope is typical of most other slopes in the area. The upper slope has a moderately steep convex profile grading into concavity or a gentle ($<5^0$) downslope segment (Woo and Steer 1982). The break-of-slope forms a depression which holds a late-lying or semi-permanent snowpack (Fig. 2.8). Below the depression, surface flow commonly occurs throughout summer. Further down slope is a natural gully where flow measurement equipment could be installed easily. Total relief of the slope is 23 m over a horizontal distance of 232 m, giving an average slope of 10% (Steer 1982). The upper slope is moderately steep (10%) and consists of gravelly material over which little surface flow occurs. The lower slope averages 4% and its central portion is occupied by a vegetated tongue which receives lateral flow from slope drainage and meltwater from snow banks. This tongue merges

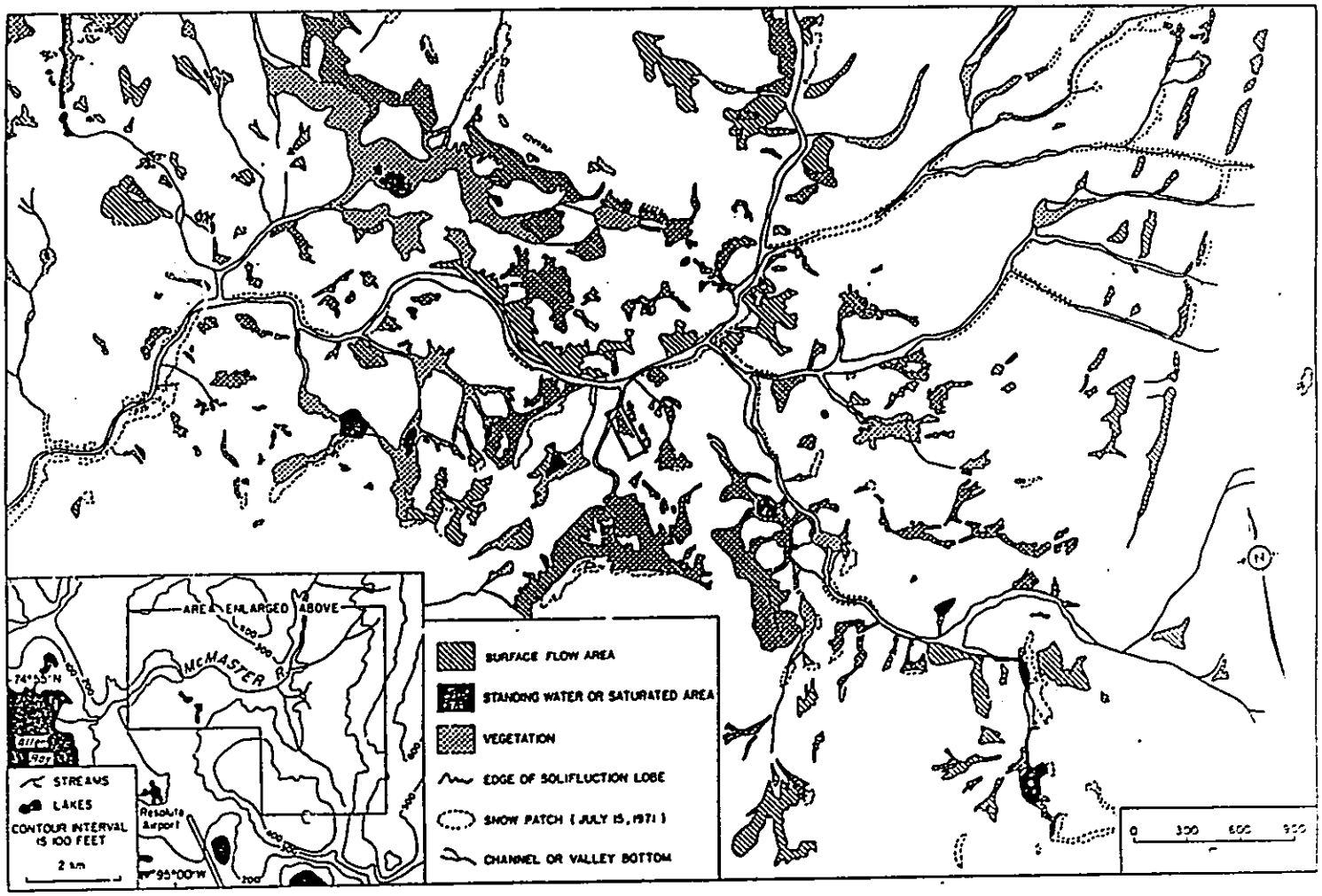

Figure 2.7 Surface condition of part of the study area shown in aerial photographs taken on July 15, 1971. The slope chosen for intensive study is indicated with a black box.

Figure 2.8 Aerial photograph of the study slope. Contours are at 1 m intervals. Topographic boundary of the slope is also marked.

laterally into gravelly areas.

2.2.2 Soil Properties

Figure 2.9 shows grain size distribution from six sample sites on the slope (Woo and Steer). Sites (1), (2), and (3) are dry polar desert lithosols with 60-70% gravels, 20-35% sand and about 5% silts and clays. Site (4) is wet polar desert lithosol where the surface sample is composed of 60% gravel, 25% sand and 15% silts and clays. Near the permafrost table the proportion of gravel increases to 85%, with 5% sand and 10% silts and clays (Steer 1982). Bog soil occupies sites (5) and (6) where samples below the vegetation mat produce a gravel content of 5% and the remaining 95% is almost equally split between sand or silt and finer materials (Steer 1982). Subsurface lateral drainage is affected by the slope material.

Measurements of hydraulic conductivity in saturated materials show that for polar desert the rate averages 2.95 ± 3.91 m/day, but in boggy areas the rate drops to 0.10 ± 0.10 m/day (Woo and Steer 1982).

Thermal property varies depending on the slope material too. The thawed zone in gravel soil area is deeper than in bog area as gravel soil has stronger thermal conductivity than bog soil. The combined effects of deeper thawing front frost table development and higher hydraulic conductivity in gravelly soil

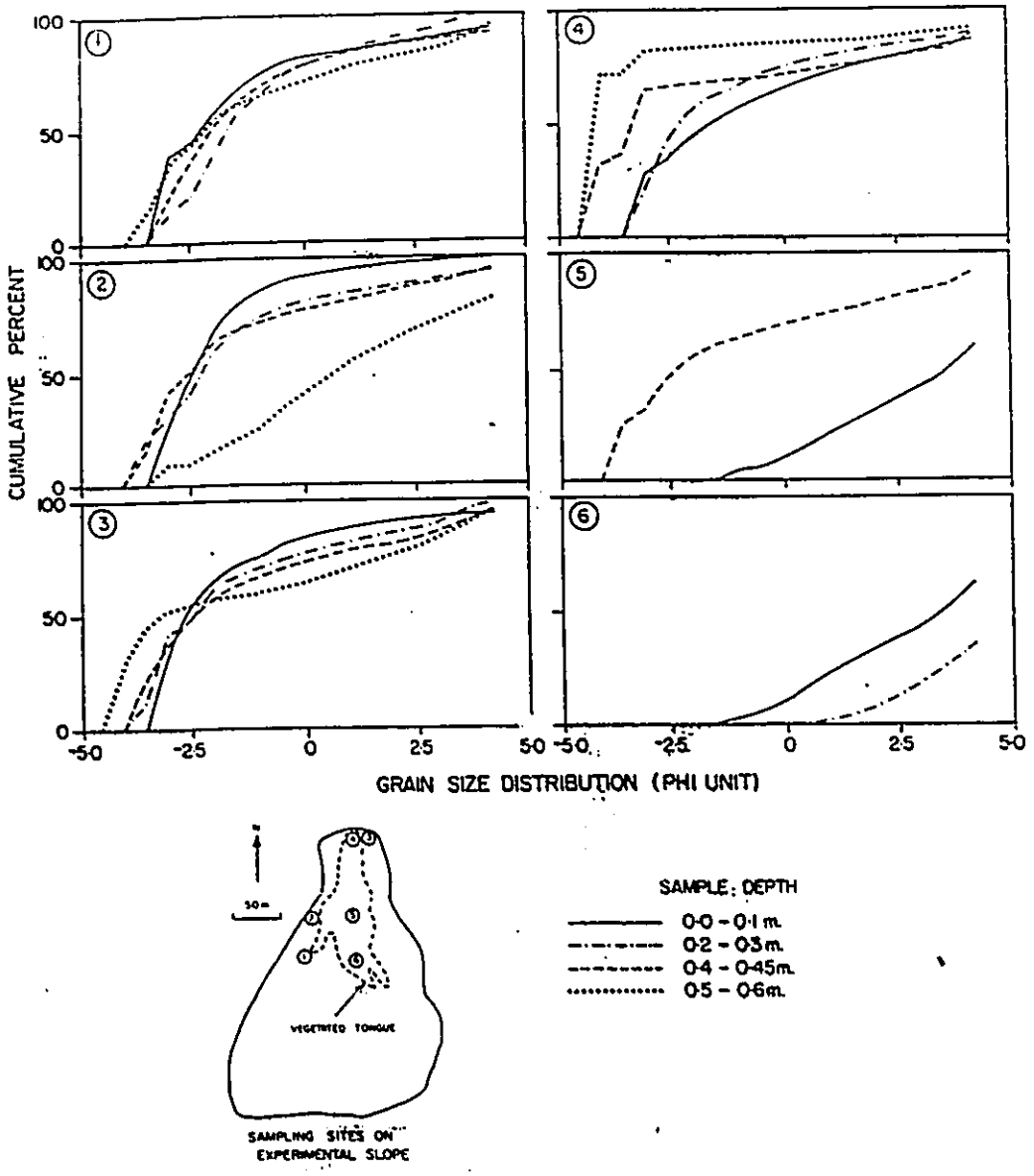

Figure 2.9 Grain size distribution of soil samples obtained from the experimental slope. Samples were obtained from several depths in the active layer. Sites (1) and (2) have dry gravelly soil, site (3) has dry polar desert soil, site (4) has wet polar desert soil, sites (5) and (6) have saturated tundra gley and bog soils.

zones will produce a lower water table than in the central bog area.

The gravelly areas on the slope support patchy growths of purple saxifrage (*Saxifraga oppositifolia*), arctic willow (*Salix arctica*), mountain avens (*Dryas integrifolia*), arctic poppy (*Papaver arctica*), *Draba alpina* and various species of lichen (Steer 1982). The mosses occupying the central boggy strip are closely related to those of areas farther west and, although not precisely identified, are probably typical of mosses found in moist calcareous habitats (Steer 1982). Some grasses and sedges occur near the western edge of the wet strip. Vegetation growth increased the soil organic content significantly (Hinzman, D.L., D.L. Kane, R.E. Gieck and K.R. Everett 1990).

The microtopography of the slope surfaces is uneven. When the water table rises above the ground, many puddles develop to satisfy depression storage requirements before lateral surface flow begins. In wetter areas, water usually moves as sheets or seeps through moss. Where there are such patterned ground features as stripes, nets, circles, polygons, or earth hummocks, local depressions and cracks facilitate flow concentration and water moves along an integrated network of ephemeral rills (Woo and Steer 1982). Since meltwater is a major scurce of surface runoff, convex and steep slopes with shallow snowpacks seldom experience significant surface flow

(Lewkowicz 1981, Lewkowicz and French 1982). However, the bases of concave and gentle slopes are favorable sites where the water table lies above the ground in the wet season (Woo and Steer 1982). The bog area at the bottom of the slope receives water supplied by lateral drainage and from upslope and is often the preferred location for saturation overland flow.

2.3 Instrumentation and Methods

Figure 2.10 shows the main sites where measurements were made at the intensive study slope of McMaster River basin for the previous studies and for the two major field seasons in 1988 and 1989. The most comprehensive data were collected at the main meteorological site where several variables were continuously recorded. Other sites were visited once a day for manual observations. The data collected at the study site are of three basic types; (1) input data to run the models, (2) parameters for developing empirical equations dealing with model construction, (3) frost table and water table data for model calibration and testing.

2.3.1 Weather Station Data

Since the Atmospheric Environment Service weather

station at the Resolute Airport was close to the research site, many meteorological observations were not duplicated. The station data also provided back-up information to allow missing data for the intensive study slope to be estimated. The fluxes of total incident shortwave radiation, diffuse shortwave radiation, reflected shortwave radiation and net radiation over a different ground surface that were measured at the weather station are directly transferable to the study site (Heron 1985). Other variables that could be used without major adjustments include precipitation and temperature. Missing air temperature, precipitation, and short wave radiation data were estimated from the station data using equations derived by linearly regressing the site and station data for the period when concurrent measurements were made at both sites. All of the above data were available on an hourly basis except precipitation which was six hourly.

In addition to climatic data, the weather station also provided daily ground temperature data (gravelly soil) at depths of 1, 5, 10, 20, 50, 100, 150, 300 cm.

2.3.2 Meteorological Data from Experimental Site

Meteorological data used as input for model calibration and testing were measured at the main meteorological site in

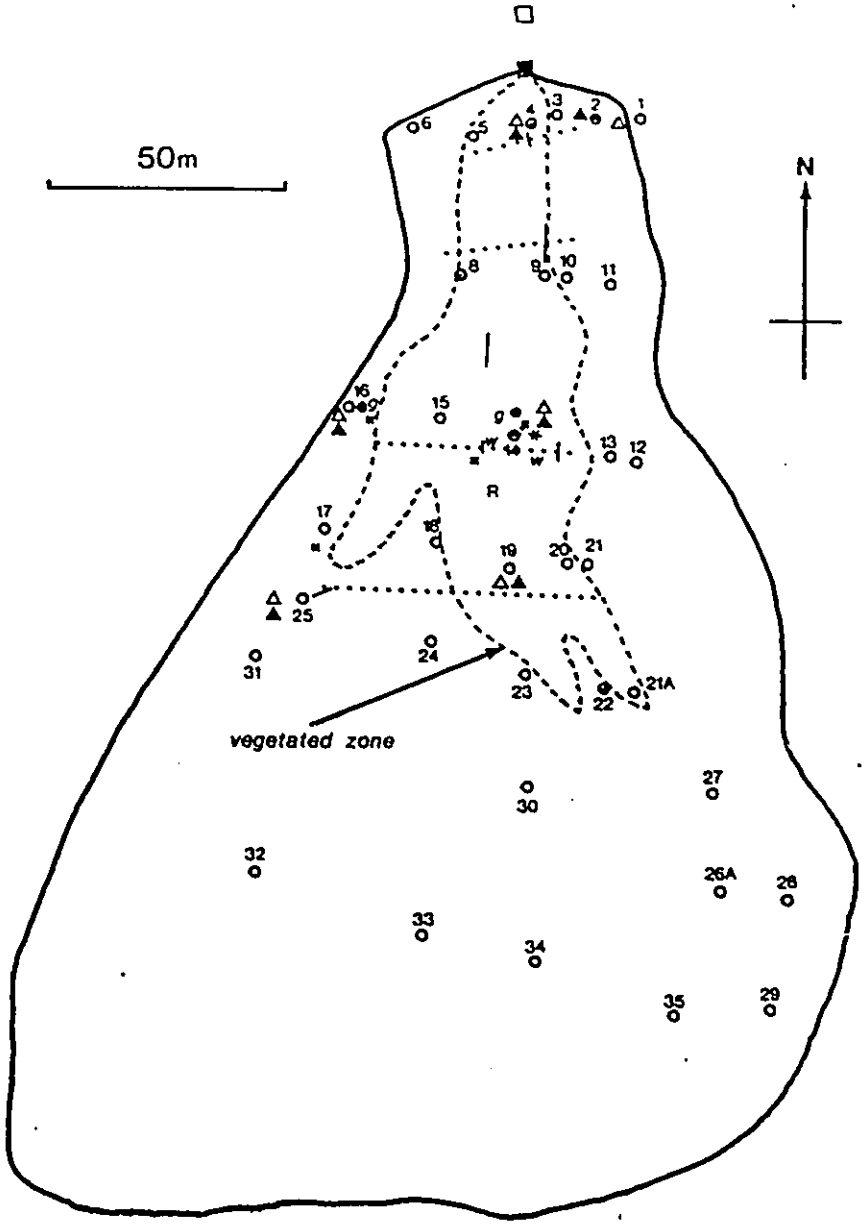

o ground water observation well
⊙ instrumented groundwater observation well
• soil moisture access tube
△ soil sample site
▲ specific yield sample site
g ground temperature site
w water temperature site

R net radiometer
* surface water depth recorder
■ surface flow collector
□ subsurface flow collector
····· microtopography profile line
| dye experiment site
× lysimeter

Figure 2.10 Location of Instruments and Measurements on the Study Slope

1988 and 1989 summer seasons (Fig. 2.10).

2.3.2.1 Precipitation

Total winter storage and snow distribution over the study site was determined by a late winter snow survey. In 1988 and 1989, more than 50 depth measurements along seven transects across the study site were surveyed. These snow depths were converted into water equivalent units using 23 snow densities determined with a Meteorological Service of Canada snow sampler.

In summer, rainfall was recorded using a Weather-Measure tipping bucket rain gauge attached to an event recorder (Campbell CR 21 data logger), at main meteorological site. A manual rain gauge (orifice diameter, 154 mm; orifice height, 250 mm) was placed nearby for comparison purposes. The gauge was checked and emptied after each storm and the accuracy of rainfall measurements is considered to be +/- 0.1 mm. Trace rainfall was determined using a method described by Woo and Steer (1979) and is accurated to +/- 5%.

2.3.2.2 Radiation

A Swissteco net radiometer was set up at the main meteorological site on the gravelly soil surface. A second net

radiometer was set up first over the top of snow surface and moved along with snow pack retreat. After the snow disappeared, it was set up on the fen surface and remained there throughout the entire thawed season. The signals from both instruments were recorded with a Campbell CR-21 data logger on hourly intervals. Latimer (1971) suggested that these instruments have an error of 5 percent, for keeping the sensors level over the melting snow, a more realistic error is 10 percent.

The incoming shortwave radiation received at the site and at the weather station did not correspond exactly because of the instrument error and the slightly different cloud coverage over both sites. All the radiometers were strongly affected by low solar elevations that occurred at the early and late hours of the day. The difficulty in maintaining a level sensor compounded the innerent sensor errors at low sun angles (Latimer 1971).

2.3.2.3 Air Temperature and Humidity

Air temperature and relative humidity were obtained using a Weathermeasure hygrothermograph housed in a Stevenson screen located 1 m above the ground surface. Temperature records were calibrated daily with a mercury thermometer and the resulting error was approximately 0.2 ^{0}C.

Relative humidity was checked against daily measurements obtained using an Assman psychrometer. The error was approximately 5 percent. From these data, the vapour pressure was obtained using the empirical equations given by Dilley (1978).

2.3.3 Hydrological Data and Soil Parameters

Hydrological data and soil parameters were observed for model calibration and testing.

2.3.3.1 Hydraulic Conductivity

Hydraulic conductivity was measured using the single auger hole method (Luthin, 1966). ABS plastic pipe with 100 mm inner diameter was punctured with 10 mm boles and dug down to the permafrost table which forms an essentially impermeable layer. Pumping tests enable the determination of hydraulic conductivity. The position of the water table in the pipe was noted before water was pumped out and the amount of drawdown recorded. By measuring the rate at which the water table rises in the pipe, the hydraulic conductivity (k) may be calculated as follows:

$$k = (523000r^2/dt)\,[\log_{10}(Y_o/Y_1)] \qquad (2.1)$$

where k is hydraulic conductivity in m/day, r is the radius of the auger hole in m, dt = $t_1 - t_0$ where t_0 is the starting time and t_1 is the finishing time in seconds, $Y_0 = d - Y_0'$ and $Y_1 = d - Y_1'$ where d is the height of the water table above the permafrost table in cm, Y_0' is the starting level and Y_1' is the finishing level, both in cm.

2.3.3.2 Bulk Density and Porosity

Bulk Density (Total Unit Weight or Wet Unit Weight) is defined as the ratio of the total soil mass (m) to the total volume (V)

$$\rho_t = \frac{m}{V} = \frac{m_s + m_t}{V} \qquad (2.2)$$

where m_s is the total mass of soil moisture and m_t is the dry weight of the sample soil. Soil samples were obtained from several sites using a sampler constructed from a steel pipe, and were weighed on an Ohaus triple beam balance in 1988 and

1989. The soil bulk densities observed in three different soil segments are listed in Table 2.1.

Porosity is defined as the ratio of the Volume of the voids to the total volume of the soil

$$\phi = \frac{V_v}{V} \qquad (2.3)$$

where ϕ is soil porosity; V_v is voids volume; and V is total volume of soil sample.

Table 2.1 Soil Bulk Densities of the Study Site

Soil Segment	Sample Depth (m)	Bulk Density kg/m^3
Gravelly	0.00 - 0.17	1540
Gravelly	0.18 - 0.34	1640
Gravelly	0.35 - 0.56	1690
Polar desert	0.00 - 0.30	1650
Polar desert	0.30 - 0.50	1709
Peaty	0.00 - 0.15	640
Peaty	0.16 - 0.30	1010

The soil density and porosity survey were carried out at the late summer 1988, and were continued in 1989. The observed mean value of soil porosity is 0.4 for the gravelly soil, 0.5 for peaty soil, and 0.7 for the vegetation cover including grasses, sedges, and mosses .

2.3.3.3 Specific Yield and Retention

The volumetric fraction of water which can be drained from the soil column by gravity is called the *specific yield*. The difference between porosity and specific yield gives the *specific retention*.

To obtain specific yield and specific retention, an undisturbed soil sample was saturated for 48 hours (Meinzer 1923). Then, any water ponded on top of the sample was decanted and the sample was then let drain through a mesh screen for 48 hours. The amount of water drained was recorded, and then the sample was dried in the oven to remove the rest of the water.

The specific yield S_y and specific retention S_r were calculated as:

$$S_y = \frac{V_{dw}}{V} \qquad (2.4)$$

$$S_r = \frac{V_{rw}}{V} \qquad (2.5)$$

where V_{dw} is volume of water drained from the saturated soil sample; V_{rw} is the volume of retained water in drained soil sample; V is the volume of the sample.

2.3.3.4 Soil Moisture and Water Table

At three experimental sites, gamma access tubes were installed down to the permafrost table in late August 1987 (Fig. 2.11). Changes in the frozen and unfrozen water stored in the active layer were determined using a twin-probe gamma density meter. Measurements began in June 1988 and continued at frequent intervals throughout the summer. Moisture profiles were obtained at 5 cm increments, with each measurement accurate to ±2 mm of water. The results have been reported by Woo and Marsh (1990).

Changes in the suprapermafrost groundwater table were measured across several lines of observation pipe (Fig. 2.10). Each well was a ABS pipe with 50 mm inner diameter perforated throughout its length, and installed to the depth of the permafrost table. A reference point was marked on the top of each pipe and distance down to the water table measured with

a steel rule. In 1988 and 1989 respectively, two and three observation wells were monitored continuously using Leupold-Stevens type F water level recorders. The observed water table fluctuation for well No.8 was shown in Fig. 2.12. The sharp rise in water level on August 7 (Julian day 217), 1989 was caused by heavy rain, amounting to 14.2 mm at our research sites.

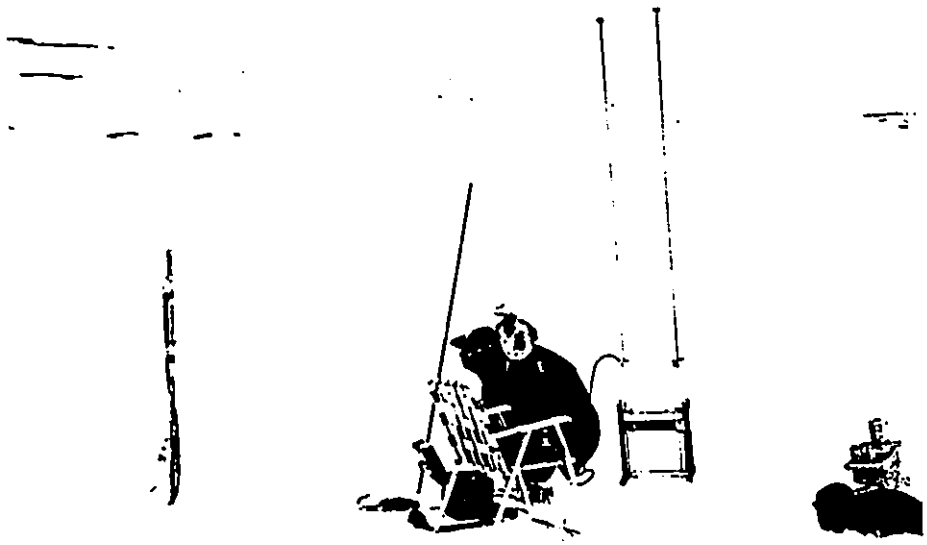

Figure 2.11 Using Gamma Probe to Determine Soil Moisture Changes in the Active Layer. The Measurement Was Started at the Beginning of the Melt Season.

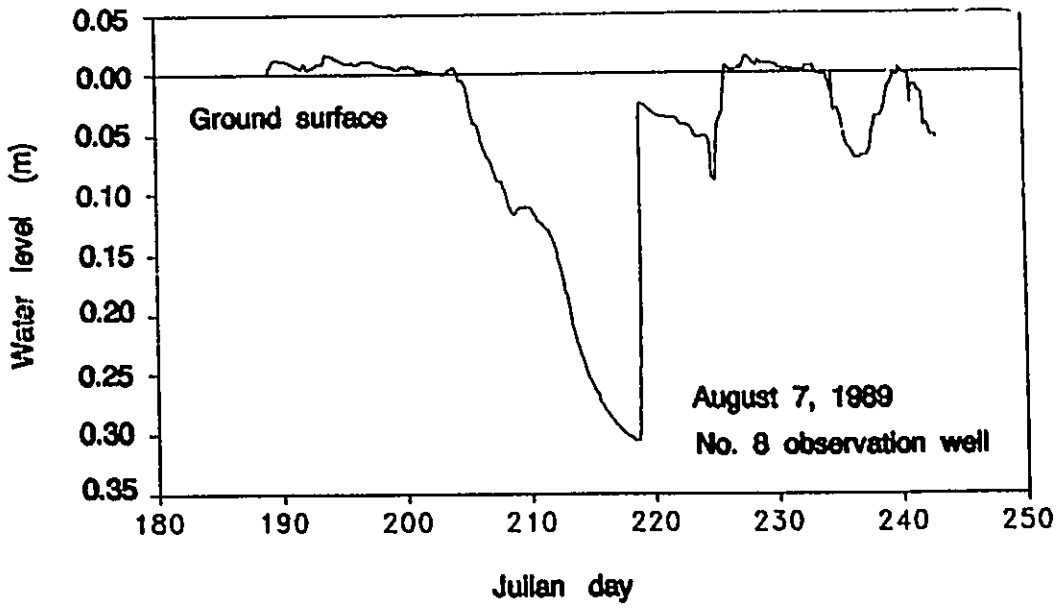

Figure 2.12 The Water Table Fluctuation at No. 8 Observation Well, Measure with Leupold-Stevens Type F Water Level Recorder

2.3.3.5 Soil Structure and Composition

Two pits one in gravelly and one in peaty soil were dug in late summer 1988 and soil samples were obtained for soil classification, composition analysis, density and porosity survey. The stratigraphy of the soil column at both sites is shown in Fig. 2.13.

The estimated fractions of various soil components,

including porosity, at 0.15 - 0.20 m depth, as determined for

Table 2.2 Soil compositions in gravelly and peaty soils

Soil Types	Gravelly Soil	Peaty Soil
Minerals	0.58	0.35
Organic Matter	0.02	0.15
Water	0.20	0.40
Air	0.20	0.40
Ice	0.00	0.00
Porosity	0.40	0.50

August 15, 1988, are given in Table 2.2. Both ice content and soil moisture are subject to change, according to the hydrologic conditions of the site at different times.

2.3.3.6 Ground Temperature and Frost Table

Ground temperatures in gravel and peat-covered soils were measured at five levels; 2, 5, 10, 25 and 50 cm depths (Fig. 2.10). Fenwall JA41J1 disc thermistors calibrated at

McMaster University, were inserted into plexiglass tubing and then firmly glued to a wooden stake at the desired intervals.

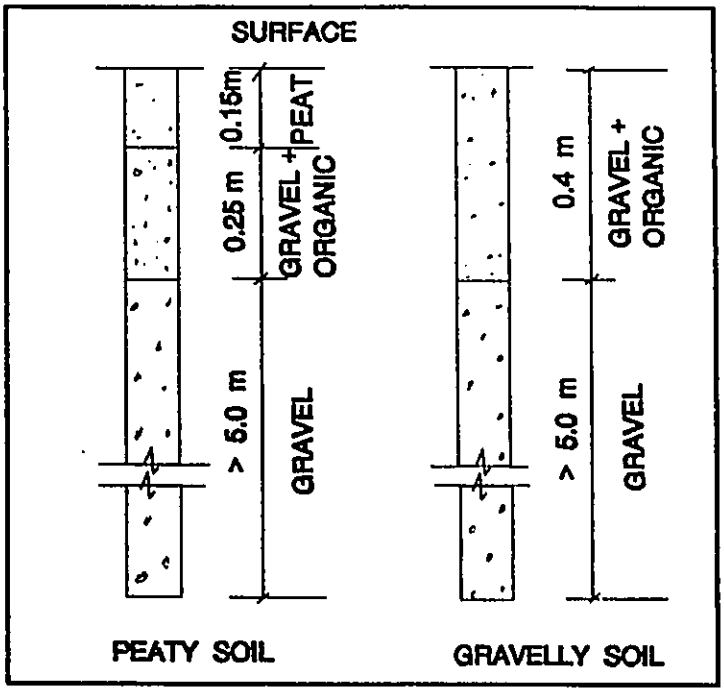

Figure 2.13 The stratigraphy of soil structures of the study site

Each thermistor rod was then tamped into holes drilled in the active layer using a Cobra drill. Resistance across the thermistor was measured using a digital multimeter.

The depth to the frost table was probed daily at 35 different observation points alongside the observation well

(Fig. 2.10). The probe was a steel rod and the depth of penetration of the rod was recorded to the nearest 0.005 m. Repeated measurements frequently had to be performed because the rod encountered gravel size material before reaching the frost table. These data could be used to test the model performance.

CHAPTER 3

ONE DIMENSIONAL MODEL FOR CONTINUOUS PERMAFROST

3.1 Woo and Drake (WAD) Model

The Woo and Drake model is a one-dimensional model developed to simulate the daily hydrological and thermal conditions of a vertical profile in the permafrost active layer. The major physical processes active in a continuous

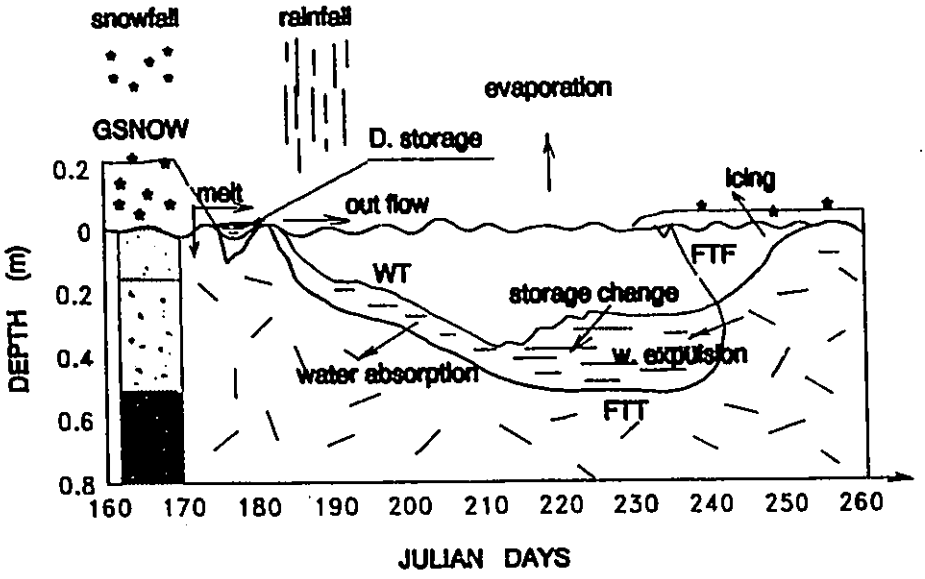

Figure 3.1 Major Physical Processes Represented by the Model

permafrost environment are shown in Figure (3.1). All these processes are represented in the model so that any changes in the magnitude and timing of the processes and the effects on the freeze-thaw and water discharge from the active layer, can be reproduced numerically.

3.1.1 Physical Background

The vertical structure and composition of the soil are entered as inputs to the model. The vertical column is divided into 100 slabs, each of a thickness DZ specified by the user. Individual slabs can be of different materials as specified by the user. Five material types are recognized including bedrock, gravel, fine sand and clay, peat and water. These are materials commonly found in the profile of an active layer in a continuous permafrost environment.

3.1.1.1 The Winter Season

In winter, snow accumulates on the column and the amount of snow on the ground varies depending on the type of terrain in which the column is located. In spring, snow melt proceeds according to the energy supply and the amount of snow storage. Meltwater can infiltrate into non-saturated frozen soil and may also fill up the surface depressions.

Once the depression storage is satisfied, outflow occurs. An increase in heat supply at the surface also warms the soil, though the presence of a snow cover prevents the temperature of the ground surface from rising above 0 ^{0}C and the ground will thaw when its temperature gets above the freezing point. Since ice has a volume approximately 1.1 times that of water, thawing of the ice leaves 10% of the soil with voids which need to be filled with water. It is also found that the fractional volume of air in some frozen materials may be different from the fractional volume of air in its equivalent thawed state. The consequences are that water is absorbed by a thawing soil, but expelled from a freezing soil. The latter condition is noticeable in the freeze-back period when the descent of the freezing front may be accompanied by water expulsion to the surface to form icings.

7.1.2 The Summer Season

Throughout the thawed season, the column receives water from meltwater, rainfall, inflow from upslope, and losses of water to evaporation and outflow. The result of this water balance is a net change in water storage in the thawed zone, which is manifested partially by the position of the water table. The water table defines the upper limit of the saturated zone, but its location is governed by (1) the

water balance noted above, and (2) the position of the thawing front below which the column is generally considered to be impervious. Thus, the saturated zone is considered to be perched upon the frost table whose position changes daily as the thawing front advances or retreats; (3) the exchange of water with the depression storage and the gain or loss of water through the freezing (expulsion) or thawing (absorption) of the ground; (4) the amount of water taken up or released by the non-saturated zone above the water table.

When the water table rises above the ground to exceed the maximum level of depression storage, surface outflow occurs. The saturated zone below the water table is prone to lateral subsurface flow. It has been found, however, that subsurface flow is orders of magnitude below surface runoff in permafrost region and that heat flux due to ground water flows is negligible in this environment (Woo 1986, McMillan 1983). Since the water table position and the thickness of the saturated zone are intimately related to the frost table, a coupling of the hydrological and thermal regimes in the permafrost environment is the physical essence of the model.

3.1.2 Flow Diagram for the Model

A flow-chart summarizing the Woo and Drake model is given as Figure (3.2). The column is built up by the user

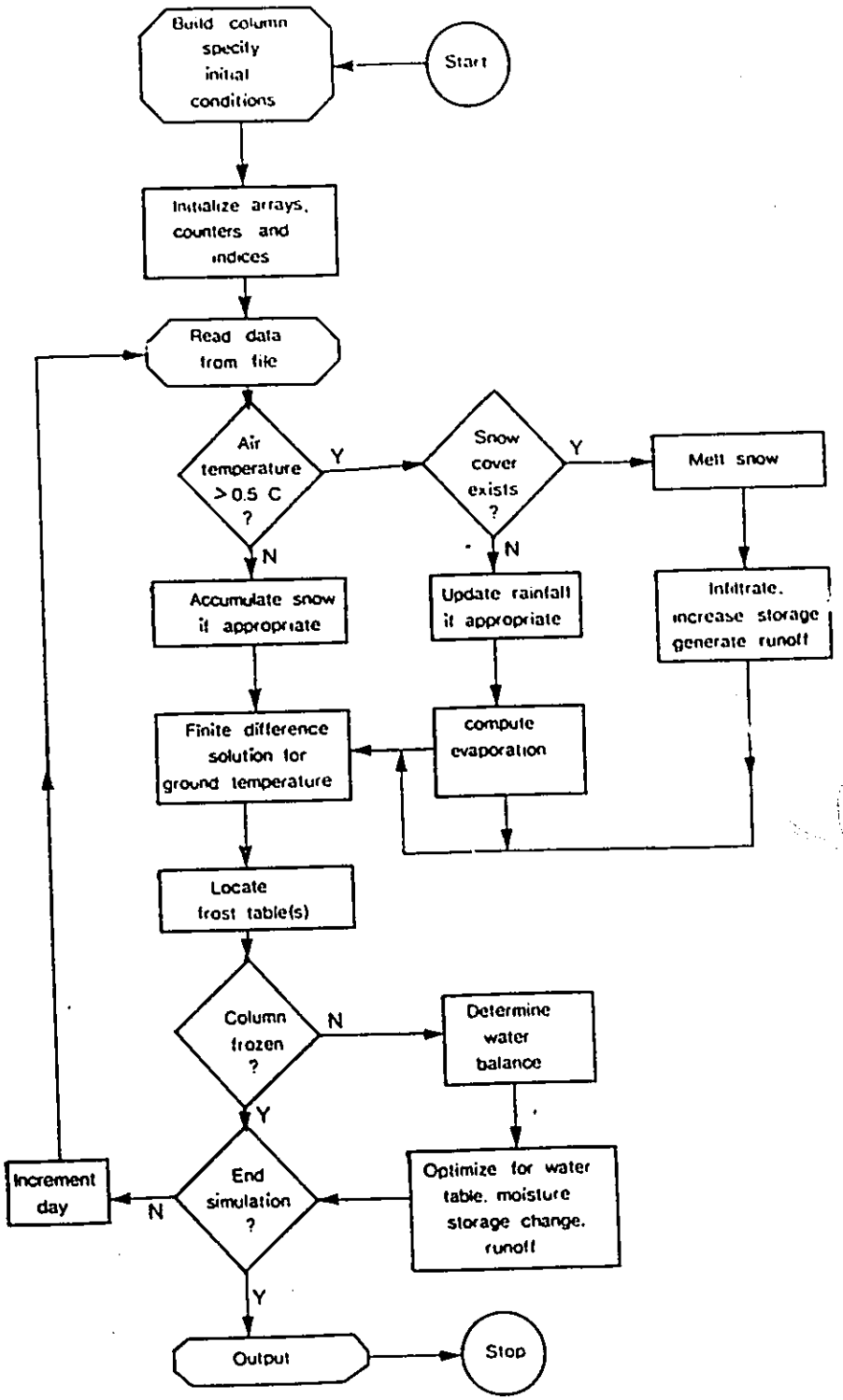

Figure 3.2 Flow-chart of Woo and Drake Model

interactively at the computer terminal. The requisite initial conditions are also set. The model reads from a pre-processed file the daily data for air temperature (^{0}C), precipitation (mm) and solar radiation (MJ m^{-2}) from a base station, and the optional data for inflow to the column (m d^{-1}). On a daily basis, the snow on the ground is updated and its accumulation is calculated during a cold period. In the melt season, snowmelt is computed and so is the basal-ice melt, if appropriate.

On a daily basis, ground temperatures are computed from a finite difference solution, and this allows the frost table to be determined. Evaporation, water storage and runoff are obtained. These results allow the daily water balance to be performed and the water table position as well as the soil moisture profile are updated. Lateral runoff depends on the amount of surface flow generated and the elevation of the water table relative to the ground surface. Such information, together with the magnitude of all the major hydrological processes, the location of the frost and water tables in the column, and the amount of snow and ice, will be reported for every simulation day. At the end of a simulation year, summary statistics pertaining to the water balance and storage change are also produced.

3.2 Model Description

The Woo and Drake model encompasses several major components which are described in detail, as submodels, in the following sections.

3.2.1 Snow Accumulation and Melt Submodel

3.2.1.1 Snow Accumulation

Snow accumulation is a major component in the winter season in a continuous permafrost environment. In the open treeless areas of high Arctic, snow drifting gives rise to an extremely uneven distribution of snow, depending on the type of terrain (Woo et al. 1984). An indexing approach can be used to relate the snow cover water equivalent of various terrains $P_{s(i)}$ to the snowfall recorded at the nearby base station (P).

$$P_{s(i)} = INDEX(i) * P \qquad (3.1)$$

where i denotes terrain i. The indices can be obtained by comparing the station snowfall with the results of field surveys of snow on the ground. Snow density also varies according to terrain type, and the mean densities can be determined from field surveys. Using snow density $\rho_{s(i)}$ and water equivalent $P_{s(i)}$, snow depth on the ground (GSNOW) can be

obtained as

$$GSNOW(i) = \frac{P_{s(i)}}{\rho_{s(i)}} \qquad (3.2)$$

GSNOW is expected to decrease as the φ_s increases during the snow ripening period. In the Arctic, however, the snow is often highly compacted by drifting before the melt events, and the change in φ_s during the ripening period is less significant compared with the temperate latitudes.

3.2.1.2 Snow Melt Processes

3.2.1.2.1 Snow Melt Computation

Mean daily air temperature is used to distinguish between snowfall and rainfall, with 0.5 ^{0}C as the appropriate demarcation point. Freshly fallen snow is considered to be 'dry' snow which is not yet ripe for melting. Snowmelt takes place when the energy available for melt (Q_M) becomes positive:

$$Q_M = Q^* + Q_H + Q_E + Q_P + Q_G \qquad (3.3)$$

where Q^* is net radiation, Q_H and Q_E are sensible and latent heat fluxes, Q_P is energy added by rainfall, Q_G is ground heat flux which is negative for the permafrost area during the

melt season because the ground is often colder than the snow. Q_K can be determined if all the terms on the right hand side are known (e.g. Price and Dunne 1976). In the present model, a limited amount of meteorological information is assumed to be available, and various energy components have to be estimated. Radiation melt Q^* can be estimated from short-wave radiation (K↓):

$$Q^* = a_0 + a_1 K\downarrow \tag{3.4}$$

where a_0 and a_1 are empirical coefficients (Davies 1967). Rain-on-snow melt can be calculated as

$$Q_P = \rho_w C_w P_r (T_A - M_P) \tag{3.5}$$

where ρ_w is water density, C_w is heat capacity of water, P_s is rainfall at temperature T_h and M_p is the melting point of snow ($\approx 0\ ^0C$). Wind data, which is necessary to calculate Q_H and Q_E, are generally not available for the remote region, nor are the data easily transferrable from site to site. The magnitude of these fluxes are combined ($Q_T = Q_H + Q_E$) and field measurements allow the turbulent fluxes to be estimated as

$$Q_T = \rho_s \lambda M - Q^* - Q_P \tag{3.6}$$

where M is measured daily melt, converted into energy units using snow density ρ_s and the latent heat of fusion λ. The values of Q_T thus obtained were related to air temperature so that empirical coefficients c_0 and c_1 were derived

$$Q_T = c_0 + c_1 T_A \qquad (3.6a)$$

This approach of using several equations to estimate the various components of the energy balance has advantages over a strictly empirical degree-day method for melt calculation. Not only is the physical structure preserved, but each component is considered to operate independently and additively.

3.2.1.2.2 Melting Front Advance

As meltwater propagates downward through the cold, dry snow, the zone behind the meltwater front (MF) will be ripen (i.e. becomes saturated at a temperature of 0 ^{0}C). Melting front advance (ΔMF) is calculated as (Colbeck 1976).

$$\Delta MF = \frac{M}{\phi_s \theta + TSNOW \frac{C_{ice}(1 - \phi_s)}{\rho_w \lambda}} \qquad (3.7)$$

where $\theta \approx 0.07$ is the irreducible water saturation, C_{ice} is the heat capacity of ice ($1.9 * 106$ Jm^{-3} K^{-1} at 0 ^{0}C), TSNOW is the below-freezing snow temperature, and ϕ_s is the snow porosity, related to snow and ice density by

$$\phi_s = 1 - \frac{\rho_s}{\rho_i} \tag{3.8}$$

with ρ_i = 910 kg m^{-3}. The position of the melting front on day t is (Fig. 3.3):

$$MF_{(t)} = MF_{(t-1)} + \Delta MF \tag{3.9}$$

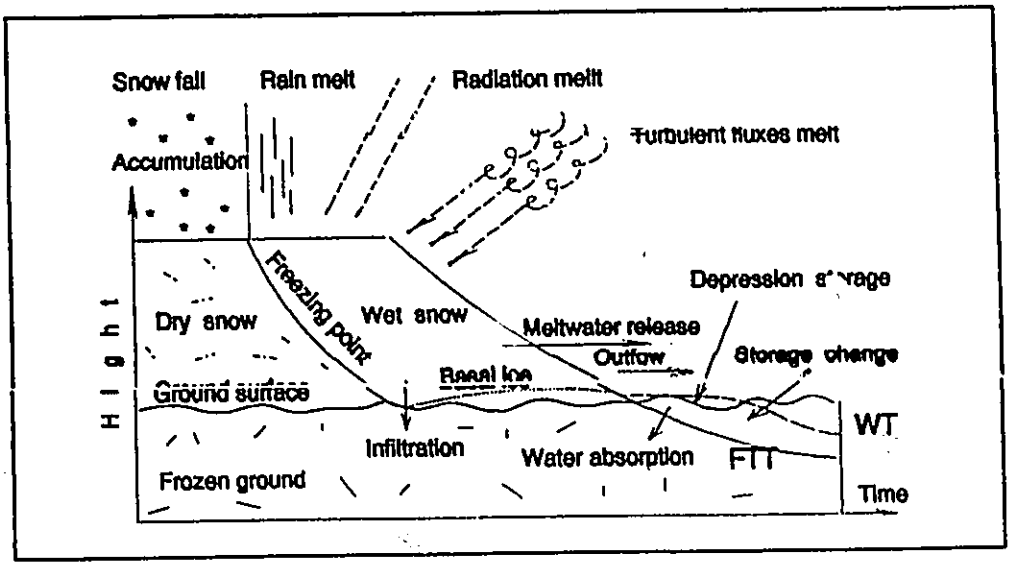

Figure 3.3 Snow Accumulation and Melt Processes

Several other processes, including thawing front development, meltwater movement into the snow and the frozen ground, basal ice formation, meltwater release, storage change and outflow, are also shown in Fig. (3.3)

3.2.1.2.3 Basal Ice Formation

When the melting front reaches the bottom of the snow cover (MF ≥ GSNOW), meltwater is able to infiltrate the frozen soil (Granger et al. 1984, Kane and Stein 1983). In the model, infiltration is assumed until the ground is saturated. Then, additional meltwater supply will refreeze at the base of the snow cover because the substrate remains intensely cold. Basal ice is formed instead of meltwater release. Field measurements showed that the maximum basal ice thickness ($BICE_p$) is strongly affected the total depth of snow accumulated prior to the commencement of melt (GSNOW before the melt event).

$$BICE_P = \sqrt{g_0 + g_1\ GSNOW} \qquad (3.10)$$

where g_0 and g_1 are empirical coefficients. Basal ice growth ceases only when the total ice thickness has reached the potential limit (i.e. BICE > $BICE_p$, where

$$BICE = \frac{\rho_w}{\rho_i} \sum_{i=1}^{c} M_i \qquad (3.10a)$$

with M_i being the snow-melt amount for day i (Heron 1985).

The effect of meltwater front advance and basal ice growth in the cold snow cover is to retard the loss of mass and to delay meltwater release from the snow. The water released will first satisfy the depression storage, and when the depression storage capacity (DSMAX) is exceeded, outflow is generated. The snowmelt submodel remains active until the snow on the ground is completely gone.

3.2.2 Ground Temperature and Frost Table Submodel

Ground temperature changes as heat is conducted or convected through the soil. In the Arctic, heat convected by ground water flow is not significant compared with conduction (McMillan 1983). Although latent heat transfer through refreezing of meltwater infiltrated into frozen soil may be important (Woo and Heron 1981), this effect is noticeable only when infiltration occurs in the snowmelt season. Therefore, only heat conduction is considered in the model.

3.2.2.1 Heat Conduction and Finite Difference Approach

To solve the heat conduction problem in a continuous permafrost environment, the model breaks up the soil profile into 100 slabs to evaluate the temperature at each slab by the finite difference approach noted previously. The frost table is represented by the depth of thawing front. When an ice cover, a snow cover or a shallow water layer is present, the total number of slabs will be adjusted accordingly.

The one-dimensional heat conduction equation is

$$c\frac{\partial T}{\partial t} = -\frac{\partial}{\partial z}\left(k\frac{\partial T}{\partial z}\right) \qquad (3.11)$$

where c is the heat capacity of the soil and k is its thermal conductivity. T is temperature which changes with time (t) and depth (z). The temperature at any particular depth i and for time j can be obtained if the initial and boundary conditions and the thermal properties, C and k, are functions of soil type, soil structure and soil moisture conditions, which can be calculated at each time step. In the model, a finite difference scheme was used to solve for the T's.The equivalent finite difference form for equation (3.11) is

$$c\,\Delta z\,\frac{(T_i^{j+1} - T_i^j)}{\Delta t} = \left\{ \begin{array}{l} \dfrac{k_I(T_{i-1}^{j+1} - T_i^{j+1}) + k_{II}(T_{i+1}^{j+1} - T_i^{j+1})}{\Delta z} + \\ \dfrac{k_I(T_{i-1}^{j} - T_i^{j}) + k_{II}(T_{i+1}^{j} - T_i^{j})}{\Delta z} \end{array} \right. \qquad (3.11a)$$

Equation (3.11a) is solved using the Thomas algorithm described in Wang and Anderson (1982).

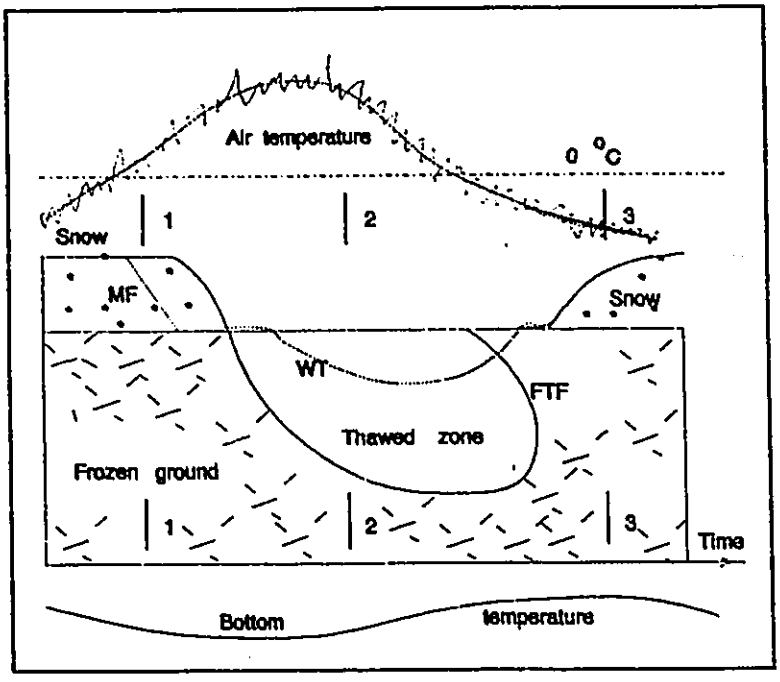

Figure 3.4 Boundary Conditions for the Ground Temperature Submodel

3.2.2.2 Boundary Conditions

In the model, the boundary conditions are the daily temperatures at the surface and the bottom of the column. Figure (3.4) shows the boundary conditions and the development of the thawed zone. In this chart, the numbers 1 - 3 showed the positions of different vertical profiles, along with time development, in Figure (3.5).

3.2.2.2.1 Bottom Temperature

Bottom temperature or temperature at the lowest slab of the column assumes an annual sinusoidal wave.

$$T_{b(t)} = T_b + A_b \cos\left[2\pi \frac{(t + SHIFT)}{365}\right] \qquad (3.12)$$

where $T_{b(t)}$ is bottom temperature on day t, T_b and A_b are the annual mean and annual amplitude of the temperature at the bottom slab and SHIFT is the Julian date when bottom temperature reaches the mean.

3.2.2.2.2 Surface Temperature

One method to obtain surface temperature is to

equilibrate it against the surface energy balance. This approach was used in the Outcalt model to simulate snow and soil thermal regimes (Outcalt et al. 1975). The inadequacy of meteorological data for most permafrost areas prevents the adoption of this method. Instead, the surface temperature is estimated from the air or snow temperatures (Woo et at. 1988) using empirical relationships derived from the field experiments, (Fig. 3.5):

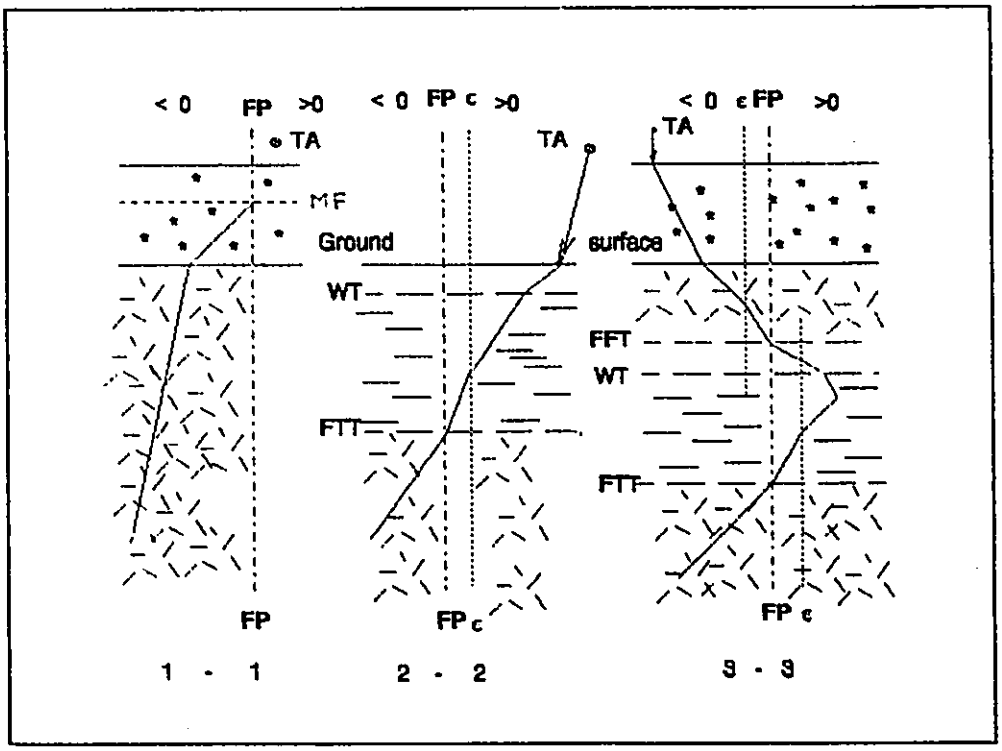

Figure 3.5 Hypothetical Temperature Profiles During Spring, Mid-summer and early fall

Figure (3.5) shows the hypothetical temperature profiles during late winter, mid-summer and early fall. In this diagram, MF is meltwater front, TA and TS are air and column surface temperatures, WT is water table, FTF and FTT are freezing and thawing fronts, FP is freezing point temperature, and ε is a temperature range around the freezing point within which temperature changes are retarded by the dissipation of latent heat of fusion to melt the ground ice.

The estimated air and column surface temperatures in the model are

$T_s = T_A$, if there is dry snow and s is the snow surface,

$T_s = 0\ ^0C$, if there is a melting front in the snow, and s is at the front.

$T_s = b * T_A$, if there is water on the surface, and s is the ground surface,

$T_s = a + b * T_A$, if the surface is not saturated, and s is the ground surface.

3.2.2.3 Initial Temperature Profile

The model uses daily air temperature, the estimated bottom temperature and the temperature profile of the past

period to compute the temperature profile for the next day.

The initial temperature profile is seldom available and the model simply assumes an exponential temperature profile between the bottom and surface temperatures of the first day.

$$T_{(z)} = T_s \exp(-\beta z) \tag{3.13}$$

where T_s is the surface temperature of the modeled soil column. z is the depth of the column vertical profile, and β is estimated from the surface and bottom temperatures:

$$\beta = \frac{\ln T_s - \ln T_b}{z_b} \tag{3.14}$$

with z_b being the total column depth. The effect of this artificial initial condition becomes unnoticeable after several months of simulation. It is therefore advisable to start the simulation in the middle of winter when there are no significant hydrological activities so that the erroneous temperatures due to the unrealistic initial profile will not seriously affect the performance of the hydrological submodels.

3.2.2.4 Thermal Conductivity and Heat Capacity

The thermal properties are calculated using the thermal conductivity and heat capacity of individual soil components of organic, mineral, air water or ice (Farouki 1981, Williams 1982):

$$k = \prod_{i}^{n} k_i^{f_i} \qquad (3.15)$$

and

$$c = \sum_{i=1}^{n} c_i f_i \qquad (3.16)$$

where f is the fractional volumetric content of each component i. The values of k and c varies in each slab of the soil column, depending upon the changing status of soil moisture (or water content), and freeze and thaw (or water and ice content).

It is also noted that a certain fraction of the soil is always occupied by air so that the saturated water content is the effective porosity,

$$\phi_e = \phi - f_a = S_y + S_r \tag{3.17}$$

where ϕ is soil porosity, f_a is the air content that cannot be displaced by water or by ice, and s_y and s_r are the specific yield and specific retention of the soil. The model also recognizes the possibility that f_a for frozen soil may be different from f_a for thawed soil.

4.2.2.5 Apparent Thermal Capacity

The freezing and thawing of the soil involves a phase change, which is ice formed or melted. This results in a latent heat gain or loss which causes the freezing-point isotherm to linger at a particular depth for a longer duration than if the change of state is absent (Woo and Drake, 1988). To model this zero curtain effect (Muller 1945), an apparent thermal capacity term is introduced.

$$C_{app} = C + \rho_i \lambda \frac{f_{ice}}{\varepsilon} \tag{3.18}$$

where ε is an arbitrary temperature range, above or below

the freezing point (FP), within which the temperature wave propagation is retarded by the phase change. The soil slab which contains the freezing point isotherm is considered to have a heat capacity of C_{app} instead of c and the effect of this term is diagrammatically represented in Figure (3.5). Although this routine is an approximation of the freeze-thaw process, it preserves reasonable accuracy while eliminating the need for an iterative solution that is often required by the usual methods.

3.2.2.6 Frost Table and Active Layer

This model assumes that all the soil water freezes once the freezing front has moved through a slab. This is a simplification of reality because it is well known that there is unfrozen water in soils with temperatures several degrees below 0 ^{0}C (e.g. Ad Hoc Study Group on Ice Segregation and Frost Heaving 1984), and this phenomenon was considered by the Nakano and Brown (1972) model of the thermal regimes in tundra soils. However, given the approximate nature of Equation (3.13 - 3.18) and an expected field measurement error of 0.02 m, the simplified approach is acceptable to the model.

The freezing or thawing front is located at the slab whose temperature has crossed the freezing point. The depth

of the front is obtained by linearly interpolating with respect to the mean temperatures of the slabs close to the front to locate the position of the freezing point. The thawing front represents the frost table and its maximum depth defines the thickness of the active layer. When the descending freezing front coalesces with the rising thawing front in the fall or winter, the entire column is frozen and an index is set to signal the termination of most hydrological computations described in the water balance, soil moisture and water table submodel.

3.2.3 Evaporation Submodel

Evaporation is computed when the ground is snow-free and when the net coming energy Q^* is greater than ground heat flux.

3.2.3.1 Priestley and Taylor model

The Priestley and Taylor (1972) model has been found to be highly suitable for the computation of daily evaporation for the continuous permafrost environment (Marsh et al. 1981, Roulet and Woo 1986, Rouse et al. 1977). Evaporation (E) is computed using radiation energy, air temperature and an empirical function α which varies with

surface conditions:

$$E = \alpha\sigma \frac{Q^* - Q_G}{\rho\lambda(\sigma + \gamma)} \qquad (3.19)$$

where Q^* is net radiation, Q_G is ground heat flux, σ is the slope of vapor-pressure-temperature curve, γ is the psychrometric constant, and $\rho\lambda$ is used to convert the energy into water equivalent units.

3.2.3.2 Ground Heat Flux

For the model, Q^* can be estimated from short wave radiation but with the two coefficients in Eq. 3.4 determined empirically for different surface types. The ground heat flux can be obtained from the heat flow equation

$$Q_G = k_s \frac{\partial T}{\partial z} \qquad (3.20)$$

Using the temperature of the soil slabs near the surface, we could have

$$Q_G = k_s \frac{T_s - T_{s-1}}{DZ} \qquad (3.20a)$$

where s denotes the surface slab, and DZ is the slab thickness. The value of $\sigma/(\sigma + \gamma)$ is a slowly changing function of temperature, and σ can be approximated without much error using the air temperature and a functional relationship given by Dilley (1968).

For the ponded areas, the ground heat flux can be obtained as the water temperature change over a time period DT (Roulet and Woo 1986). Q_G is obtained then as

$$Q_G = \rho C_w \frac{Z_w(T_w - T_{w1})}{DT} \qquad (3.21)$$

where Z_w is depth of the water, T_w and T_{w1} are the water temperatures for the time steps t and t-1.

3.2.3.3 Empirical Coefficient α

The value of α has been subject to much discussion (Drake 1979). It was found that $\alpha \approx 1.3$ for water surfaces, and it is quite correct to assume that $\alpha = 0$ for bedrock because the latter undergoes little evaporation. Rouse et al. (1977) found that for subarctic lichen heath, $\alpha \approx 1$ when the surface is no longer saturated. This condition of $\alpha = 1$, known as equilibrium evaporation, is considered in the model to be applicable also to fine sand and clay.

For gravel soil in the Arctic, Marsh et al. (1981) obtained the empirical relationship with surface soil moisture (SM_s)

$$\alpha = \frac{1.3}{\exp(b_0 + b_1 SM_s + 1)} \qquad (3.22)$$

where b_0 and b_1 are coefficients, and SM_s can be obtained from the soil moisture submodel.

3.2.4 Soil Moisture, Water Table and Runoff Submodel

Soil moisture is updated daily during the thaw season, and so is the water table which represents the upper limit of soil saturation. Saturation occurs when the soil moisture equals the effective porosity $\phi_e = \phi - f_a$, with ϕ being the soil porosity, and f_a is the fraction of air that, for simplicity, is assumed to be sealed against water or ice intrusion. The value of ϕ_e (frozen) need not be the same as ϕ_e (thaw) for the same soil material (Woo and Drake 1987).

3.2.4.1 Water Balance

The submodel first calculates the surface water balance as the sum of melt, rainfall, inflow and the residual

surface depression storage, minus the evaporation loss. Water may also be expelled from the pores of a slab that is saturated or is near-saturation; or absorbed by the slab as it thaws. The reason for this is that the fractional volume of 'hydrologically inactive' voids, f_a may be different for thawed and for frozen soils. in this model, it is assumed that f_a in thawed soils is not larger than f_a in frozen soils. The amount of water that is expelled (XPEL) or absorbed (TAKEUP) is calculated as

$$\begin{cases} XPEL = [SM - \phi_{\theta(frozen)}/1.1]\,DH, & XPEL > 0 \\ TAKEUP = [\phi_{\theta(frozen)}/1.1 - SM]\,DH, & TAKEUP < 0 \end{cases} \tag{3.23}$$

where DH is the zone which has undergone change in state as a result of a rising freezing front or descending thawing front (both of which allow water to be absorbed by the soil), or a rising thawing front or descending freezing front (both of which lead to water expulsion). Such processes as soil water migration towards the frozen zone, are not represented in the model.

3.2.4.2 Apparent Water Balance

In this model, the surface water balance and the

amount of water expelled or absorbed as the soil freezes or thaws are summed to yield an apparent water balance (APPWB). The apparent water balance can be positive or negative and this amount is used to determine the daily change in the soil moisture content of the column. APPWB < 0 leads to a fall in the water table and a reduction in soil moisture in the non-saturated zone, and the reverse happens when APPWB > 0. Figure (3.6) shows the various change of water table and frost table positions.

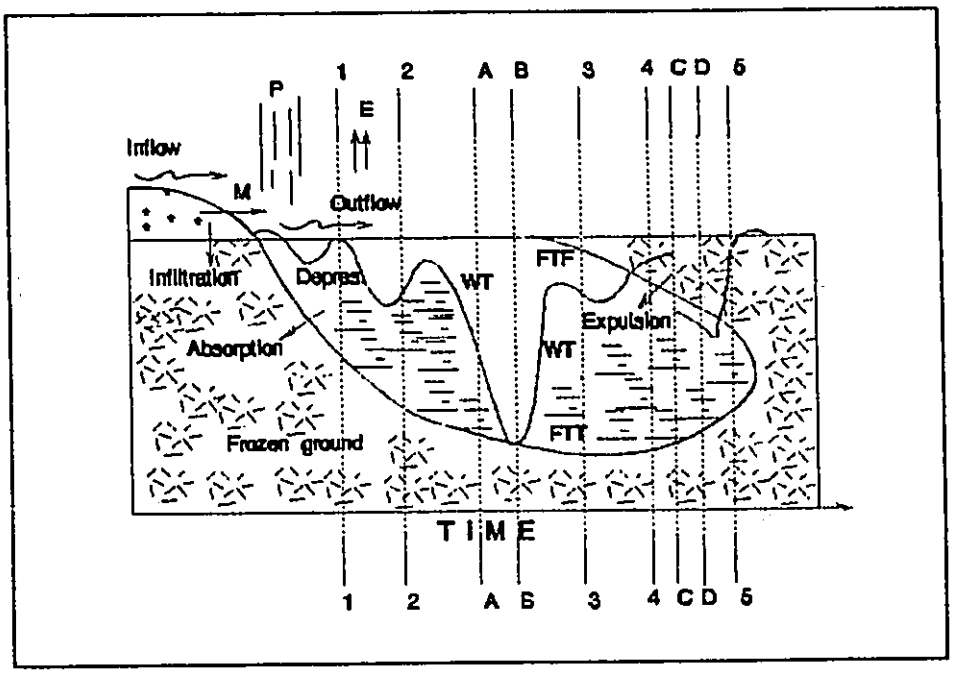

Figure 3.6 The Seasonal Water Table and Frost Table Development Patterns. The lines 1, 2, 3, 4, 5, A, B, C and D are the positions of vertical moisture profiles in Fig. 3.7

Diagrammatic representation of the surface water balance (WB), and the apparent water balance (APPWB) are shown in Figure (3.6). The surface water balance and apparent water balance could be computed as

$$\begin{cases} WB = P + M + INFLOW + DEPRES - INFILTRATION - E - OUTFLOW \\ APPWB = WB + EXPULSION - ABSORPTION \end{cases}$$

3.2.4.3 Soil Moisture Profile

The basic form of the soil moisture profile is that (1) the soil moisture below the water table reaches the effective porosity, which may have different values for the thawed and frozen conditions; (2) soil moisture decreases linearly with distance above the water table:

$$S_M(z) = g(W_T - z) \qquad (3.24)$$

where W_T is the depth at which the water table is located, $S_M(z)$ is soil moisture at depth z, and g is an empirically determined value for a particular soil; (3) the soil moisture normally decreases to some minimum value > 0.0, but can fall to 0.0 when the water table drops to the position of the

thawing frost; (4) in the frozen surface zone, the frozen moisture content does not change unless the water table rises into this zone. Then, the rising water table can fill up the available voids until the effective porosity of frozen soil is attained. The various possibilities of soil moisture and water table position changes, given a change in the APPWB, are shown in Figure (3.7)

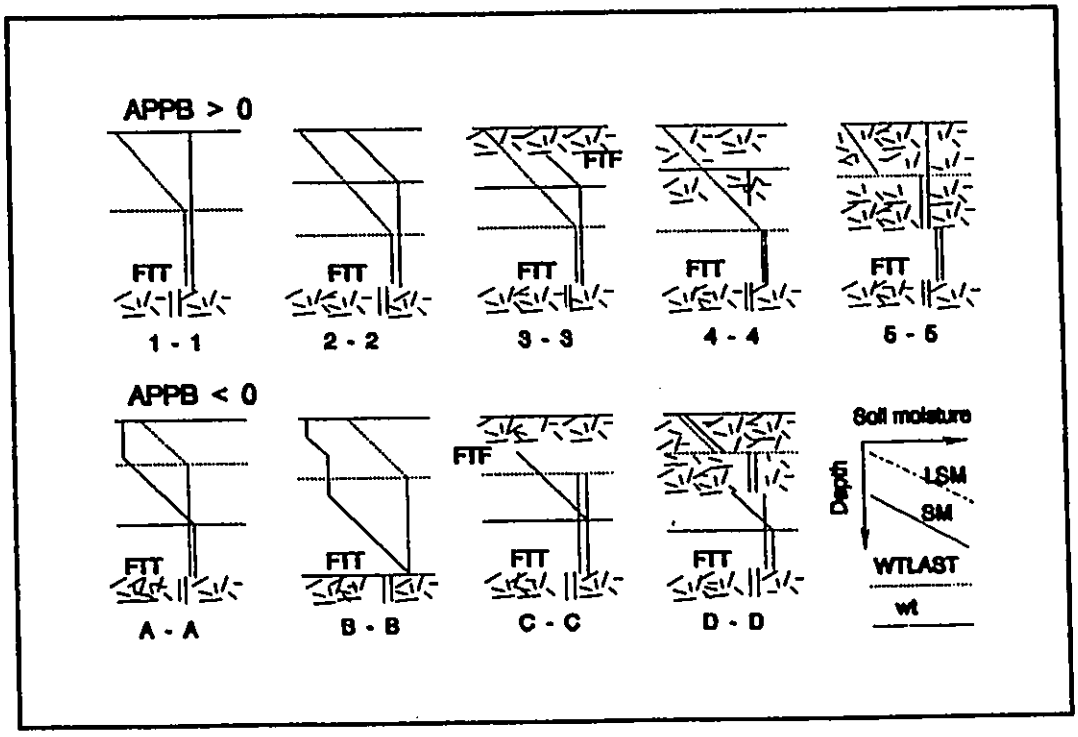

Figure 3.7 Various Cases of Vertical Soil Moisture Profile Changes. The profiles are located at different times of the year as shown in Fig.3.6

We may find that the vertical soil moisture profile changes with the apparent water balance changes and as the freezing (FTF) and thawing fronts (FTT) migrate. In the diagram, SM and WT are the soil moisture profile and water table of the present period; LSM and WTLAST are the soil moisture profile and water table of the previous day.

3.2.4.4 Storage Change and Outflow

Subject to the conditions mentioned above, the new soil moisture profile is obtained by optimization such that the difference between the new profile (SM) and the profile of the previous day (LSM) will satisfy the apparent water balance excess or deficit; i.e.

$$\int_z [S_M(z) - LS_M(z)]\,dz + EXCESS = APPWB$$
$$EXCESS = 0 \qquad when \qquad W_T \geq 0 \tag{3.25}$$

where Z is the column thickness, EXCESS is the amount of water available for depression storage and outflow when the entire column is saturated (i.e. Water table rises above the surface for $W_t \leq 0$. The situation when EXCESS > 0 often arises in spring when a large supply of meltwater cannot be

accommodated by a shallow thawed zone; in summer and autumn during heavy rainstorms particularly if the soil is already at a high moisture level; in winter when freezing expels water that escapes to the surface to form icings or frost blisters (Pollard and French 1983, van Everdingen 1982). This model does not consider frost heave but assumes that the expelled water can go above the ground.

Water rising above the ground will first be held as depression storage. Outflow occurs when the depression storage capacity is exceeded.

3.3 Input and Output of WAD Model

3.3.1 Input

Two types of input information are required: the data file and the interactive input with which the soil column is built and the parameter are initialized.

3.3.1.1 Description of Data File

There are five columns in the data file. From left to right, the columns are: julian day, total daily precipitation (m water equivalent), global solar radiation (MJ m^{-2}), mean daily air temperature (^0C) and surface inflow (m d^{-2}). The format of the data file is user-specified in the interactive

input described in Section 3.3.1.2.

Several points about the input data file should be noted:

(1) There is no allowance in the program for missing input data.

(2) The simulation must be started in mid-winter so that the temperature profile can stabilize before the season of active layer than begins (see Section 3.2.2.3). Also, the soil column is initialized as 'frozen' (SOLID = 1) and, therefore, the simulation must be started when this condition would be physically true.

(3) If the simulation is conducted on two or more sequential years, each year of input data have to be separated by the appropriate end-of-year marker. The computer program of the WAD model recognizes the value, 8888., in any one or all of the four meteorological data input columns, as the end-of-year marker. On encountering this marker, the program summarizes the yearly totals of several hydrological variables and re-initialises others automatically.

3.3.1.2 Interactive Input

The program of the WAD model has been written for

microcomputers. The data should be stored in the computer before the simulation run is performed. When the model is run, information will be requested by the program on the interactive interface. The user will be prompted by a question mark for all the answers required.

3.3.2 Output

The output of WAD model has been formatted as a table. The first page of the simulation output is a listing of the user-input information as well as the values assigned to various hydrological properties. Then, it is followed by eight pages of daily output, plus one page of year-end hydrological statistics.

The outputs are divided into five categories: (1) physical data, (2) hydrology of the soil column, (3) surface flows, (4) water balances, and (5) characteristics of the surface of the soil column. Included in the first category are the julian day (JD), the year number of the simulation (YR), precipitation in m water equivalent (PREC) and air temperature in ^{0}C (TA), depth (m) of snow on ground (GS) and the difference between net radiation and ground heat flux in MJ m^{-2} (Q^{*} - QG).

The hydrology of the soil column, the second category, is described by evaporation (EV) and snowmelt (ACTM) rates

(m d^{-1}), and the depths (m) of the water table (WT) and freezing (FTF and thawing (FTT) frost tables. The position of the water table is listed along with the soil type (SOIL) and volumetric soil moisture (SM) of the slab in which the water table is located. When the water table is above the ground surface, water is retained in depression storage (DS) which is expressed as a depth of water in m.

ACTM (actual melt) differs from MELT (the contribution of snowmelt to the surface water balance) by the amount of snow meltwater which infiltrates the frozen soil on a daily basis.

The third category, surface flows, consists of surface inflow (IN) and outflow (OUT), both of which are in m d^{-1}.

There are two water balances listed under the fourth category. The surface water balance (SURFACE) is the sum of all surface hydrological inputs and outputs. The net water balance (NET) is the sum of the surface water balance plus any water losses or gains resulting from the movement of the freezing and/or thawing fronts.

The fifth category comprises the final two columns of the daily output table which characterize the soil column (or snow) surface. Listed are the volumetric soil moisture of the uppermost slab in the soil column (SM), and the temperature (TS) of the uppermost slab in the snowpack (if GS > 0) or the uppermost slab in the soil column (if GS = 0).

The yearly output consists of a summary of the hydrological events of that year. Yearly totals (m) of precipitation, rainfall, snowfall (water equivalent), evaporation, melt, surface inflow and outflow are included. The total number of data records processed is also shown.

3.4 Model Testing

3.4.1 Parameters and Variables

Field work was carried out near Resolute in 1988 and 1989 to determine parameters and variables to be used in the WAD model.

3.4.1.1 Premelt Snow Parameters

Premelt snow parameters which may affect the model performance include: premelt snow depth and snow density, which are functions of total precipitation in winter and snow cover properties. To examine the spatial variability of these properties within each study site near Resolute, a snow survey was carried out in early June of 1988 and 1989. Snow pits were dug in which detailed stratigraphic measurements were made. The 1988 survey comprised 12 pits and a total of 68 depths measured along two transects. In 1989, a similar scheme was employed, using 9 pits and 46 depths measured

along two profile lines.

One face of each pit was cleaned off with a wire brush or a scraper to highlight individual strata. These strata were usually well defined in terms of snow hardness and were easy to recognize. Within each layer the following measurements were made:

(1) Layer thickness, with a folding carpenter's rule,

(2) Snow density, with snow cutters ranging in size from 50 to 250 cm^3. Samples were weighed in the field on a Geotest temperature compensated snow density scale housed in a case with a plexiglass door to protect it from the wind. Generally, two samples were obtained from each layer, but a few pits were sampled in greater detail to determine the variability within layers.

The measured snow density in weighted mean value and the mean depth in each simulation site are given in Table 3.1. The snow density and water equivalents at these two adjacent sites were not significantly different.

Table 3.1 Snow Density and Depths

Model Site	Snow Density kg/m^2	Snow Depth in m	Snow Depth Water Equv. (m)
Gravelly	325	0.34	0.11
Peaty	324	0.40	0.13

3.4.1.2 Coefficients for Calculating Net Radiation

Net radiation Q^* may be estimated from short-wave radiation K↓ using an empirical relationship:

$$Q^* = a_0 + a_1 K\downarrow \qquad (3.4)$$

here a_0 and a_1 are empirical estimated coefficients.

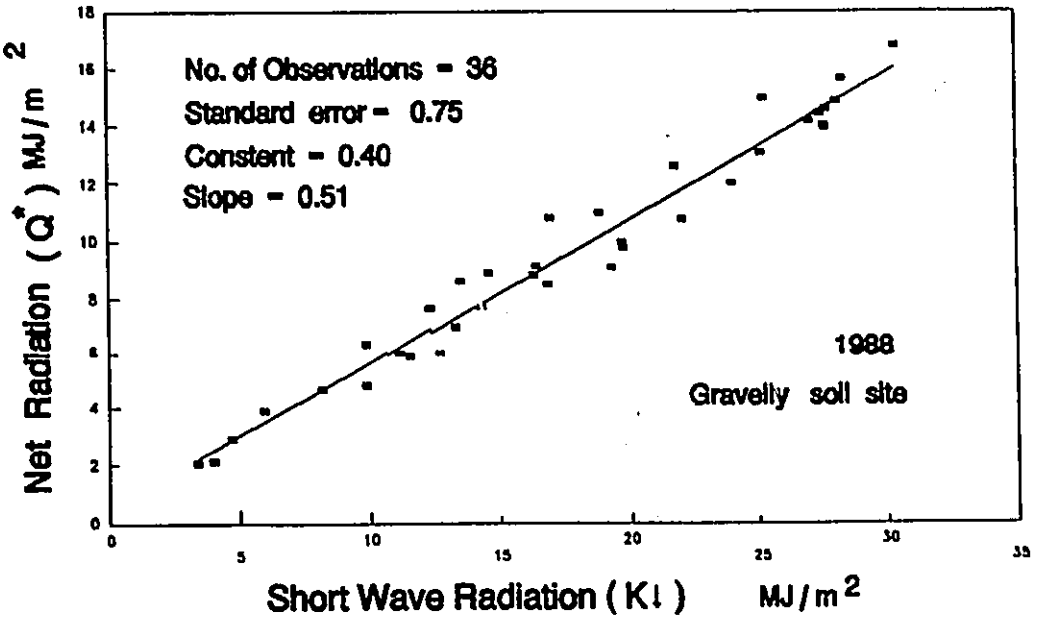

Figure 3.8 The Regression of Q^* to K↓ at Gravelly Soil Site, in The Year 1988

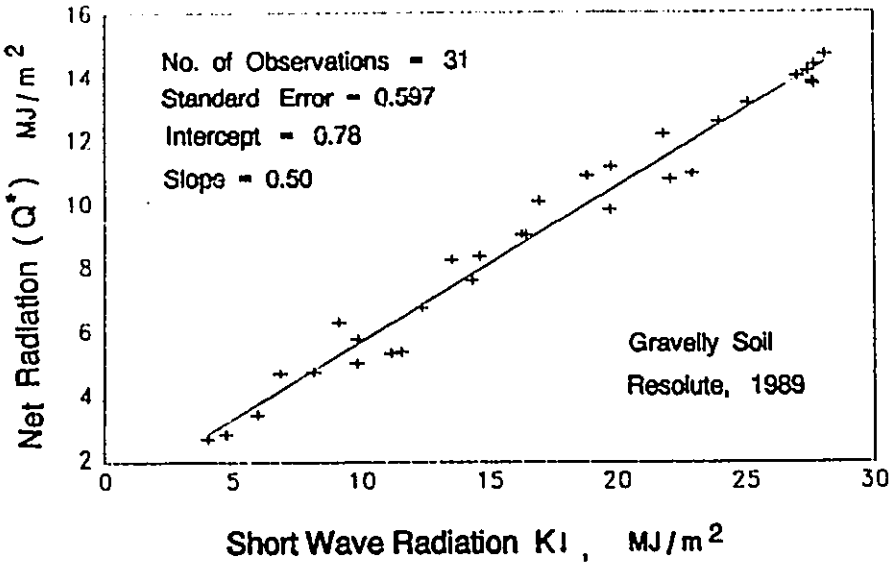

Figure 3.9 The Regression of Q^* to $K\downarrow$ at Gravelly Soil Site in 1989

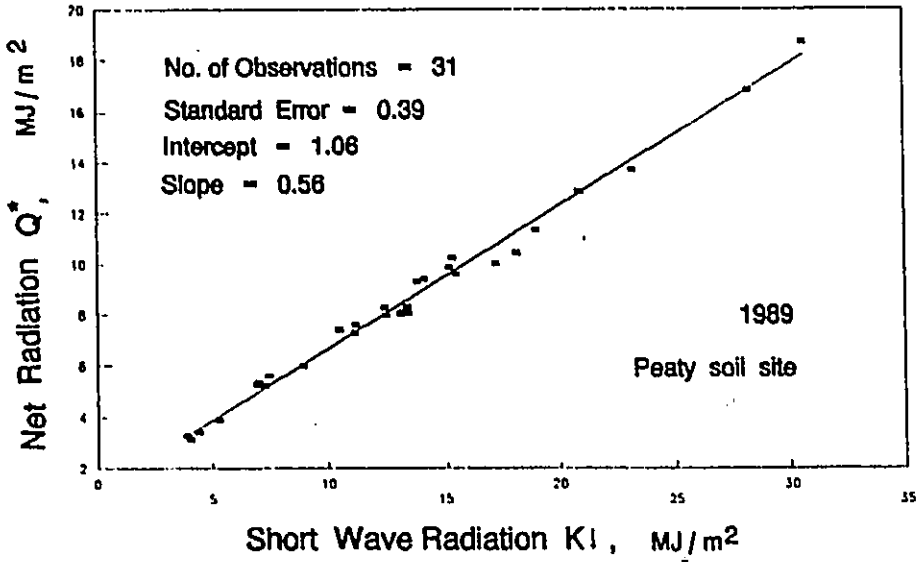

Figure 3.10 The Regression of Q^* to $K\downarrow$ at Peaty Soil Site in 1989

To estimate a_0 and a_1, net radiation and incident short-wave radiation were measured in the field seasons 1988 and 1989. Net radiation was measured with Swissteco net radiometers over the two typical surface types, and short wave radiation was measured with an Eppley pyranometer.

The regression results show different relationships between net radiation and short wave radiation (Figure 3.8, 3.9 and 3.10), for the gravelly soil site and the peaty soil site. The reason is that at the peaty soil site, the surface always ponds more water than in gravelly site, so this may decrease surface albedo value and increase net radiation. The results of the regression for gravelly soil site in 1988 and 1989 are similar and these data are pooled to give a single equetion (Table 3.2):

Table 3.2 Parameters for the Empirical Equation 3.4

Model Site	a_0	a_1
Gravelly	0.59	0.51
Peaty	1.06	0.56

3.4.1.3 Coefficients for Estimating Turbulent Fluxes

Turbulent heat flux Q_T is the combination of the sensible heat and latent heat fluxes ($Q_T = Q_H + Q_L$). This can be obtained from the energy balance relationship

$$Q_T = \rho_s \lambda M - Q^* - Q_P \qquad (3.6)$$

where Q_P is the energy added by rainfall, ρ_s is snow density λ is latent heat of fusion and M is measured daily snowmelt. The magnitude of Q_T may be related to air temperature through the following empirical equation (3.6a):

$$Q_T = c_0 + c_1 T_A \qquad (3.6a)$$

To estimate c_0 and c_1, Q_T was obtained from Eq. 3.6 and regreesed against T_A. The regression results are shown in figure (3.11). The parameters used for equation (3.6a) are $c_0 = 0.04$ and $c_1 = 0.006$.

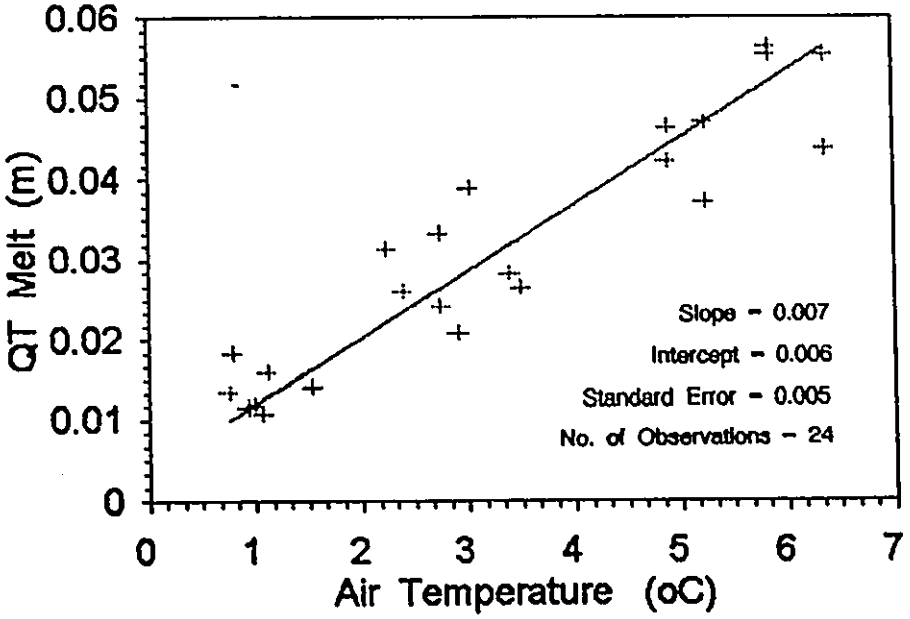

Figure 3.11 Regression of Snow Melt with Turbulent Heat Flux to Air Temperature

3.4.1.4 Parameters for Soil Moisture Estimation

In the thawing period, soil moisture is considered as a function of the distance below or above the water table. Below the water table, soil moisture may reach its maximum value which is less than or equal to the effective soil moisture, but it may also be considered to be close to zero below the frost table. Above the water table, soil moisture is assumed to decrease linearly until it reaches its minimum

value which is equal to its specific retention. The rate of the soil moisture decrease can be described with the equation (3.24)

$$S_M(z) = g_o + g_1(W_T - z) \qquad (3.24)$$

Parameters g_0 and g_1 vary with soil type and soil structure. For the particular soil in the model testing site, g was estimated empirically by Figure (3.12) and (3.13).

The rate of soil moisture decrease is smallest in

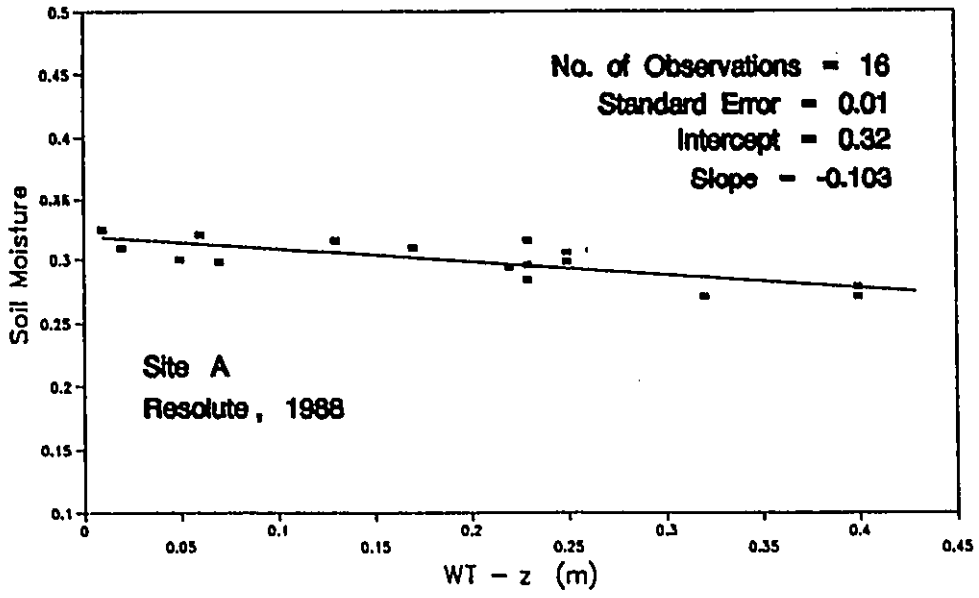

Figure 3.12 The Regression of Soil Moisture to Water Table in Gravelly Soil Site

clay and fine sandy soil, larger in peaty soil, and is the largest in gravels. Site A, one of the model testing sites, is characterized by lot of fines and organic material at the surface, and the moisture decreasing rate is less than in peaty soil.

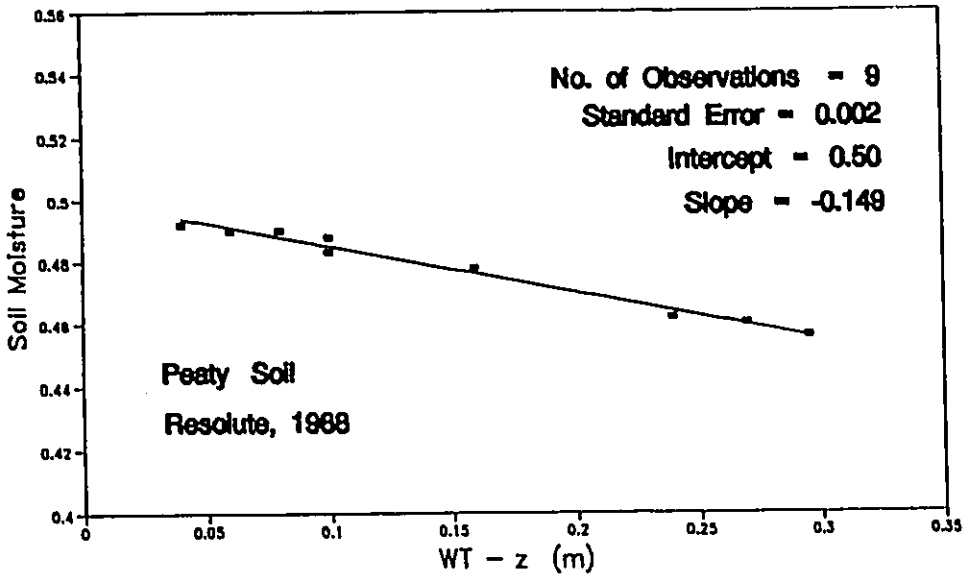

Figure 3.13 The Regression of Soil Moisture to Water Table Position, in Peaty Soil Site

3.4.1.5 List of Parameters Used in WAD Model

Table (3.3) lists the various parameters for WAD model as applied to Resolute, N.W.T.

Table 3.3 Surface Type-dependent Parameters

Parameters	Gravelly Soil Site	Peaty Soil Site	In Equation or Figure
a_0	0.59	1.06	3.4
a_1	0.51	0.56	3.4
a	1.15	0.87	Fig. 3.5
b	1.23	0.90	Fig. 3.5
g	-0.08	-0.15	3.24
DSMAX	0.009	0.018	
ϕ	0.40	0.50	3.23
S_r	0.20	0.25	3.23
f_0	0.02	0.15	3.15; 3.16
f_N	0.58	0.35	3.15; 3.16
f_a'	0.10	0.15	3.15; 3.16
f_a	0.05	0.10	3.15; 3.16

The ground temperature at a depth of 5 m was used to provide the lower boundary conditions for the finite difference thermal equation. The temperature record from Resolute weather station (1985 to 1986) provided an estimate of the average conditions of T_b, A_b and SHIFT for equation

3.12. In the model, the vertical soil column is divided into 100 steps (MAXS = 100), and the freezing temperature is considered to be -0.00001 ^{0}C as freezing point. For basal ice growth (equation 3.10), the coefficients used by Heron (1985)are adopted for the model. DSMAX is the maximum depression storage that has to be satisfied before runoff occurs. Optional values provided by the WAD model were used. All these parameters are listed in Table 3.4.

Table 3.4 Miscellaneous Parameters:

Parameter	Value used	In Equation
T_b	-10.00 ^{0}C	3.12
A_b	4.00 ^{0}C	3.12
SHIFT	270 ^{0}C	3.12
FP	-0.00001 ^{0}C	
MAXS	100	
b_0	5.24	3.22
b_1	21.5	3.22
c_0	0.04	3.6a
c_1	0.006	3.6a
g_0	-0.0012	3.10
g_1	0.0156	3.10

3.4.2 Model Calibration

The model was calibrated with two year's field observations made in 1988 (Jun, 8 to Aug. 23) and 1989 (Jun 15 to Aug. 25) from a site Resolute, N.W.T. ($74^0$43'N, $94^0$59'W). Two plots, underlain by gravels, one with peaty soil cover and vegetation in wet area and the other in a dry and bare area were selected as the simulation sites for the model calibration and testing. This site was chosen because (1) previous work in the area (e.g. Woo and Steer, 1983) allows access to a seven year data base and (2) the area is close to a first class weather station which provides long climatic records that can be used as input data for model testing.

3.4.2.1 Error Estimation

Most hydrological models have parameters which require calibration. In this case the calibration procedure must produce a set of parameter values which, when used in the model, reproduce the hydrological response to some desired degree of accuracy or "goodness of fit". This accuracy must be based on a set of criteria for hydrologic modelling in order to minimize error. The error sources could be the following:

(1) Bias in the simulated output due to incomplete or biased model structure

(2) Bias in the simulated output due to unreasonable estimation of parameters

(3) Random and systematic errors in the input data e.g., rain, radiation or temperature, due to incomplete or inaccurate measurements

(4) Random and systematic errors in the measured output, e.g., frost table, water table, or evaporation used for comparison with the simulated output.

Parameter estimation may be based on minimization of root-mean squares between measured and simulated outputs.

$$RMSE = [\, N^{-1} \sum_{i=1}^{N} (P_i - O_i)^2 \,]^{0.5} \qquad (3.26)$$

where RMSE is root-mean-square error which is an index of goodness of fit

N is number of values or record at daily time intervals

P_i is the ith simulated value of a hydrologic variable.

O_i is the ith observed value of the same variable.

For example, if we consider frost table change during

the thawing period as the only variable to be fitted, we use the root-mean square value of the differences between observed and simulated thawing depth, as shown in equation (3.26). This procedure applies to the other variables likewise.

3.4.2.2 Model Structure and Parameter Calibration

To calibrate the model structure and corresponding parameters, two series of field experiments were set up in the years 1988 and 1989. The main experiment was in 1988, and the one in 1989 provided auxiliary data. Meteorological data (global radiation, air temperature and precipitation) as the model inputs are taken directly from field measurements. For the model structure calibration, first we break the WAD model into a number of sub-models, according to different hydrological processes. Each sub-model was run separately, and the simulated results were compared with field measurements. When these sub-models produce satisfactory goodness of fit with observed values according to the required level of accuracy, we put them together and calibrated the entire model and its parameters.

The first step for the calibration of model parameters is to simulate hydrological processes in the year 1988 and

compare them with field measurements; determine the goodness of fit, then adjust some parameters by trial and error until the results of simulation satisfy the pre-specified level of acceptance. The parameters are then defined as optimal parameters. For the WAD model the parameters defined by optimization included the air contents in thawed and frozen state of different soils (f_a in Eq. 3.17) and inflow rate as input in peaty soil site (test site B).

Figures (3.14) and (3.15) show the calibrated results of water table and frost table simulation in both gravelly and peaty soil sites, using their optimized parameters with the data from 1988. GS is ground snow depth, WT is water table, FTT is thawing front, FTF is freezing front, and symbols are measured values in charts.

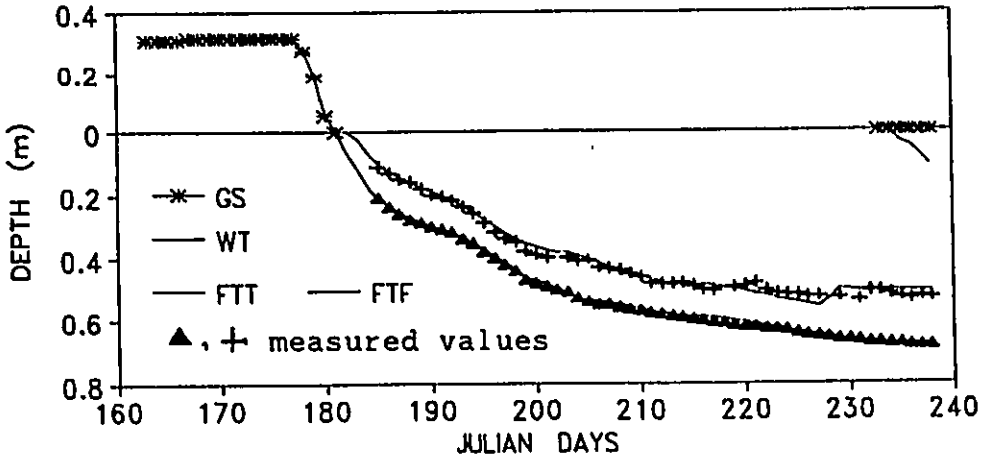

Figure 3.14 Calibration of the WAD Model with Gravelly Soil Site Data

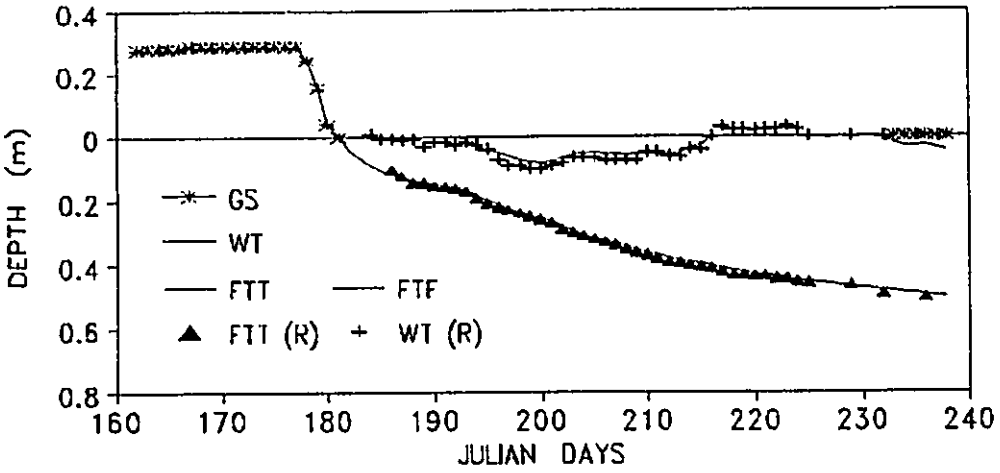

Figure 3.15 Calibration of the WAD Model with Peaty Soil Site Data

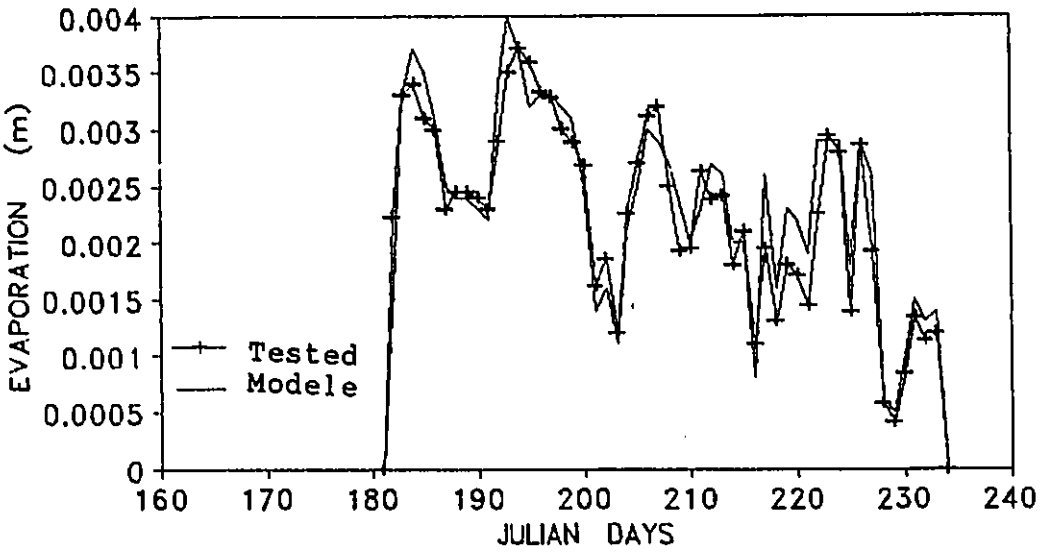

Figure 3.16 Evaporation Calibration of the WAD Model with Priestley and Taylor Calculations for Peaty Soil Site

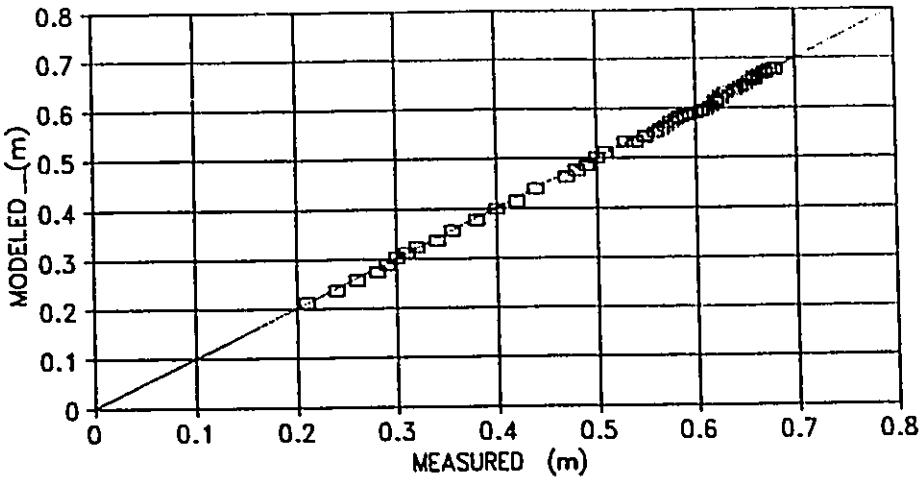

Figure 3.17 Comparison of Simulated Frost Table depth with Field Measurements at Gravelly Soil Site

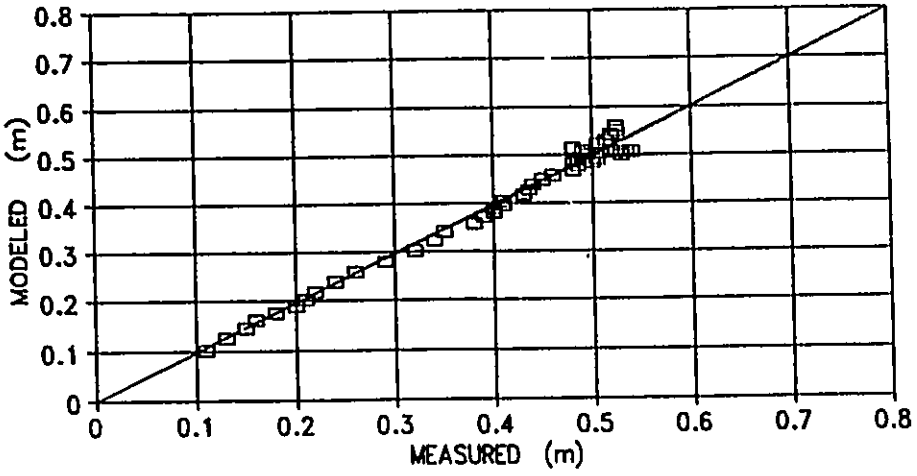

Figure 3.18 Comparison of Simulated Water Table Depths with Field Measurements at Gravelly Soil Site

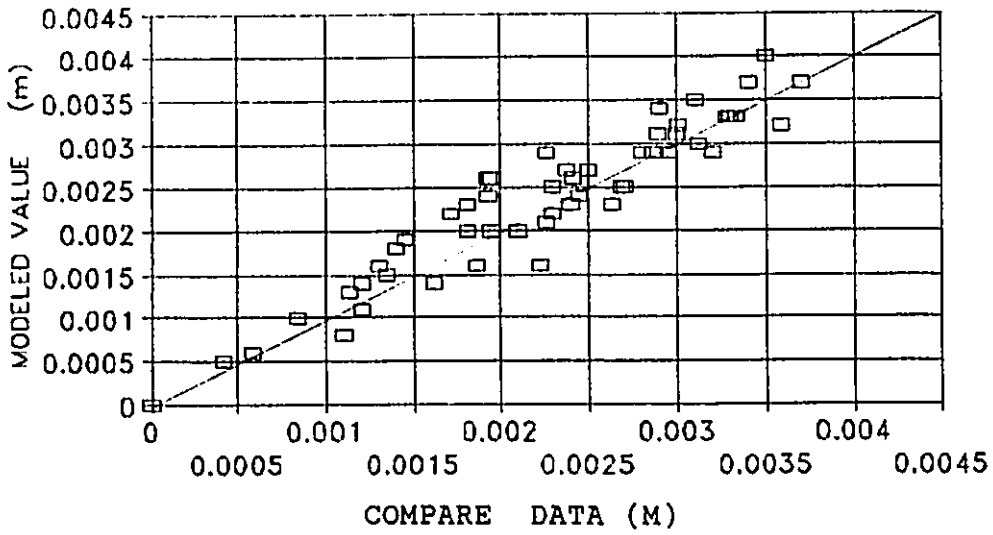

Figure 3.19 Comparison of Modeled Evaporation with Priestley and Taylor Model

evaporation for this year. In terms of comparison with field measurements, the simulated frost table compares better than the simulated water table which is better than the evaporation simulation. Figures (3.17), (3.18) compare the simulated frost table and water table with corresponding field measurements at the gravelly soil site, Figure (3.19) shows evaporation comparisons for the year 1988. There is a larger scatter of data about the 1:1 line for daily evaporation than for frost or water tables.

3.4.2.3 Inflow Calibration at the Peaty Soil Site

Peaty soils occur at a fen site which receives lateral inflow from melting snowbanks located upslope (Woo and Marsh 1990). This source of water input to the fen site cannot be ignored in the water balance considerations, but the amount of inflow has not been measured directly in the field. To incorporate this water source in the model runs, some approximation of its magnitude was required, and the data for 1988 was used for this purpose.

To estimate the total inflow for this year, the model was first run without the inflow, and the computed deficit in the seasonal water balance was assumed to be the total inflow. This amount was then distributed uniformly over all the days when air temperature exceeded 0.5 ^{0}C (non-frozen conditions) to serve as daily inflows to the test site. Thus, in 1988, the total estimated inflow was 193 mm and there were 58 days when air temperature exceeded 0.5 C, yielding an average inflow of 4 mm/day to the site during the thawed period. This value is in close agreement with the field estimated value of 4.5 mm/day determined by Woo and Marsh (1990) during the thawed period of July 5 to August 10 1988. An average daily inflow value of 4 mm/d was applied to all subsequent model runs for the peaty soil site.

3.4.2.4 The Initiation Time Calibration

To determine the stabilization time required for the model to stabilize, initialization experiments were performed over simulation periods of one to six years. The thermal ard hydrological outputs were compared with the observed values using the root-mean square criterion. Table 3.5 shows that the outputs of the peaty soil site converged to stable values of RMSE error estimation after a one year initiation simulation. This proved that it is not necessary for a long warm-up period for running the WAD. Similar conclusions can be reached for the gravelly soil site.

Table 3.5 The Calculated RMSE Values for Model Proper Initiation Calibration

Outputs	Between 0 year and one year	Between 1 year and two year
Ground snow	0.00919	0
Thawing front	0.0016	0
Freezing front	0.00025	0
Evaporation	3.1E-05	0
Water table	0.00051	0

3.4.2.5 Field Measurements Calibration

Two types of field measurements were calibrated, one was used as input data for the model simulation including precipitation, global radiation and air temperature. The other type was for checking the model outputs.

Measured input data were calibrated with the data measured at Resolute weather station. Any missing observation was filled and corrected linearly with empirical equations. Figure (3.20), as a example, shows the correlation of air

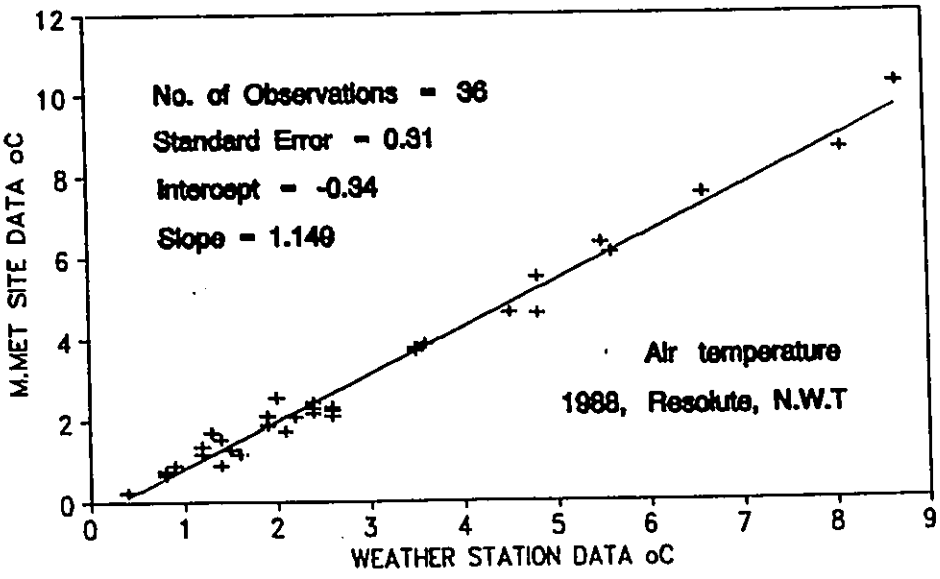

Figure 3.20 The Regression of Air Temperature Measured in Weather Station to Our Measurements

temperature measured at our own climate station with the air temperature measured at the first class weather station at Resolute.

Field measurements of frost table positions were used to check the WAD model output. Frost table changes were measured daily by hammering a steel rod into the ground until the frost table prevented further penetration. The problem with this field method is that the steel rod may destroy the top plastic zone of the frost table. As the frozen soil in this zone is warmer than the soil below, this plastic frozen soil is weaker than the deeper soil in the elastic state. This is because the strength of the frozen soil is a function of temperature. Equation (3.27) shows the relationship of the ultimate compressive strength of frozen soil with its temperature:

$$\sigma_{ul}^{cm} = a + b(\theta)^n \qquad (3.27)$$

where a, b and n are parameters and θ is the absolute value of the negative temperature. σ_{ul}^{cm} is the ultimate compressive strength of frozen soils. From this equation, we know that $\sigma_{ul}^{cm} = a$ when temperature $\theta = 0$, or that the minimum ultimate

compressive strength of frozen soils equals the minimum ultimate compressive strength of unfrozen soils if it is saturated. One reason may be that not all the water in the soil freezes at exactly 0 ^{0}C, and the more unfozen there is in the soil, the weaker is the soil resistance to the penetration of the frost rod. Figure (3.21) shows curves of $\sigma_{ul}^{cm} = f(-\theta)$, obtained by professor N. A. Tsytovich (1975), for three frozen soils: sand, sandy loam, and clay. Similar

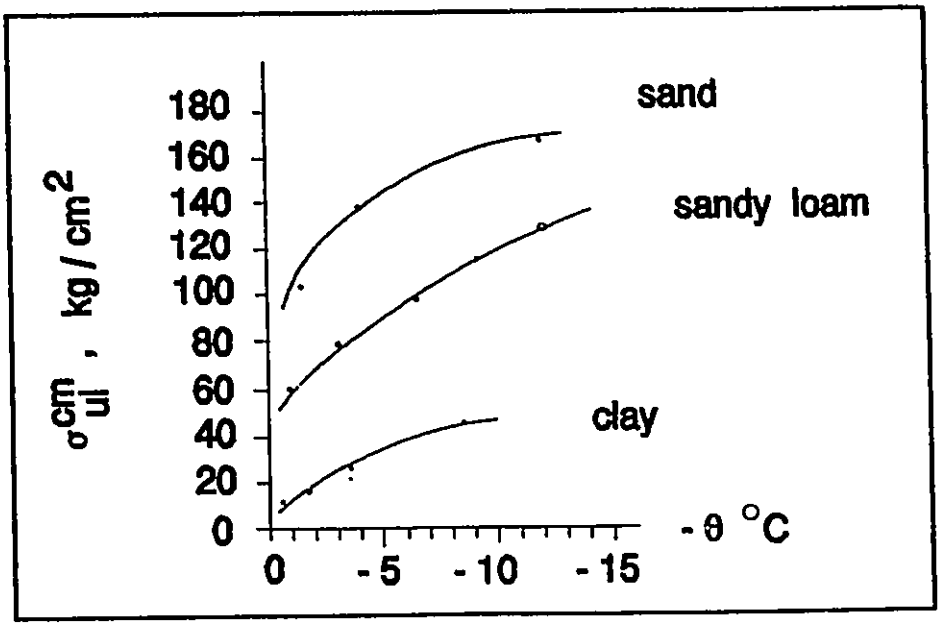

Figure 3.21 Ultimate Compressive Strength of Frozen Soils as a Function of Negative Temperature

results were obtained by other investigators.

The above discussion suggests that when the soil temperature is close to 0 ^{0}C, it may be difficult to get accurate frost depth measurement using simple method such as hammering steel rod into the soil. A series of experiments were made in 1988, using different type of steel rods to measure frost table depth (Fig. 3.22). Figure (3.23) shows that the error of frost table measurement is different for different soils using steel rods with different tips.

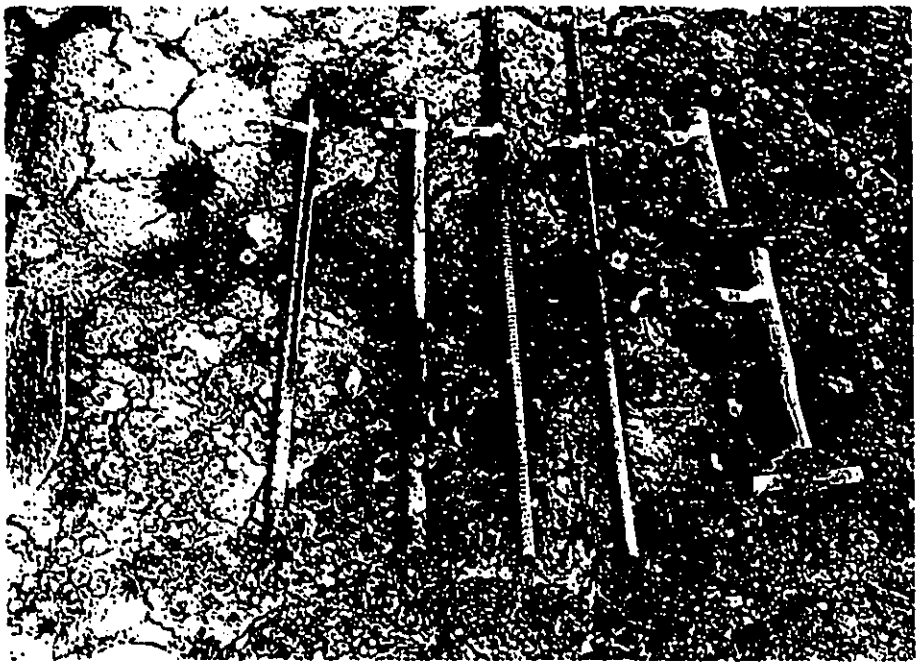

Figure 3.22 The Steel Rods and Hammers Used for the Frost Table Measurement Calibration

The range of the measurement error is 2 to 4 cm for gravelly soil site and is 3 to 5 cm for the peaty soil site. The rods tend to overestimate frost depth because the strength of the frozen soil was the lowest near the freezing point. This bias in the field data should be taken into consideration when calibrating modelled results.

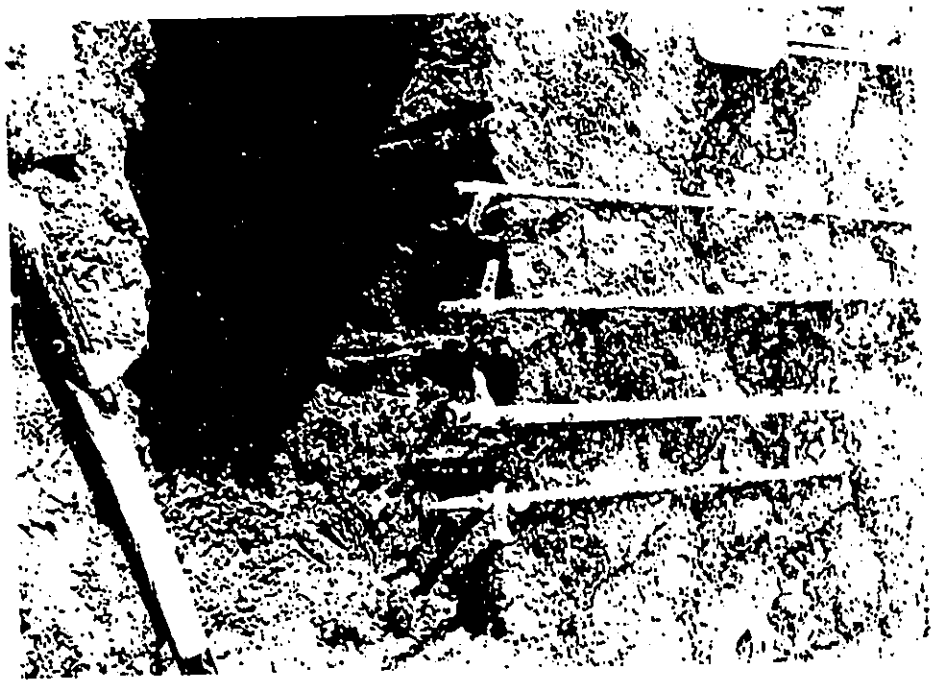

Figure 3.23 The Soil Profile and the Error Comparatione Measured with Different Steel Rod

3.4.3 Model Testing

The model was tested on a gravelly and a peaty soil plot using parameters derived from field experiments and from optimization with the 1988 data set. Meteorological data from 1989 used as inputs for model testing are shown in Figures (3.24), (3.25) and (3.26).

Figures (3.27), (3.28) illustrate the results of the model testing at the gravelly soil site and the peaty soil

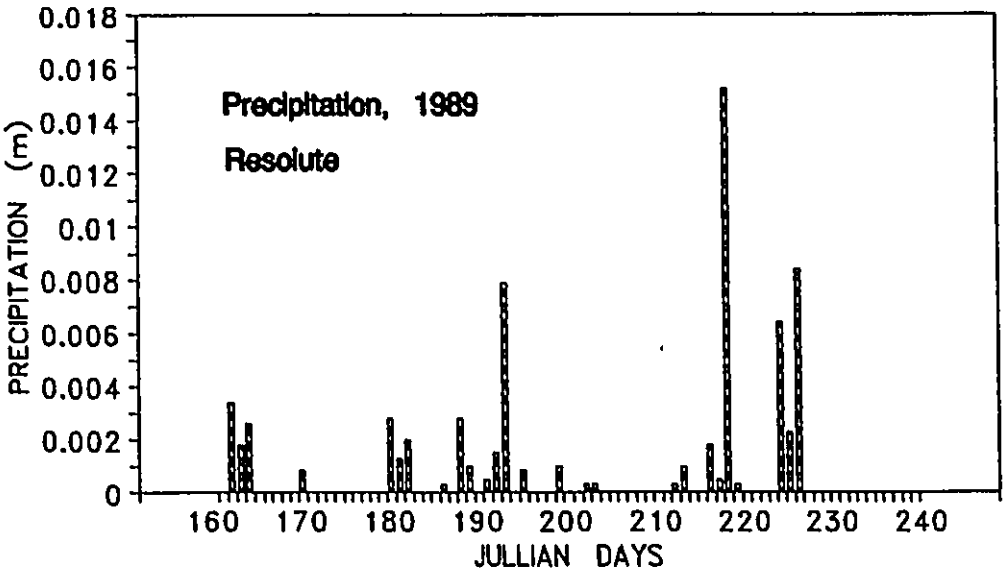

Figure 3.24 Precipitation Distribution in the Thawing Season of the Year 1989

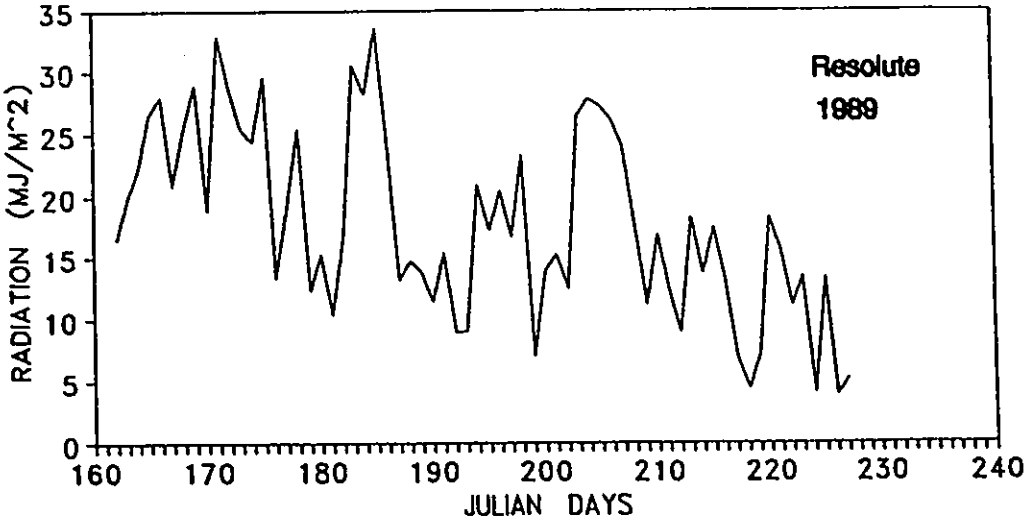

Figure 3.25 Radiation Distribution in the Model Testing Period

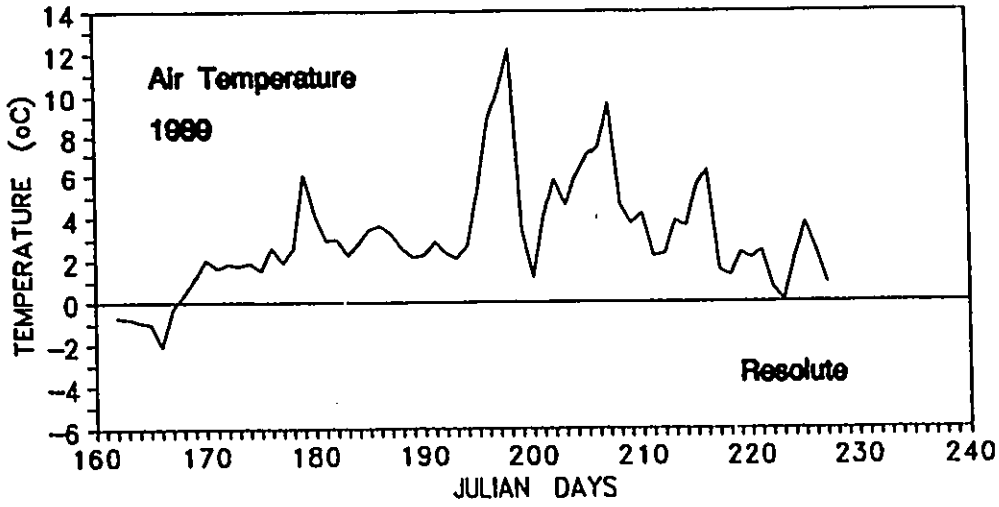

Figure 3.26 Air Temperature Variation in the Model Testing Period

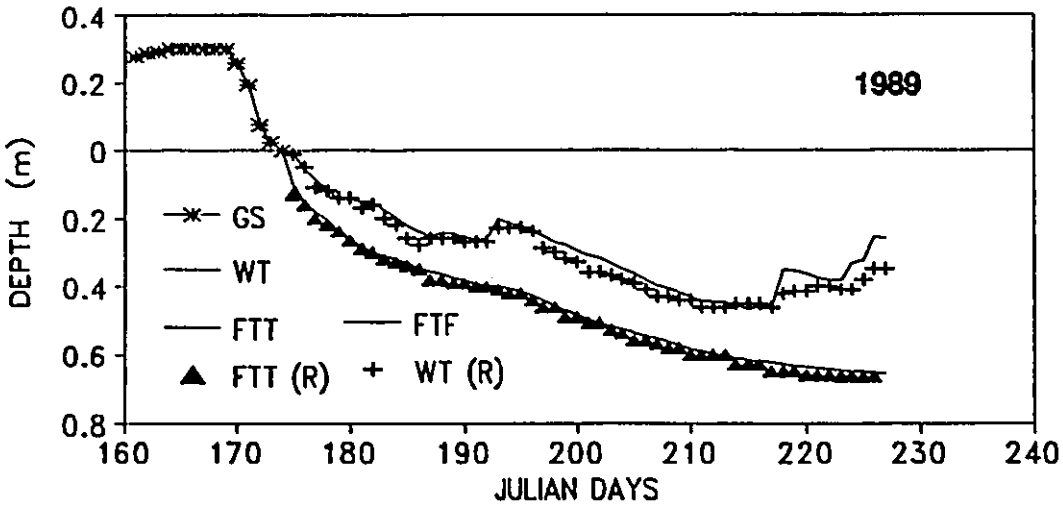

Figure 3.27 Verification of the WAD Model Results for Peaty Soil Site

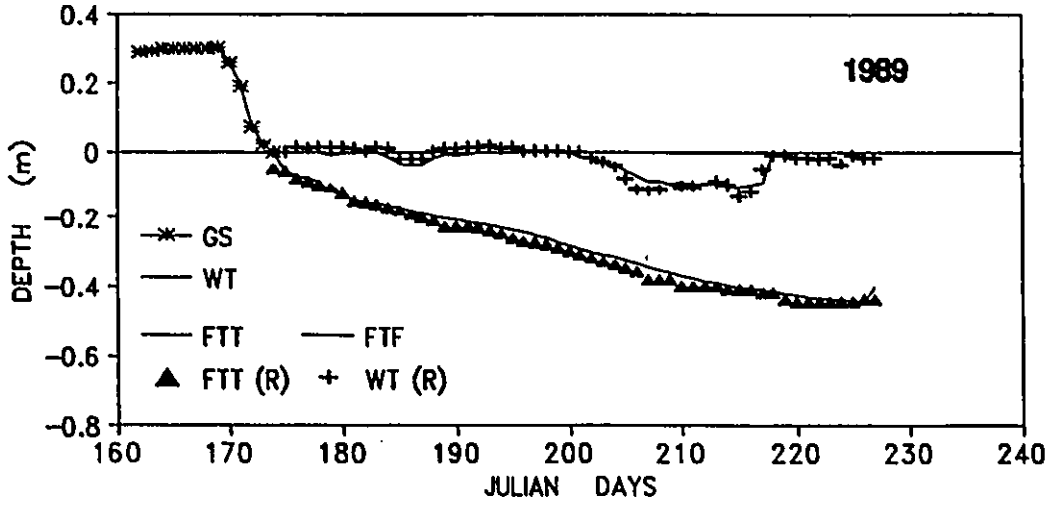

Figure 3.28 Verification of the WAD Model Results for Peaty Soil Site

site separately. GS is ground snow depth, FTT is thawing front frost table, FTF is the freezing front position and WT is the water table height. The initial conditions for the model testing were specified only once on Julian day 162 of 1989. At this time, the frozen ground was considered to be fully saturated, and the depth of the snow cover, defined by detailed snow survey at the both testing site, was related to snow depth at the weather station data using an index method. Compare with field measurements, both frost table and water table simulations all achieved satisfactory goodness of fit in both gravelly and peaty soils. The associated root-mean square errors are shown in Table 3.6, with the frost tables yielding smaller errors then the water tables. One reason is that water table fluctuation is governed also by the frost table change, so that the error from the frost table modeling is transmitted to the water table estimation.

Comparing the simulated results for both test sites, we find that the frost table development in the gravelly soil site was very fast at the beginning of the thawed season. The reason is that the entire soil column was fully saturated at the beginning of simulation yielding a higher thermal conductivity than when the soil dried out. As the thawed zone was not fully saturated later in the season the thermal conductivity of the soil column decreases gradually and the curve of the frost table descent became slower. In a

contrast, frost table development at the peaty soil site was uniform through time because its water table was always very high and the soil was almost fully saturated. The shallower thawed depth compared with gravels was due to differences in thermal conductivity between the two materials (organic soils have lower thermal conductivity).

Table 3.6 The Accuracy of the Model Simulation (m)

Model Test Site	Error for Frost Table Modeling	Error for Water Table Modeling
Gravelly Soil	0.015	0.035
Peaty Soil	0.018	0.026

3.4.4 Model Application

The model was applied to the simulation of the thermal and hydrological conditions for six years (1976 to 1981), using input data from Resolute first class weather station. This simulation was also validated against field data acquired between early Jun and late August in 1977, 1978, 1980 and 1981.

3.4.4.1 Simulation with Historical Data

Six years of daily precipitation, short wave radiation and air temperature, supplied by Resolute first class weather station, were used as model input data (Fig. 3.29). During the simulation period, 1977 and 1979 had less rainfall, but more snowfall, than the other years. Most of the snow events in the year 1977 occurred in the latter half of the year and concentrated mainly in October and November. This built up a deep ground snow cover for 1978 before melt started. The year 1981 was the wettest because of its high summer rainfall and considerable snowfall in winter. The rain events in the summer of the year 1981 were unevenly distributed, concentrating in the late summer, and this might have caused high water tables and enhanced evaporation.

The incoming solar radiation was distributed more evenly, though it was a little higher in 1980 and 1981 and lower in 1979.

From the air temperature record, the years 1977, 1980 and 1981 were warmer than the other 3 years. 1976 and 1979 had more negative degree-days in the winter and fewer positive degree-days in summer. The maximum daily mean high temperature was found in 1976 and the lowest was at the beginning of 1979.

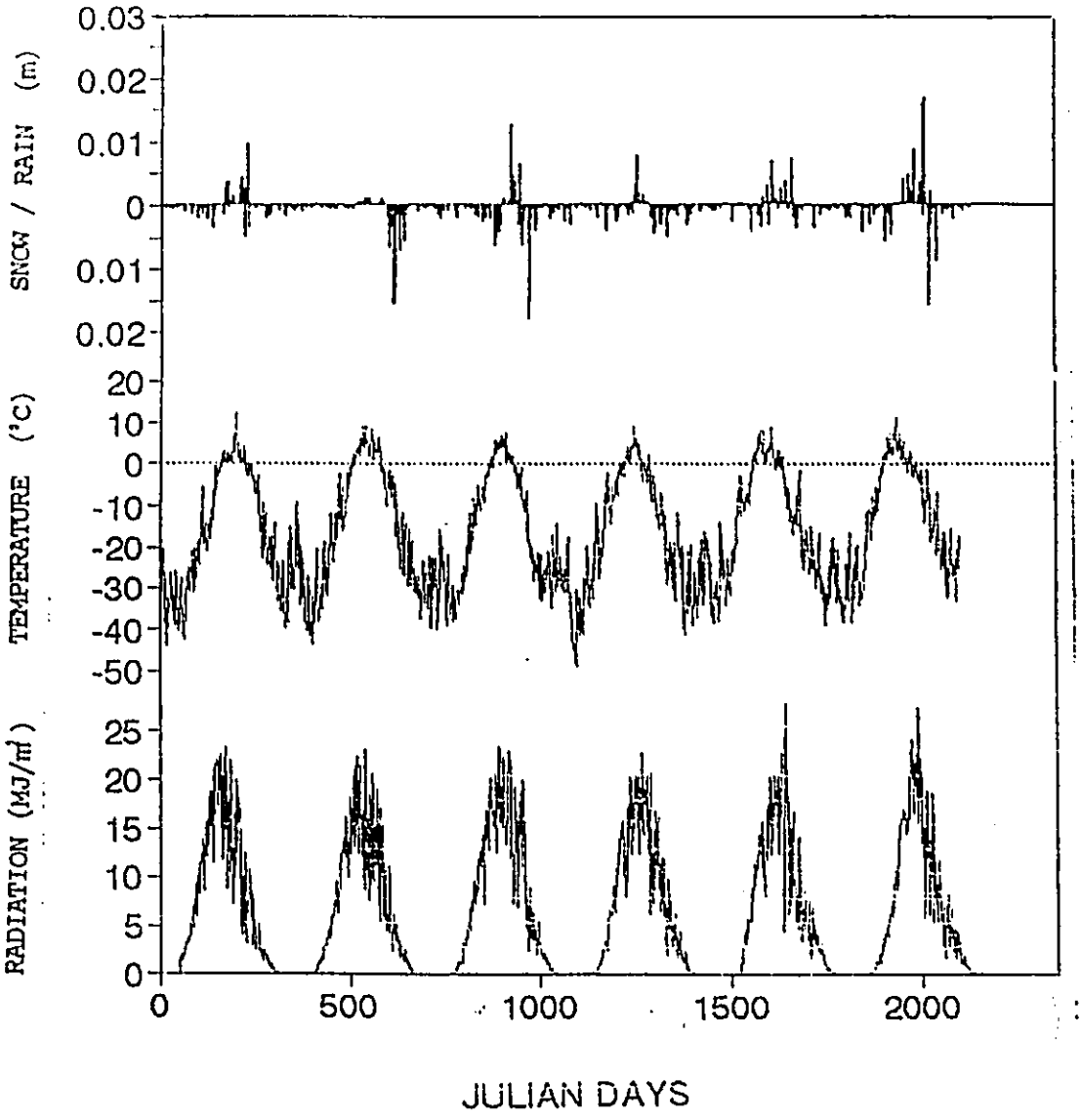

Figure 3.29 The Input Data of Six Year Hydrologic Modeling of The Active Layer in a Continuous Permafrost Environment

3.4.4.2 Hydrological Modeling Results

The 1976 to 1981 modelled results of snow accumulation and melt, thawing front and freezing front development, and water table fluctuation for both the gravelly soil site and the peaty soil site are shown in Fig.3.30 and 3.31. The observed field data were also plotted for comparison with the simulated results. As there were more snow events in the winter seasons between the year 1977 and 1978, the snow accumulation reached its highest value before the melt season started in 1978. The maximum thickness of the snow cover reached 400 mm in the peaty soil site by middle June, 1978. This thick snow cover delayed the melt season. In contrast, there was less snow accumulated in the 1976-77 winter, and it reduced the time duration of snow melt, thus extended the time period for ground thawing.

The daily rate of thawing front descent in gravelly soil site was greater than the one in peaty soil site. The reasons were that the gravelly soil has more minerals which have higher thermal conductivity than the organic-rich peaty soil; and the latter has more ice content, requiring more heat thaw the frozen soil. Moreover, the water table was usually higher at the peaty soil than the gravel soil. Freezing of this soil produced more ground ice in the winter. In spring and summer, more energy is use for phase change,

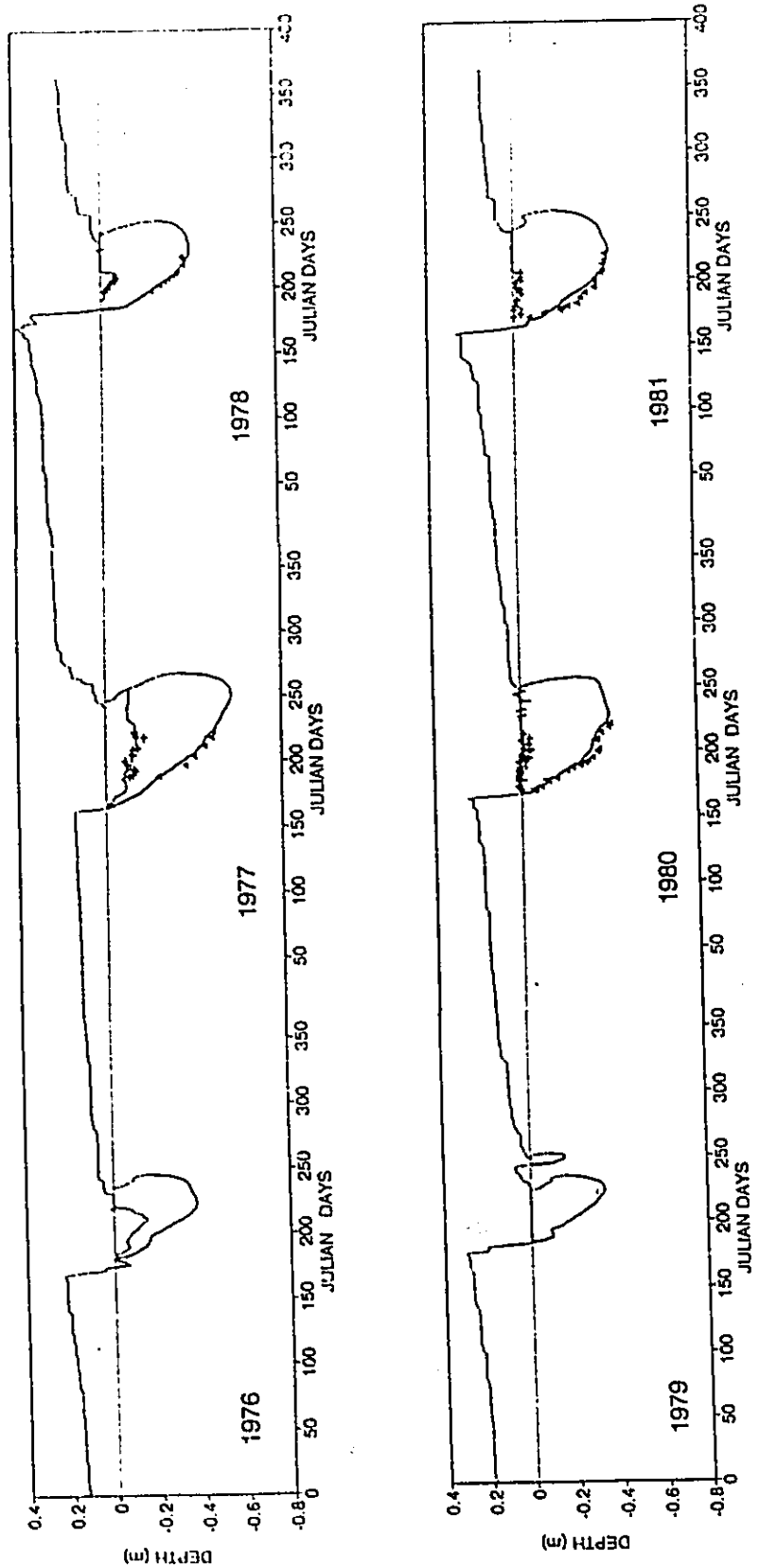

Figure 3.30 The Output of Six Year Hydrological Modeling in Gravelly Soil Site, Resolute, N.W.T.

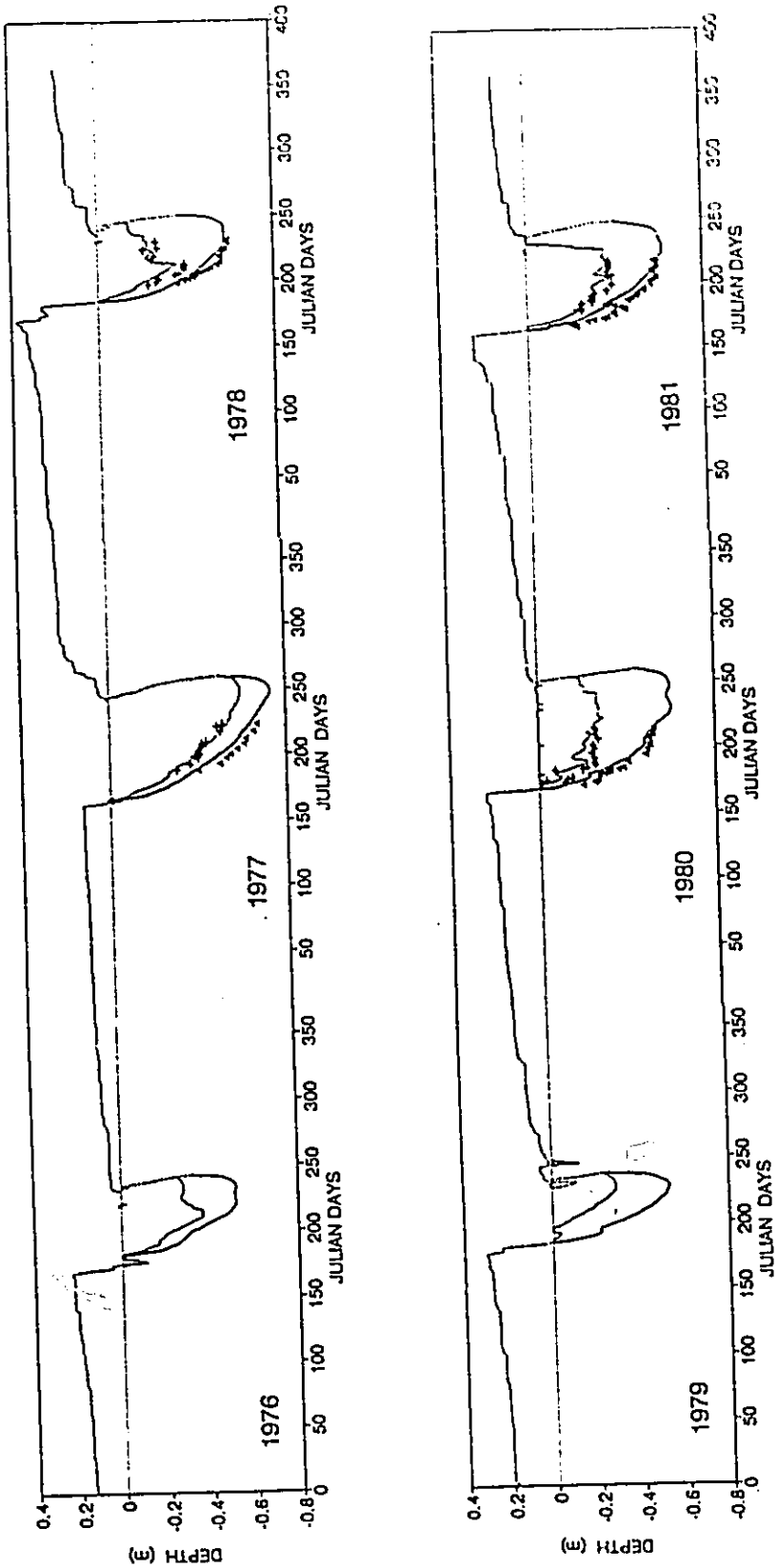

Figure 3.31 The Output of Six Year Hydrological Modeling in Peaty Soil Site

from ice to water, and this retards the rate of thawing front descent. On other hand, water table was usually low at the gravel site, yielding less ice in winter and therefore, the same amount of energy penetration into the gravelly soil can produce a greater thawing depth.

At the gravelly soil site, the water table was high at the beginning of the thawing seasons. In summer, the water table rose during rain events but dropped down as evaporation increased. Water table also responded to the soil ice content and frost table development of the testing site, as it is the lower boundary. As more ice content was stored in the soil column from the previous year, more energy is needed to thaw this ice and this retards frost table development. The year 1977 was a warm year, and the thawing front reached the deepest among the 6 simulation years. A deep frost table and low summer rainfall caused the water table to be the lowest among the 6 years.

Unlike the gravelly soil site, which receives water input only from rainfall and snowmelt, the peaty soil site also receive lateral surface and subsurface inflows from upslope. The modeled water table in the peaty soil site was quite high. Throughout the thawed seasons of 1976 to 1981, the soil column was fully saturated before each summer season ended. The high moisture content yielded high ice content in winter time which subsequently reduced the depth of summer

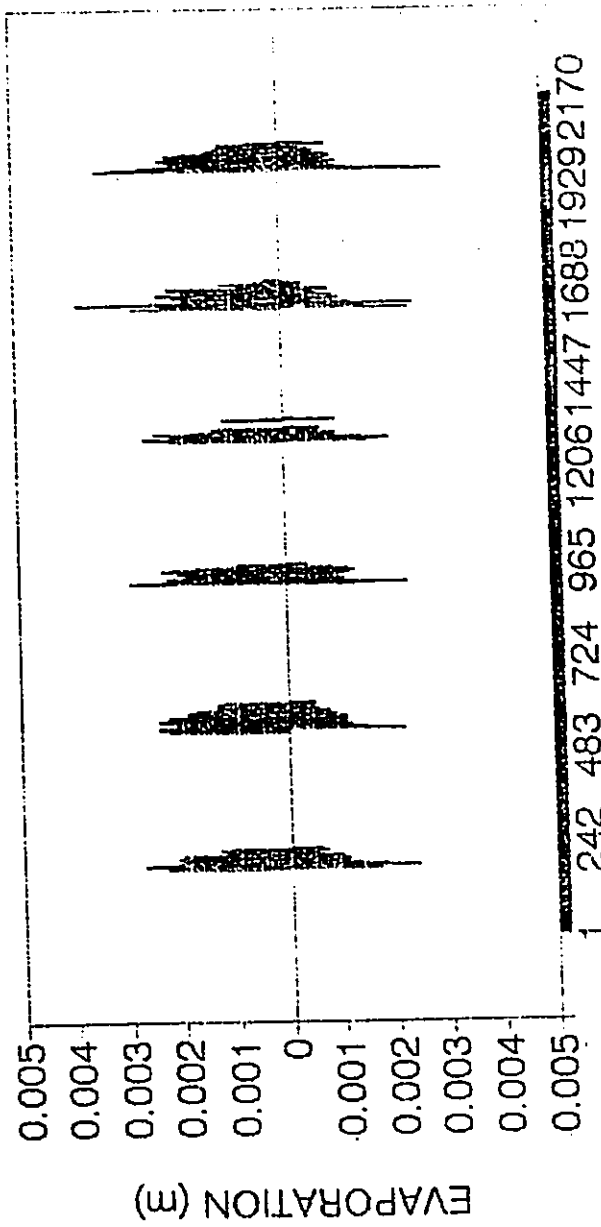

Figure 3.32 The Simulated Evaporation Variation from 1976 to 1981. Top Shows Evaporation from Peaty Soil and Bottom Shows Evaporation from Gravelly Soil

thaw. The frequent availability of moisture in a polar desert environment explains the presence of vegetation cover, and why the peaty soil could develop.

The modeled evaporation variation is shown in Fig. 3.32. It is clear that evaporation was higher at the peaty soil site than at the gravelly soil site under the same climatic regime. The dominant factor is that water was not limited in peaty soil site as its water table was always close to the surface. Evaporation is also a function of precipitation, temperature and radiation. The years 1977, 1980 and 1981 had more evaporation, as they were warmer than the other years (Table 3.7). Unlike many areas with seasonal

Table 3.7 The Total amount Evaporation Simulated from 1976 to 1981

Simulation Year	Evaporation (m) Peaty Soil	Evaporation (m) Gravel Soil
1976	0.0657	0.0382
1977	0.1015	0.0473
1978	0.0770	0.0420
1979	0.0637	0.0387
1980	0.0777	0.0411
1981	0.0943	0.0526
SUM (76..81)	0.4739	0.2599

frost, maximum daily evaporation always happened in the melt season at the continuous permafrost, gravel site. This was due to the ample water supply at the surface during the melt period when solar radiation also reached its maximum. Afterwards, low summer rainfall and reduced radiation input limit the supplies of moisture and energy, thereby causing evaporation to drop.

The modeled evaporation for the peaty soil site in 1977 was special, as there was little snow accumulation in the previous winter and meltwater supply was therefore limited. There was no evidence of higher evaporation in the spring and the evaporation rate tended to be more evenly distributed in the summer, as moisture was supplied by the ground ice melt and by lateral inflow. The duration of thawed period varied from year to year, being longer in the three warm years of 1977, 1980 and 1981.

The modeled freezing front penetration was also correlated with the freezing degree day index. The process of freeze-back in the active layer occurs in two directions, i.e. downward from the ground surface and, upward from the permafrost table. If the air temperature falls slowly in late summer, upward freezing will play a more important role. The simulated freezing front descent was deeper at the gravelly than the peaty soil site. One reason is that the larger amount of minerals in gravel soil yields higher thermal

conductivity. The other reason is that the higher water content in the peaty soil releases more latent heat as its water freezes. This effect of moisture content on soil freezing can also cause the freezing front descent to vary from year to year at the same site. At the end of the dry summer of 1977, the water tables at both the gravel and the peaty soil sites were lower than the other years, and this year experienced the deepest freezing front frost table penetration at both sites.

3.4.4.3 The Output Test with Field Measurements

Field measurements were available in 1977, 1978, 1980 and 1981 to provide comparison with simulated results. The root mean square errors are shown in Table 3.8, and the observed data are plotted as symbols on Fig. 3.30 and 3.31. The systematic underestimation of frost table depths by the model may be due to the bias in the field measurements. As the frost table measurements (obtained by hammering a steel rod into the ground) may have a positive error of 3 - 4 cm (see section 3.4.2.5), this can account for some difference with modelled results.

In terms of evaporation, the modelled output compared favourably with values calculated using field input data

Table 3.8 The Estimated Error for Frost Table and Water Table Modeling

Year	Frost Tab (m) P.S. Site	Water Tab (m) P.S. Site	Frost Tab (m) G.S. Site	Water Tab (m) G.S. Site
1977	0.02	0.01	0.04	0.02
1978	0.02	0.01	0.03	0.03
1980	0.02	0.02	0.04	0.04
1981	0.03	0.02	0.04	0.03

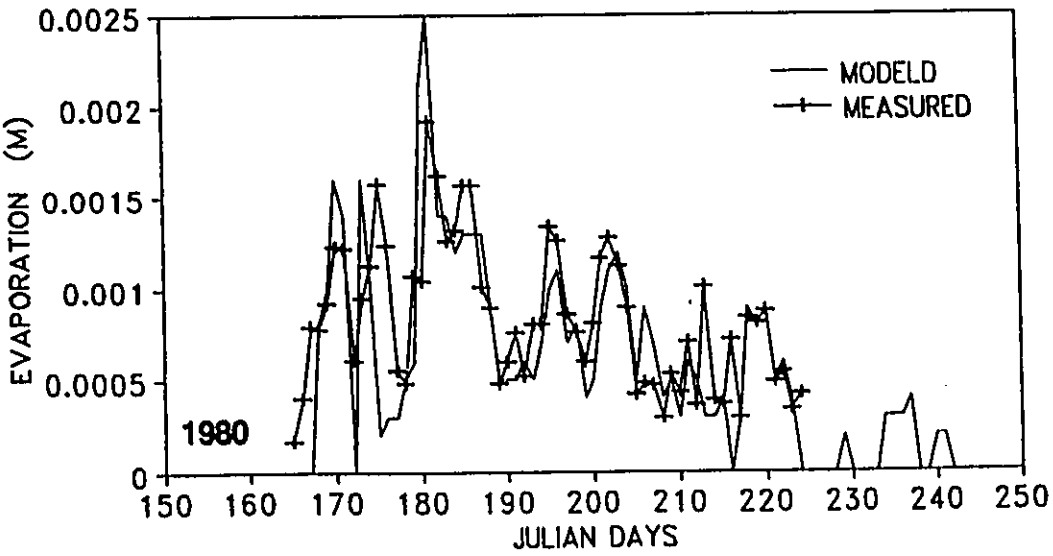

Figure 3.33 The Simulated Evaporation Variation in the Year 1980

(Fig. 3.33). The root-mean square error for evaporation modelling in 1980 was 0.00038 m.

3.4.4.4 Simulated Active Layer Water Balance

The modeled hydrologic water balance of 1976 to 1981, is shown in Table 3.9. Annual precipitation was separated into snowfall and rainfall, and the term melt means total contribution of snow meltwater to the active layer water balance. The magnitude of total meltwater may not equal to the total snowfall as they are computed for different time periods. The snow which produces meltwater was accumulated over the previous winter before melt started. Annual precipitation as snow was computed from the first day of January to the last day of December. Q_{in} and Q_{out} are total inflow and outflow. Evap. is total evaporation and DS is soil moisture deficit of active layer at the year end. The active layer storage experienced a slightly net loss for the gravelly soil site, but a large net gain for the peaty soil site. The loss at gravelly soil site was largely due to evaporation and to lateral flow. The modeled evaporation loss was large for the peaty soil site, but this was more than made up by the net gain from lateral inflow.

Table 3.9 Summary of Modeled Hydrologic Events of Six Historical Years (m)

Year	1976	1977	1978	1979	1980	1981
G.Site						
Snow	0.072	0.092	0.135	0.108	0.074	0.106
Rain	0.034	0.008	0.043	0.024	0.037	0.077
Melt	0.077	0.040	0.100	0.098	0.074	0.093
Q in	0.000	0.000	0.000	0.000	0.000	0.000
Q out	0.069	0.033	0.093	0.098	0.084	0.082
Evap.	0.035	0.045	0.030	0.036	0.036	0.050
DS	0.000	0.033	0.015	0.000	0.000	0.000
P.Site						
Snow	0.072	0.092	0.135	0.108	0.074	0.106
Rain	0.034	0.008	0.043	0.024	0.037	0.077
Melt	0.078	0.056	0.178	0.125	0.147	0.112
Q in	0.064	0.113	0.083	0.066	0.095	0.104
Q out	0.066	0.066	0.173	0.138	0.124	0.142
Evap.	0.065	0.100	0.086	0.070	0.084	0.102
DS	0.000	0.000	0.000	0.000	0.000	0.018

CHAPTER 4

TWO DIMENSIONAL MODEL FOR ACTIVE LAYER THAW

4.1 Background of the Study

Ground conditions in continuous permafrost areas may be considered to comprise a number of segments, each underlain by different materials experiencing non-uniform hydrological conditions, and subject to differential surface heating (Brown 1956, 1962). As a consequence, the active layer under each ground segment will have different rates of thaw. Spatial variations in thaw depths may have implications for landform development, vegetation growth and the stability of man-made structures.

Given adequate data on the soil properties, the hydrological behaviour and the surface temperature regime, various numerical methods, e.g. finite difference or finite element (Outcalt 1975; Goering and Zarling 1985), can determine the thaw depth along a stretch of the ground. However, detailed climatic and hydrological data are often

not available to run such models. If only mean surface temperature and average hydrological information are often not available, an alternative method is needed to predict frost table positions under the influence of climatic variability and change.

A model will be developed for this purpose, applying the Green Theorem to solve the heat flow equation for an active layer zone with the frost table as its lower boundary. The ground is divided into contiguous segments of various lengths, each with different thermal and hydrological properties and under different surface temperature conditions. The effect of variable ground ice content on the descent of the thawing front is achieved by thaw retardation, and the average moisture content for different periods is considered in the calculation of the thermal conductivity.

4.2 Development of the Model

In 1947, Carslaw and Jaeger expanded the Green theorem to make it possible to obtain solutions to heat transfer problems. Lachenbruch (1957) made use of their solutions and applied to model the thermal effect of the ocean on the permafrost in the adjacent land. In the present study, the Green theorem is also used as a basis to provide solutions for permafrost heat transfer problems. However, several major

differences exist between the current application and the model used by Lachenbruch:

1) Lachenbruch's model was limited to two adjacent soil segments with different thermal characteristics and boundary conditions. The model proposed can handle multiple segments.

2) The earlier model solved the heat conduct equation as diffusion equation using constant soil thermal conductivity and heat capacity, without considering the effects of soil moisture variations.

3) The effect of phase change due to the melting of ground ice was not considered by the earlier model.

4) In the present study, the Laplace equation for heat transfer was treated as a Cauchy problem, and was solved by selecting a special Γ-function different from that used by Carslaw and Jaeger.

In the following section, a brief description of heat transfer equation and the Green theorem are presented.

4.2.1 Active Layer Heat Transfer Processes

In the general case, the transfer of energy may take place by one or more of the three basic modes of heat

The first two methods are not associated with mass transfer, whereas the third is dependent on mass transfer. In addition to these modes of heat transfer, we may encounter energy transfer due to mechanical work, and energy liberation by electrical, chemical, physical, or other means, like latent heat of phase change from ice to water or from water to vapour state. An energy balance for any selected thermodynamic system may be established for the each of individual cases. From these energy balances, an equation of the temperature as a function of the space coordinates, time, and the velocity components, along with some properties of the medium, may be written (Lunardini 1981).

In the following discussion, emphases will be placed on heat conduction with and without phase change and with phase change (Anderson 1973, Bondarev 1959).

4.2.1.1 Heat Transfer Equations

Heat conduction follows the empirical relation known as "Fourier's law".

$$q = -k\frac{dT}{dx} \qquad (4.1)$$

where the flow of energy q across a unit area is proportional to the temperature gradient dT/dx with the proportionality coefficient k being the thermal conductivity of the medium. Equation (4.1) can be generalized to the three-dimensional case and

$$q = -\bar{k}\nabla T \qquad (4.2)$$

Consider an element of soil volume dV having side lengths dx, dy, and dz. The net flow of energy into and out of this volume of material must equal to the change in stored energy in the system

$$Q_i - Q_o + Q_g = \Delta Q_s \qquad (4.3)$$

where Q_i, Q_o are net heat energies transferred across the boundaries into and out of the system

Q_g is the energy developed within the system

ΔQ_s is the change in stored energy.

ΔQ_s is the change in stored energy.

The side lengths of the element are dx, dy and dz. The time interval over which our observations will be made is dt. The face perpendicular to the x axis and closest to the origin passes through the point x, y, z.

The energy transfer across the soil boundaries in the form of heat may take place by conduction and by radiation. Heat transferred by the flow of mass (such as water) is ignored here for simplicity. The energy transfer by conduction may be computed by applying Fouriers equation to each of the three directions. Take the face perpendicular to the x-axis and passing through the point x, y, z, the energy transfer by conduction for an orthotopic material, in the time dt is

$$dQ_{cx} = k_x \, dy \, dz \, \frac{\partial T}{\partial x} \, dt \qquad (4.4)$$

at x + dx is

$$dQ_{c(x+dx)} = \left[k_x \frac{\partial T}{\partial x} + \frac{\partial}{\partial x} \left(k_x \frac{\partial T}{\partial x} \right) dx \right] dy \, dz \, dt \qquad (4.5)$$

The net flux of energy is the difference between these two values

$$dQ_{xc} = \frac{\partial}{\partial x}\left(k_x \frac{\partial T}{\partial x}\right)\, dV\, dt \qquad (4.6)$$

Similar equations may be written for dQ_{yc} and dQ_{zc} for the net energy transfer by conduction in the y and z direction. Then the net energy into the system by conduction is the sum of the energy fluxes in the three directions

$$dQ_c = \left[\frac{\partial}{\partial x}\left(k_x \frac{\partial T}{\partial x}\right) + \frac{\partial}{\partial y}\left(k_y \frac{\partial T}{\partial y}\right) + \frac{\partial}{\partial z}\left(k_z \frac{\partial T}{\partial z}\right)\right]\, dV\, dt \qquad (4.7)$$

The energy transfer by the radiation process will depend on the "radiation geometry", the emissivities and temperatures of the surroundings and the material within the boundaries. Since this will be a complex function, it will be left in a general form. The net energy transferred by radiation will be

$$dQ_r = q_r\, dV\, dt \qquad (4.8)$$

where q_r is the net radiant energy into the system per unit volume, per unit time. The term Q_i and Q_o in Eq. (4.3) may now be written

$$Q_i - Q_o = dQ_c + dQ_r \tag{4.9}$$

In the permafrost environment, heat transfer into and out of the soil often involves freezing or thawing processes. We will express this energy term in a general form.

$$Q_g = q_g \, dV \, dt \tag{4.10}$$

where q_g is the energy released or absorbed per unit volume and per unit time in freezing or thawing processes.

For practical considerations, the change in heat energy storage in the soil volume can be determined as

$$\Delta Q_s = C \frac{dT}{dt} \, dV \, dt \tag{4.11}$$

where C is volumetric heat capacity of the soil.

The general energy equation Eq. (4.3) may now be

rewritten

$$k\nabla^2 T + q_r + q_g = C\,\frac{DT}{Dt} \qquad (4.12)$$

here ∇^2 is the usual operator. For a Cartesian coordinate system

$$\nabla^2 = \frac{\partial^2}{\partial x^2} + \frac{\partial^2}{\partial y^2} + \frac{\partial^2}{\partial z^2} \qquad (4.13)$$

4.2.1.2 Heat Transfer Processes

Assume that the soil material is isotropic. The radiation term only affects the ground surface of the active layer, so it will be handled as a boundary condition. Then Eq. (4.12) becomes the general conduction equation.

$$\frac{\partial}{\partial x}\left(k_x \frac{\partial T}{\partial x}\right) + \frac{\partial}{\partial y}\left(k_y \frac{\partial T}{\partial y}\right) + \frac{\partial}{\partial z}\left(k_z \frac{\partial T}{\partial z}\right) + q_g = c\frac{\partial T}{\partial t} \qquad (4.14)$$

For the system of an active layer in a continuous permafrost environment the term q_g is mainly due to the latent heat of fusion associated with the phase change from water to ice or from ice to water. Other types of energy released such as latent heat of vaporization within the soil, tend to be insignificant compare with latent heat of fusion. Then the term q_g in Eq. (4.14) may be written as

$$q_g = -\lambda \frac{\partial \varphi}{\partial t} \tag{4.15}$$

where λ is the volumetric latent heat of fusion from ice to water ,

φ is ice content in soil.

Finally, the equation describing heat balance at any point in an active layer may be written as

$$k_x \frac{\partial^2 T}{\partial x^2} + k_y \frac{\partial^2 T}{\partial y^2} + k_z \frac{\partial^2 T}{\partial z^2} = c \frac{\partial T}{\partial t} + \lambda \frac{\partial \varphi}{\partial t} \tag{4.16}$$

4.2.2 Green's Theorem

Let us introduce an important relation between the line integral and area integral, first, the Green's theorem which provides the base for the Green Function.

4.2.2.1 General Description

Suppose a closed region Ω in the XY-plane can at the same time be represented by inequalities $a \leq x \leq b$, $f(x) \leq y \leq g(x)$ and by inequalities $c \leq y \leq d$, $h(y) \leq x \leq i(y)$, where f, g, h, and i are functions with continuous derivatives in their respective domains (Fig. 4.1).

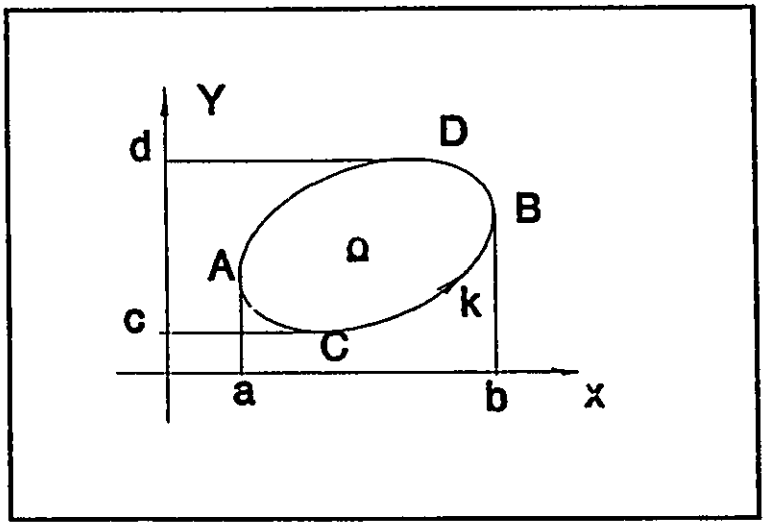

Figure 4.1 The coordinates and the domain of the basic Green's theorem

Consider now the double integral

$$I = \int_{\Omega} [U'_x(x,y) - V'_y(x,y)] \, dA \qquad (4.17)$$

where U and V have continuous partial derivatives in an open region containing Ω. In terms of two perpendicular coordinates the following may be obtained:

$$
\begin{aligned}
I &= \int_{\Omega} U'_x(x,y)\ dA - \int_{\Omega} V'_y(x,y)\ dA \\
&= \int_c^d dy \int_{h(y)}^{i(y)} U'_x(x,y)\ dx - \int_a^b dx \int_{f(x)}^{g(x)} V'_y(x,y)\ dy \\
&= \int_c^d [U(i(y),y) - U(h(y),y)]\, dy - \int_a^b [V(x,g(x)) - V(x,f(x))]\, dx
\end{aligned}
\tag{4.18}
$$

Introducing k as the boundary curve of Ω, assigned in a counter-clockwise direction, we further consider the line integral

$$
J = \int_k V(x,y)\ dx + U(x,y)\ dy = \int_k V(x,y)\ dx + \int_k U(x,y)\ dy \tag{4.19}
$$

which may be rewritten as follows:

$$
\begin{aligned}
J &= \int_{ACB} V(x,y)\ dx - \int_{ADB} V(x,y)\ dx + \int_{CBD} U(x,y)\ dy \\
&\quad - \int_{CAD} U(x,y)\ dy \\
&= \int_a^b V(t,f(t))\ 1\ dt - \int_a^b V(t,g(t))\ 1\ dt + \int_c^d U(i(t),t)\ 1\ dt \\
&\quad - \int_c^d U(h(t),t)\ 1\ dt
\end{aligned}
\tag{4.20}
$$

This completes the proof of Green's theorem for the region Ω considered:

$$\oint_k V(x,y)\ dx + U(x,y)\ dy = \int_\Omega [U'_x(x,y) - V'_y(x,y)]\ dA \tag{4.21}$$

or

$$\oint_k V\ dx + U\ dy = \iint_\Omega \left(\frac{\partial U}{\partial x} - \frac{\partial V}{\partial y}\right)\ dxdy \tag{4.22}$$

Here the circle with an arrow on it introduced in the formula simply emphasizes that the path of integration k, as mentioned, is to be traversed in the counterclockwise direction (Bak and Lichtenberg 1966).

4.2.2.2 The Green's Identities

Define a region Ω with its boundary ∂Ω. The Laplace operator acting on a function $u(x) = u(x_1,\ldots,x_n)$ of class C^2 in the region may be written as

$$\Delta = \sum_{k=1}^{n} D_k^2 \tag{4.23}$$

where $D_k = \partial / \partial x_k$ is the Cauchy differentiation symbol. For $u, v \in C^2(\bar{\Omega})$ we may write Green's first identity (John, 1982)

$$\int_\Omega v \, \Delta u \, dx = - \int_\Omega \sum_i v_{xi} u_{xi} \, dx + \int_{\partial\Omega} v \frac{du}{dn} \, dS \tag{4.24}$$

where n is a vector, outward normal to the boundary $\partial\Omega$ of the region Ω. Similarly, interchanging v and u, we have

$$\int_\Omega u \, \Delta v \, dx = - \int_\Omega \sum_i v_{xi} u_{xi} \, dx + \int_{\partial\Omega} u \frac{dv}{dn} \, dS \tag{4.25}$$

Subtracting Eq. (4.25) from (4.24) we obtain

$$\int_\Omega v \, \Delta u \, dx = - \int_\Omega u \, \Delta v \, dx + \int_{\partial\Omega} (v \frac{du}{dn} - u \frac{dv}{dn}) \, dS \tag{4.26}$$

here d / dn indicates differentiation in the direction of the exterior normal to $\partial\Omega$. Eq. (4.26) is the common expression of the Green's second identity.

The special case v = 1 yields the another identity

$$\int_\Omega \Delta u \, dx = \int_{\partial\Omega} \frac{du}{dn} \, dS \tag{4.27}$$

Another special case of interest is v = u. From Eq. (4.43), we then find the energy identity

$$\int_{\Omega} \sum_{i} u_{xi}^2 \, dx + \int_{\Omega} u \, \Delta u \, dx = \int_{\partial\Omega} u \frac{du}{dn} \, dS \qquad (4.28)$$

If $\Delta u = 0$ in Ω and either $u = 0$ or $du / dn = 0$ on $\partial\Omega$, it follows that

$$\int_{\Omega} \sum_{i} u_{xi}^2 \, dx = 0 \qquad (4.29)$$

The above results are valid in either two or three dimensions. To proceed further, we follow the special cases.

4.2.2.3 Green's Representation

One of the principal features of the Laplace equation

$$\Delta u = 0 \qquad (4.30)$$

is its spherical symmetry. The equation is preserved under

rotations about a point ξ, that is under orthogonal linear substitutions for $x - \xi$. This makes it plausible that there exist special solutions $v(x)$ of Eq. (4.30) that are invariant under rotations about ξ, that have the same value at all points at the same distance from ξ. Such solutions would be of the form

$$v = \psi(r) \tag{4.31}$$

where

$$r = |x - \xi| = \sqrt{\sum_i (x_i - \xi_i)^2} \tag{4.32}$$

represents the Euclidean distance between x and ξ. By the chain rule of differentiation we find from Eq. (4.49) in n dimensions that ψ satisfies the ordinary differential equation

$$\Delta v = \psi''(r) + \frac{n-1}{r}\psi'(r) = 0 \tag{4.33}$$

Solving it yields

$$\psi'(r) = Cr^{1-n} \tag{4.34}$$

$$\psi(r) = \begin{cases} \dfrac{Cr^{2-n}}{2-n} & \text{when} \quad n > 2 \quad (a) \\ C \ln r & \text{when} \quad n = 2 \quad (b) \end{cases} \tag{4.35}$$

with C = constant where we can still add a trivial constant solution to ψ.

The function $v(x) = \psi(r)$ satisfies (4.30) for $r > 0$, and for $x \neq \xi$. For a suitable choice of the constant C, v is a fundamental solution for the operator Δ, satisfying the symbolic equation

$$\Delta v = \delta_\xi \tag{4.36}$$

Let $u \in C^2(\bar{\Omega})$ and ξ be a point in Ω. We apply Green's second identity (4.26) with v given by (4.31), (4.35 a,b). Since v is singular at $x = \xi$ we cut out from Ω a sphere $B(\xi, \rho)$ contained in Ω with center ξ, radius ρ, and boundary $S(\xi, \rho)$. The remaining region $\Omega_\rho = \Omega - B(\xi, \rho)$ is bounded by $\partial\Omega$ and $S(\xi, \rho)$. Since $\Delta v = 0$ in Ω_ρ we may have

$$\int_{\Omega_\rho} v \, \Delta u \, dx = \int_{\partial\Omega} \left(v\frac{du}{dn} - u\frac{dv}{dn}\right) dS + \int_{s(\xi,\rho)} \left(v\frac{du}{dn} - u\frac{dv}{dn}\right) dS \tag{4.37}$$

Here on $S(\xi,\rho)$ the "exterior" normal to our region Ω_ρ points towards ξ. Consequently, by (4.34), (4.35), (4.27) we may have

$$v = \psi(\rho), \qquad \frac{dv}{dn} = -\psi'(\rho) \tag{4.38}$$

$$\int_{S(\xi,\rho)} v\frac{du}{dn}\, dS = \psi(\rho) \int_{S(\xi,\rho)} \frac{du}{dn}\, dS = -\psi(\rho) \int_{B(\xi,\rho)} \Delta u\, dx \tag{4.39}$$

$$\int_{S(\xi,\rho)} u\frac{dv}{dn}\, dS = -C\rho^{1-n} \int_{S(\xi,\rho)} u\, dS \tag{4.40}$$

Since both u and Δu are continuous at ξ, the right-hand side of (4.39) tends to 0 for $\rho \to 0$ by (4.35), while that of (4.40) tends to $-C\omega_n u(\xi)$, where ω_n denotes the surface "area" of the unit sphere in $\mathbb{R}^n$. The values $\omega_2 = 2\pi$, $\omega_3 = 4\pi$ are quite familiar for n = 2 and n = 3. Thus Eq.(4.37) becomes for $\rho \to 0$

$$\int_{\Omega_\rho} v\, \Delta u\, dx = \int_{\partial\Omega} (v\frac{du}{dn} - u\frac{dv}{dn})\, dS + C\omega_n u(\xi) \tag{4.41}$$

We now choose C = 1 / ω_n in Eq.(4.35), so that

$$\psi(r) = \begin{cases} \dfrac{r^{2-n}}{(2-n)\,\omega_n} & \text{when} \quad n > 2 \quad (a) \qquad (4.42) \\ \dfrac{\ln r}{2\pi} & \text{when} \quad n = 2 \quad (b) \qquad (4.43) \end{cases}$$

We write the corresponding v in its dependence on x and ξ as

$$v = \Gamma(x,\xi) = \psi(r) = \psi(|x - \xi|) \qquad (4.44)$$

Then Eq.(4.41) may be written as

$$u(\xi) = \int_\Omega \Gamma(x,\xi)\,\Delta u\, dx - \int_{\partial\Omega} \left[\Gamma(x,\xi) \frac{du(x)}{dn_x} - u(x) \frac{d\Gamma(x,\xi)}{dn_x} \right] dS_x \qquad (4.45)$$

for $\xi \in \Omega$, where the subscript "x" in S_x and dn_x indicates the variable of integration respectively differentiation.Eq. (4.45) is also known as Green's representation.

Let $u \in C^2(\bar{\Omega})$ be "harmonic" in Ω, that is, be a

solution of $\Delta = 0$; then by Eq.(4.45) for $\xi \in \Omega$ we may have

$$u(\xi) = -\int_{\partial\Omega} \left[\Gamma(x,\xi) \frac{du(x)}{dn_x} - u(x) \frac{d\Gamma(x,\xi)}{dn_x} \right] dS_x \tag{4.46}$$

Formula (4.46) expressing u in Ω in terms of its Cauchy data u and du / dn_1 on $\partial\Omega$ represents the solution of the Cauchy problem for Ω, provided that such a solution exists.

4.2.3 Models of Heat Transfer without Phase Change

Many natural processes occur at such a slow rate that they can be analyzed in a steady-state form without a large loss in adequate accuracy. The two-dimensional steady-state heat transfer model giving below may be used to approximate non-steady state solutions to heat flow problems involving phase change in the thawing of the permafrost active layer.

4.2.3.1 Domain and Boundary Conditions

Consider a plane surface, $z = 0$, as shown in Fig. 4.3. The temperature on the plane $x < -a$ is T_1, and is T_2 for $-a < x < a$, as well as T_3 for $x > a$.

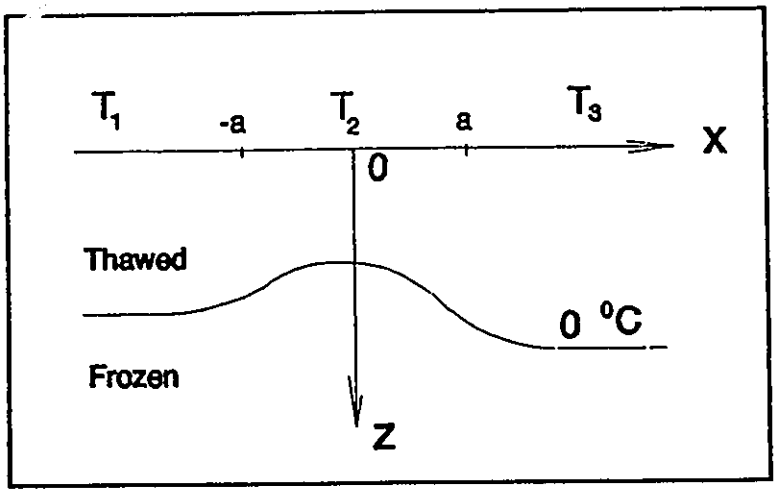

Figure 4.2 Plane Surface with Different Temperature and its Coordinates

This situation at -a<x<a may might represent a wetland surface or the floor of a large building with a temperature different from the adjacent ground surface temperatures.

Consider first the case of three-dimensional heat transfer without phase change. This can be represented by Eq. (4.16), with $\partial\varphi/\partial t = 0$, yielding

$$k_x\frac{\partial^2 T}{\partial x^2} + k_y\frac{\partial^2 T}{\partial y^2} + k_z\frac{\partial^2 T}{\partial z^2} = c\frac{\partial T}{\partial t} \qquad (4.47)$$

For simplicity, we assume freeze and thaw to occur at 0 °C. Then, the domain could be divided into two zones: the

thawed zone and the frozen zone, with the interface temperature being zero. Therefore, at the thawing front we have

$$\frac{\partial T}{\partial t} = 0 \tag{4.48}$$

and the Eq.(4.16) may be reduce to

$$k_x\frac{\partial^2 T}{\partial x^2} + k_y\frac{\partial^2 T}{\partial y^2} + k_z\frac{\partial^2 T}{\partial z^2} = 0 \tag{4.49}$$

It may further be reduced to a two dimensional problem

$$k_x\frac{\partial^2 T}{\partial x^2} + k_z\frac{\partial^2 T}{\partial z^2} = 0 \tag{4.50}$$

with the following surface boundary conditions:

$$\begin{cases} T_{(x,0,0)} = T_1 & -\infty < x < -a \\ T_{(x,0,0)} = T_2 & -a < x < a \\ T_{(x,0,0)} = T_3 & a < x < \infty \end{cases} \tag{4.51}$$

4.2.3.2 Steady State Heat Transfer Model

Consider Eq.(4.50) first, which describes heat transfer in steady state, then suppose that $k_x = k_z = k$ for the time being. It might be reduced to the Laplace equation:

$$\frac{\partial^2 T}{\partial x^2} + \frac{\partial^2 T}{\partial z^2} = 0 \qquad (4.52)$$

The Green function, Eq.(4.46) could be applied to solve the above problem. We can rewrite (4.46) into two dimensional equation, and use T instead of u to fit our common expression

$$T_{(x,z)} = \int_{\partial\Omega} \left[T\frac{\partial \Gamma}{\partial n} - \Gamma\frac{\partial T}{\partial n} \right] dS \qquad (4.53)$$

The boundary conditions of Eq.(4.53) are

$$\begin{cases} \Omega = [\ (x,z) \qquad z \geq 0, \quad -\infty < x < \infty\ ] \\ \left.\dfrac{\partial \Gamma}{\partial n}\right|_{x=-\infty} = \left.\dfrac{\partial \Gamma}{\partial n}\right|_{x=\infty} = \left.\dfrac{\partial \Gamma}{\partial n}\right|_{z=\infty} = 0 \end{cases} \qquad (4.54)$$

The above becomes the Cauchy problem for Laplace equation in domain Ω. It has no solution generally, but for our special

case, we may select a particular Γ function

$$\Gamma = \frac{1}{2\pi} \ln \left[\sqrt{(x-\xi_1)^2 + (z-\xi_2)^2} \; / \; \sqrt{(x-\xi_1)^2 + (z+\xi_2)^2} \right] \tag{4.55}$$

make it to be zero along the boundary $\partial\Omega$ of the domain Ω

$$\Gamma|_{\partial\Omega} = 0 \tag{4.56}$$

Along the boundary, we always have $\partial\Gamma/\partial n = 0$ except for the ground surface segment. In other words $\partial\Gamma/\partial n \neq 0$ only when $z = 0$ and $-\infty < x < \infty$. In this case ds can now be replaced by $d\xi_1$.

$$T_{(x,z)} = \int_{-\infty}^{\infty} T(\xi_1, 0) \; \frac{\partial\Gamma}{\partial n} \; d\xi_1 \tag{4.57}$$

Furthermore

$$\frac{\partial}{\partial n} = -\frac{\partial}{\partial \xi_2} \tag{4.58}$$

and we have

$$\frac{\partial\Gamma}{\partial n}\Big|_{\xi_2=0} = -\frac{\partial\Gamma}{\partial \xi_2}\Big|_{\xi_2=0} = \frac{1}{\pi} \; \frac{z}{(x-\xi_1)^2+z^2} \tag{4.59}$$

Substituting into Eq.(4.57), we have

$$T_{(x,z)} = \frac{1}{\pi} \int_{-\infty}^{\infty} \frac{T(\xi_1, 0)\ z}{(x-\xi_1)^2 + z^2}\ d\xi_1 \qquad (4.60)$$

Introducing heterogeneous materials for different vertical segments, the condition at the thawing front, z = h, is

$$T_{(x,h)} = \frac{1}{\pi k_{(x)}} \int_{-\infty}^{\infty} \frac{k(\xi)\ T_0(\xi)\ h_{(x)}}{(x-\xi)^2 + h_{(x)}^2}\ d\xi \qquad (4.61)$$

Here, ξ_1 is replaced by ξ for simplicity of presentation; and $T = T_0$ at $\xi_2 = 0$. For the maximum thawing depth modeling of the season we have $h = h_{max}$ and the following boundary conditions:

$$T_0(\xi) = \begin{cases} T_1 & -\infty < \xi < -a \\ T_2 & -a < \xi < a \\ T_3 & a < \xi < \infty \end{cases} \qquad (4.62)$$

for temperatures at the ground surface, and

$$k(\xi) = \begin{cases} k_1 & -\infty < \xi < -a \\ k_2 & -a < \xi < a \\ k_3 & a < \xi < \infty \end{cases} \qquad (4.63)$$

for thermal conductivities. Equation (4.61) can now be employed to model the thermal state of the active layer under steady state conditions.

4.2.3.3 Unsteady State Heat Transfer Model

Unsteady state heat transfer may be classified as follows

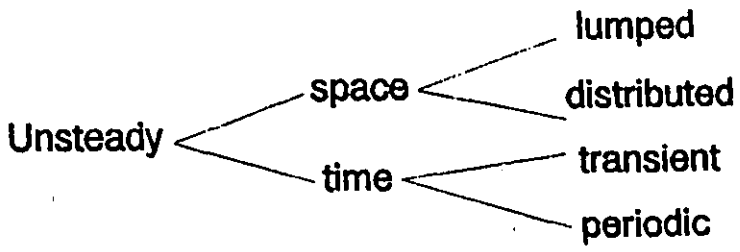

Lumping a space coordinate eliminates it from the analysis and thus leads to an initial value problem (conditions specified at any location), whereas the distributed parameter approach leads to an initial value-

boundary problem. Here we are more concerned with the time aspect, which may be solved by Green's theorem. Consider the two dimensional form of equation (4.47):

$$k_x\frac{\partial^2 T}{\partial x^2} + k_z\frac{\partial^2 T}{\partial z^2} = c\frac{\partial T}{\partial t} \qquad (4.64)$$

The unsteady state heat transfer process could be supposed to be the composite of many steady state heat transfer proceeding in small time steps. Each step should satisfy Eq. (4.64), (4.48) at the thawing front and could be modeled by

$$k_x\frac{\partial^2 T}{\partial x^2} + k_z\frac{\partial^2 T}{\partial z^2} = 0 \qquad (4.50)$$

We could solve this equation by Green's function as steady state for every steps and we also could have the solutions as

$$T_{(x,h)} = \frac{1}{\pi k_{(x)}} \int_{-\infty}^{\infty} \frac{k(\xi)\ T_0(\xi)\ h_{(x)}}{(x-\xi)^2 + h_{(x)}^2}\ d\xi \qquad (4.65)$$

However, ground thaw is not really subject to steady state

heat transfer. We find that, in summer, thawing front development proceeds differently at various ground segments, and it changes in different time periods. That means that h should be a function of both space and time, so that equation (4.65) may be rewritten as

$$T_{(x,h(x,t))} = \frac{1}{\pi\ k_{(x,h(x,t))}} \int_{-\infty}^{\infty} \frac{k(\xi, h_{(x,t)})\ T_0(\xi, t)\ h_{(x,t)}}{(x-\xi)^2 + h_{(x,t)}^2}\ d\xi \tag{4.66}$$

and could serve as an equivalent solution for unsteady state heat transfer at the thawing front of the active layer in a continuous permafrost environment.

Consider three adjacent segments, labelled a, b and c which correspond to 1, 2 and 3 in the section 4.2.3.1. Domain and Boundary Conditions, and assume that a weighted average k is applicable to the thawed zone such that k(x,z,t) = k(x,t). At the thawing front we have

$$T_{(x,h)} = \frac{1}{\pi\ k(x,t)} \left[\int_{-\infty}^{-a} \frac{k(a,t)\ T_a\ h}{(x-\xi)^2 + h^2}\ d\xi + \int_{-a}^{a} \frac{k(b,t)\ T_b\ h}{(x-\xi)^2 + h^2}\ d\xi + \int_{a}^{\infty} \frac{k(c,t)\ T_c\ h}{(x-\xi)^2 + h^2}\ d\xi \right] \tag{4.67}$$

with h = h(x,t). Samilarly for two adjacent segments, we may have

$$T_{(x,h)} = \frac{1}{\pi\, k(x,t)} \left[\int_{-\infty}^{0} \frac{k(a,t)\; T_a\, h}{(x-\xi)^2 + h^2}\, d\xi + \int_{0}^{\infty} \frac{k(b,t)\; T_b\, h}{(x-\xi)^2 + h^2}\, d\xi \right] \tag{4.68}$$

4.2.4 Model of Heat Transfer with Phase Change

The question of phase change cannot be ignored in thermal models for permafrost (Smith 1977, Brown 1978, Sheppard et al. 1978, Lachenbruch 1982). A simple representation of the system is that it consists of a thawed and a frozen zone separated by a phase change interface, or a phase change region, which is at the phase change (fusion) temperature. The duration when the phase change temperature remains at this region is dependent mainly on the soil properties, the ice content, the hydrologic conditions of the system and the ground heat fluxes.

4.2.4.1 General Expression

In general, and certainly for permafrost, the thermal properties of the frozen and unfrozen regions are different,

they are the functions of soil composition, moisture distribution, and boundary temperature. The two dimensional unsteady state heat transfer with phase change could be expressed

$$k_x\frac{\partial^2 T}{\partial x^2} + k_z\frac{\partial^2 T}{\partial z^2} = C\frac{\partial T}{\partial t} + \lambda\frac{\partial \varphi}{\partial t} \qquad (4.69)$$

Here we place our emphases on the surface temperature, the thawing front change, the heat flux consumption and the effects of hydrologic properties.

4.2.4.2 Apparent Temperature

Under thawing conditions, heat flux at the frost table is considered to be consumed in two parts. One part is to increase the heat storage and to raise the ground temperature and the other is taken up by phase change of soil moisture, from ice to water. This could be expressed as

$$q = q_i + q_{ii} \qquad (4.70)$$

where q is the total heat flux across the thawing front

q_i is the heat flux used for increasing the soil

temperatures

q_{ii} is the heat flux used for soil moisture phase change,

According to Fourier's law, Eq.(4.1), we may have

$$q = -kA \frac{\Delta T}{\Delta z} \tag{4.71}$$

As temperature at the thawing front is zero, we have

$$\begin{cases} \Delta T = T \\ \Delta Z = h_z \end{cases} \tag{4.72}$$

and we may rewrite equation (4.71) as

$$q = -kA \frac{T}{h_z} \tag{4.73}$$

In a similar manner, we may have

$$q_i = -kA \frac{T_i}{h_z} \tag{4.74}$$

and

$$q_{ii} = -kA \frac{T_{ii}}{h_z} \qquad (4.75)$$

Put q, q_i and q_{ii} into equation (4.70), we may have

$$T_s = T_i + T_{ii} \qquad (4.76)$$

where T is the ground temperature

T_i is one part of the ground temperature used for increasing soil energy and develop thawing depth

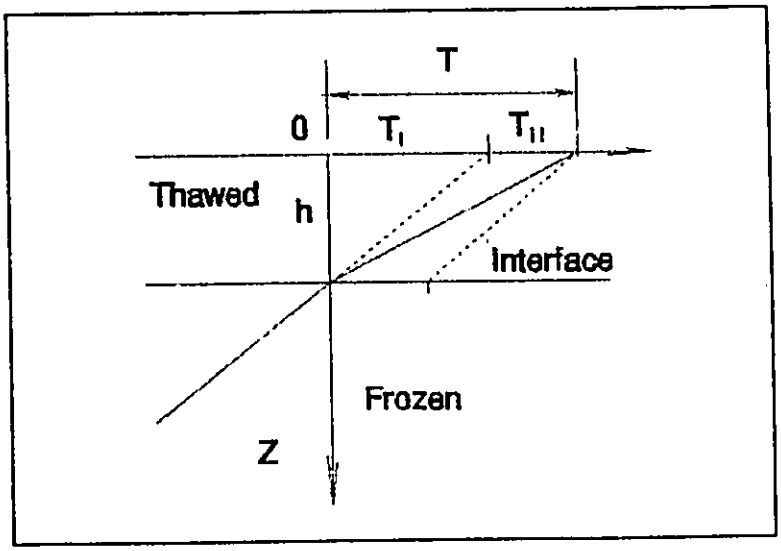

Figure 4.3 Temperature Distribution Crossing Thawing Front

T_{ii} is the other part of the ground temperature used for soil moisture phase change from ice to water

Figure (4.3) provides a schematic illustration on the temperature profile.

4.2.4.3 The Equivalent Solution

If we use apparent temperature T^* instead of T, it is possible to simplify Eq.(4.69) to an equation equivalent to heat transfer without phase change problems

$$k_x \frac{\partial^2 T^*}{\partial x^2} + k_z \frac{\partial^2 T^*}{\partial z^2} = C \frac{\partial T^*}{\partial t} \qquad (4.77)$$

where

$$T_s^* = T_i = T - T_{ii} \qquad (4.78)$$

$$T_{ii} = \frac{L\, h^2}{2kt} \qquad (4.79)$$

Equation (4.79) is the Stefan's equation with L being the total latent heat need to thaw the frozen soil. The latent heat of fusion is expressed as a function of the amount of ice content

$$L = f_i \lambda \tag{4.80}$$

where λ is latent heat of fusion from ice to water.

f_i is fraction of ice in soil

Equation (4.77) can be solved as a steady state heat transfer problem at the thawing front

$$k_x \frac{\partial^2 T^*}{\partial x^2} + k_z \frac{\partial^2 T^*}{\partial z^2} = 0 \tag{4.81}$$

$$T_{(x,h)} = \frac{1}{\pi k_{(x)}} \int_{-\infty}^{\infty} \frac{k(\xi)\ T_0^*(\xi)\ h_{(x)}}{(x-\xi)^2 + h_{(x)}^2}\, d\xi \tag{4.82}$$

using step by step replacing method to get an equivalent solution

$$T_{(x,h(x,t))} = \frac{1}{\pi\ k_{(x,h(x,t))}} \int_{-\infty}^{\infty} \frac{k(\xi, h_{(x,t)})\ T_0^*(\xi, t)\ h_{(x,t)}}{(x-\xi)^2 + h_{(x,t)}^2}\, d\xi \tag{4.83}$$

where T_0^* is a part of ground surface temperature which contributes to the increase of soil energy for developing thawing depth.

As in the case of the model of transient heat flow without phase change, we can write

$$T_{(x,h)} = \frac{1}{\pi\, k(x,t)} \left[\int_{-\infty}^{-a} \frac{k(a,t)\; T_a^*\; h}{(x-\xi)^2 + h^2}\, d\xi + \int_{-a}^{a} \frac{k(b,t)\; T_b^*\; h}{(x-\xi)^2 + h^2}\, d\xi + \int_{a}^{\infty} \frac{k(c,t)\; T_c^*\; h}{(x-\xi)^2 + h^2} \right] d\xi \tag{4.84}$$

for three adjacent segments, and

$$T_{(x,h)} = \frac{1}{\pi\, k(x,t)} \left[\int_{-\infty}^{0} \frac{k(a,t)\; T_a^*\; h}{(x-\xi)^2 + h^2}\, d\xi + \int_{0}^{\infty} \frac{k(b,t)\; T_b^*\; h}{(x-\xi)^2 + h^2} \right] d\xi \tag{4.85}$$

for two adjacent segments modeling equations.

4.3 Input and Output of the Model

4.3.1 Input

To run the model, two data sets are required. The first data set specifies site conditions, soil properties,

and temperature variations at the simulation period. The second data set specifies the hydrological status and parameters for the duration of the simulation.

Field data collected at a site near Resolute, N.W.T. ($74^0 43'N$, $94^0 59'W$) provided input information. A transect composing a strip of wetland surrounded by gravelly soils was monitored for water table fluctuations and active layer thaw during the summers of 1988 and 1989. These values were used for verification of the model.

4.3.1.1 Thermal and Soil Data

The first data set requires the detailed specification of the simulation site conditions, including dimensions of each soil segment, ground surface soil types, soil structure, profile, composition and properties. It also specifies simulation time period and ground surface temperature variations for different soil segments. From equation (4.84), the temperature at a given point, $T_{(x,h)}$, below the ground surface is influenced by the thermal conditions of three different soil segments. Changes in the surface or subsurface temperatures in any of the segments will change subsurface temperature at the point of calculation. The specified T_i^t, in equation (4.84), is a mean apparent ground surface temperature at certain soil segment i, where i = a, b, or c.

Ground surface temperatures (T_0) are estimated empirically from air temperatures (T_A):

$$T_0 = b_o + b_1 T_A \qquad (4.86)$$

where b_0 and b_1 are empirical coefficients for the linear regression T_A with T_0. Figure (4.4) shows the relationship between air temperature and the surface temperature of gravelly soil area in McMaster river basin, Resolute, N.W.T. Similar analysis was performed for the air temperature and

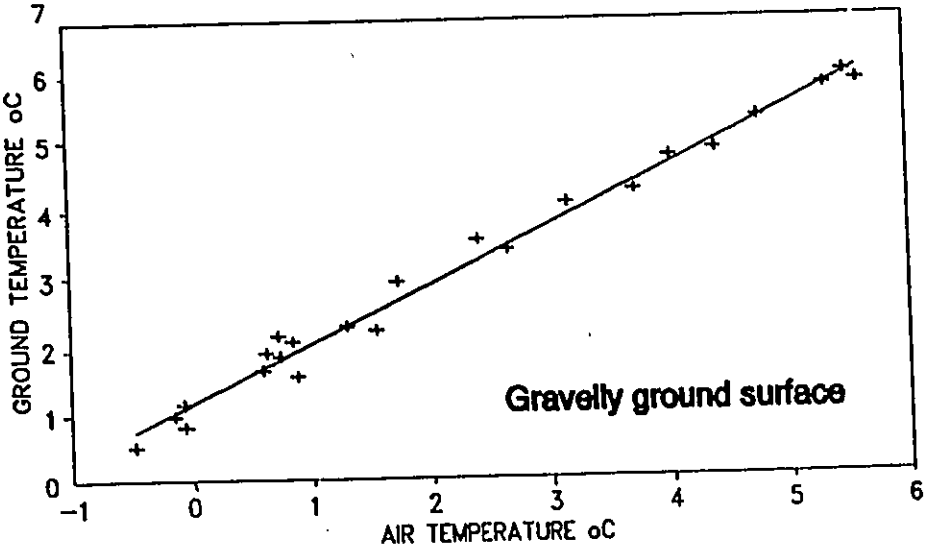

Figure 4.4 Regression of Air Temperature and Surface Temperature for Gravelly Soil

Table 4.1 Relationship between Air Temperature (T_A) and Ground Surface Temperature (T_0)

Soil Type	Gravelly Soil	Peaty Soil
Intercept b_0	1.15	0.87
Slope b_1	1.23	0.90
Correlation	0.99	0.98

surface temperature of peaty soil. In both regressions 23 observations were examined. The correlation coefficients, the slopes and the intercepts of regression are presented in Table (4.1).

Comparing the surface temperatures of the gravelly soil area with those in the peaty soil area, we find that the two surface temperatures could be different under the same air temperature conditions. Figure (4.5) shows the correlation of the surface temperature in gravelly soil area with the one in peaty soil area. The intercept is 0.04, the slope is 1.03 and the correlation coefficient is 0.98. 31 observations were used in this regression.

Soil property, soil structure and profile are very important for selecting hydrological parameters and thermal

parameters of a simulation site. To run the model we need to specify soil type, soil structures and soil profiles of different soil segment first.

At a test site in McMaster river basin, Resolute, N.W.T. three soil segments adjacent to each other were chosen. The middle segment is wet peaty soil, with a continuous cover of masses grasses and sedges. The two side segments are dry and covered with gravelly materials, characterized by a sandy loam soil with gravel, with scattered low lying Arctic plants and with good drainage conditions.

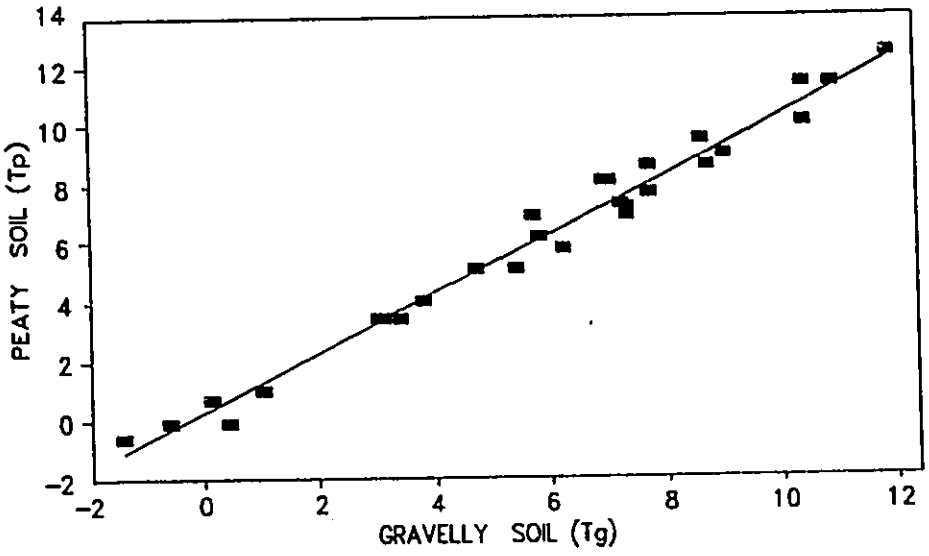

Figure 4.5 The Correlation of the Surface Temperature in Gravelly Soil Area with the Surface Temperature in Peaty Soil Area

The mean values of grain size distributions for samples obtained at 0.2 - 0.3 m below the ground surface are given in Table 4.2. The mean value of obtained soil sample from 0.2 -0.3 m under ground surface were shown in Table 4.2.

Table 4.2 Soil structure and grain size distribution

Clastic Portion	Gravelly Soil	Peaty Soil
Clay %	9	21
Silt %	19	53
Sand %	42	23
Gravel %	30	3

Thermal conductivity could be calculated by using the volumetric fractions of the various components of the soil column of each segment (Ferric 1981, Williams 1982):

$$k = \prod_{i}^{n} k_i^{f_i} \qquad (3.15)$$

where f is volumetric fractions of component

k_i = 2.93 for soil minerals

0.25 organic matter

0.57	water
2.20	ice
0.025	air

The units for k are in $W\ m^{-1}\ {}^{0}C^{-1}$. The estimated fractions of various soil components at 0.15 - 0.20 m depth, as determined for August 15, are listed in Table (2.2).

4.3.1.2 Hydrological Input Data

In the thawed zone, the general soil moisture profile is considered to consist of three sections (Fig.4.6). At the base is the saturated zone with a mean thickness during the thawing period(0,T], determined by averaging the daily differences between the frost table and water table positions (Xia and Woo 1993). In this zone soil moisture content $f_0(w)$ was supposed to be equal to the effective porosity ϕ_e determined by equation (3.17).

$$\begin{aligned} \phi_e &= \phi - f_a \\ &= S_y + S_r \end{aligned} \qquad (3.17)$$

In the middle part, the non-saturated zone, moisture content $f_z(w)$ at depth z, is assumed to decrease linearly upward to reach the specific retention value S_r. Finally, at

the surface zone, the soil moisture $f_0(w)$ equals the specific retention S_r.

$$f_z(w) = \max[\, S_r,\ \phi_e - g(z_s - z)] \qquad (4.87)$$

where z is the depth at the top of the saturated zone

g is the gradient of moisture decrease, being 2 m^{-1} for gravel, 1.5 m^{-1} for fine sand and clay and 1 m^{-1} for peaty soils.

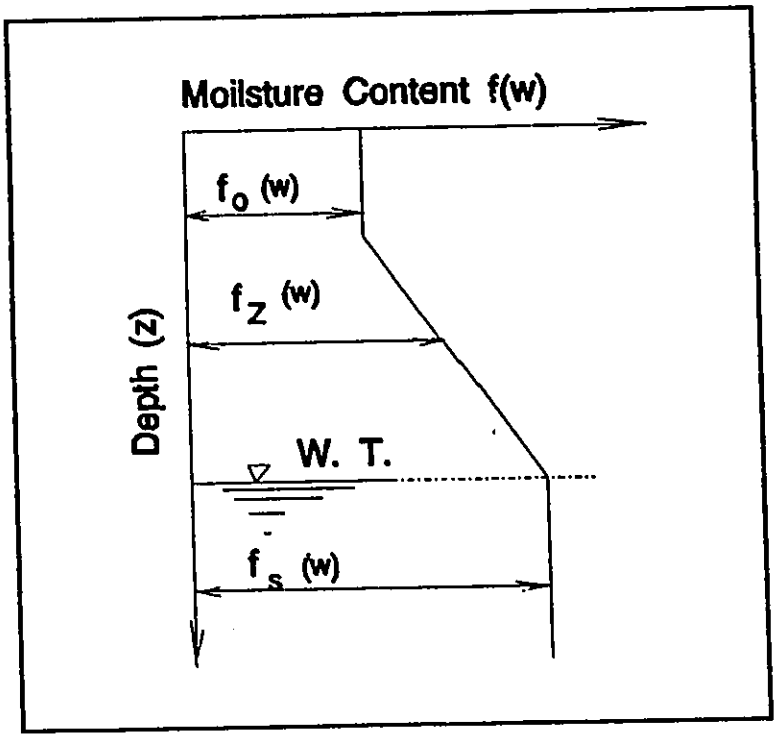

Figure 4.6 Assume Moisture Content Profile Above and Below the Suprapermafrost Water Table

The soil ice content profile is taken as the moisture content frozen at the beginning of the past winter. The zone saturated with ice is obtained by the difference between the water table and frost table at the end of the previous summer season.

4.3.2 Output

The model yields two possible outputs: the thawing front profile at a certain time period, and the maximum or minimum thawing depth for any position in a three adjacent soil segment simulation site.

4.3.2.1 Thawing Front Profile

Integrating equation (4.84) yields:

$$T_{(x,h)} = \frac{T_a^*}{\pi\, k(x,t)}\, k(a,t)\; arctg\; \frac{\xi_1 - x}{h}\Big|_{-\infty}^{-a} + \frac{T_b^*}{\pi\, k(x,t)}\, k(b,t)\; arctg\; \frac{\xi_1 - x}{h}\Big|_{-a}^{a} + \frac{T_c^*}{\pi\, k(x,t)}\, k(c,t)\; arctg\; \frac{\xi_1 - x}{h}\Big|_{a}^{+\infty} \tag{4.88}$$

This can be rewritten as

$$T_{(x,h)} = \begin{cases} \dfrac{T_a^*}{\pi\, k(x,t)}\, k(a,t)\, \left[\, \dfrac{\pi}{2} - arctg\, \dfrac{a+x}{h}\, \right] + \\ \dfrac{T_b^*}{\pi\, k(x,t)}\, k(b,t)\, \left[\, arctg\, \dfrac{a-x}{h} + arctg\, \dfrac{a+x}{h}\, \right] + \\ \dfrac{T_c^*}{\pi\, k(x,t)}\, k(c,t)\, \left[\, \dfrac{\pi}{2} - arctg\, \dfrac{a-x}{h}\, \right] \end{cases} \tag{4.89}$$

here h = h(x,t), and

$$T^* = T_i = T - T_{ii} \tag{4.78}$$

$$T_{ii} = \frac{L\, h^2}{2kt} \tag{4.79}$$

If two instead of three soil segments we used, the following equation will replace Eq. (4.89).

$$T_{(x,h)} = \begin{array}{l} \dfrac{T_a^*}{\pi\, k(x,t)}\, k(a,t)\, \left[\, \dfrac{\pi}{2} - arctg\, \dfrac{x}{h}\, \right] + \\ \dfrac{T_b^*}{\pi\, k(x,t)}\, k(b,t)\, \left[\, \dfrac{\pi}{2} + arctg\, \dfrac{x}{h}\, \right] \end{array} \tag{4.90}$$

To equations (4.89) or (4.90), if the temperature at thawing front T(x,t) = 0, the thawing depth h and distance x

has an implicit relationship. This can be seen by considering equations (4.84), (4.78) and (4.79).

The thawing depth h is a function of surface temperature T, thermal conductivity k, latent heat L, and the temperature at thawing front T(x,h). However, the computation of thermal conductivity k, latent heat of fusion L, and the temperature at thawing front T(x,h) also depend on the position of the thawing depth h. To solve for this implicit function, optimization procedure is required.

First set the temperature at thawing front T(x,h) to 0, and this is always true. Then, we assume a thawing depth h, and calculate k, L, and a new value of T(x,h), we check whether T(x,h) = 0. If not, the thawing depth is changed again and the processes is repeated until T(x,h) converges to 0. Then h is the depth required. The entire procedure can be performed easily in spread sheet format.

4.3.2.2 Maximum or Minimum Thawing Depth

As the thawing front profile is a continuous smooth curve, it must have a maximum or minimum value which could be fit the function of thawing depth with corresponding ground surface distance in a simulation site.

The position of the thawing front along the profile is

a function of the horizontal distance from the centre of the middle segment, thermal conductivity, latent heat of fusion, and duration of thaw as well as their ground surface temperatures; or h(x, k, L, t). The essential condition for having maximum or minimum thawing depth is

$$\begin{cases} \dfrac{\partial h}{\partial x} = 0 \\ h(x_0) = h_{max} \end{cases} \tag{4.91}$$

where x_0 is the x coordinate value which is the solution of the equation h' = 0.

h_{max} is the maximum thawing depth in the thawing front profile of a active layer

We may consider equation (4.89) first. Thermal conductivity is a function of soil material, soil composition, and soil moisture content and distribution, all of which are functions of distance x and time period t.

$$k(x,t) = \begin{cases} k(a,t) & -\infty < x < -a \\ k(b,t) & -a < x < a \\ k(c,t) & a < x < \infty \end{cases} \tag{4.92}$$

For three segment simulation, if the maximum or

minimum value of thawing depth occurs in the middle segment, we may have

$$T_{(x,h)} = \begin{cases} \dfrac{T_a^*}{\pi\, k(b,t)}\, k(a,t)\ \left[\ \dfrac{\pi}{2} - arctg\ \dfrac{a+x}{h}\ \right] + \\ \dfrac{T_b^*}{\pi}\ \left[\ arctg\ \dfrac{a-x}{h} + arctg\ \dfrac{a+x}{h}\ \right] + \\ \dfrac{T_c^*}{\pi\, k(b,t)}\, k(c,t)\ \left[\ \dfrac{\pi}{2} - arctg\ \dfrac{a-x}{h}\ \right] \end{cases} \tag{4.93}$$

To simplify equation (4.93), let

$$\begin{cases} a_i = \dfrac{T_a^*}{\pi\, k(b,t)}\, k(a,t) \\ a_{ii} = \dfrac{T_b^*}{\pi} \\ a_{iii} = \dfrac{T_c^*}{\pi\, k(b,t)}\, k(c,t) \end{cases} \tag{4.94}$$

then write equation (4.93) as

$$T_{(x,h)} = \begin{cases} a_i\ \left[\ \dfrac{\pi}{2} - arctg\ \dfrac{a+x}{h}\ \right] + \\ a_{ii}\ \left[\ arctg\ \dfrac{a-x}{h} + arctg\ \dfrac{a+x}{h}\ \right] + \\ a_{iii}\ \left[\ \dfrac{\pi}{2} - arctg\ \dfrac{a-x}{h}\ \right] \end{cases} \tag{4.95}$$

Obtain derivative of thawing depth h, from equation (4.94), and we have

$$\frac{-a_i\, h}{h^2 + (a + x)^2} - \frac{a_{ii}\, h}{h^2 + (a - x)^2} + \frac{a_{ii}\, h}{h^2 + (a + x)^2} + \frac{a_{iii}\, h}{h^2 + (a - x)^2} = \left[- \frac{a_i\, (a + x)}{h^2 + (a + x)^2} + \frac{a_{ii}\, (a - x)}{h^2 + (a - x)^2} + \frac{a_{ii}\, (a + x)}{h^2 + (a + x)^2} - \frac{a_{iii}\, (a - x)}{h^2 + (a - x)^2} \right] h' \tag{4.96}$$

For the above equation, the basic condition for h' = 0, is

$$\frac{-a_i\, h}{h^2 + (a + x)^2} - \frac{a_{ii}\, h}{h^2 + (a - x)^2} + \frac{a_{ii}\, h}{h^2 + (a + x)^2} + \frac{a_{iii}\, h}{h^2 + (a - x)^2} = 0 \tag{4.97}$$

Solve equation (4.97), and one solution is

$$h = 0 \tag{4.98}$$

It means that no thawing occurs. Theoretically, this is a

minimum thawing depth, but it is not the solution required. The other solution is

$$\frac{-a_i}{h^2 + (a + x)^2} - \frac{a_{ii}}{h^2 + (a - x)^2} + \frac{a_{ii}}{h^2 + (a + x)^2} + \frac{a_{iii}}{h^2 + (a - x)^2} = 0 \tag{4.99}$$

and we have

$$- a_i [h^2 + (a - x)^2] - a_{ii} [h^2 + (a + x)^2] + a_{ii} [h^2 + (a - x)^2] + a_{iii} [h^2 + (a + x)^2] = 0 \tag{4.100}$$

Then,

$$a_{iii} [h^2 + (a + x)^2] - a_i [h^2 + (a - x)^2] - 4a_{ii}ax = 0 \tag{4.101}$$

To simplify equation (4.101), let

$$\begin{cases} \omega_1 = -a_i + a_{iii} \\ \omega_2 = 2a_ia - 4a_{ii}a + 2a_{iii}a \\ \omega_3 = -a_ia^2 - a_ih^2 + a_{iii}a^2 + a_{iii}h^2 \end{cases} \tag{4.102}$$

then

$$\omega_1 x^2 + \omega_2 x + \omega_3 = 0 \qquad (4.103)$$

Equation (4.103) can be solved to find the point of maximum or minimum thaw. Two possibilities arise:

1) $\omega_1 = 0$ and we have

$$x = -\frac{\omega_3}{\omega_2} \qquad (4.104)$$

Theoretically, it is a point of extreme value, but commonly, it does not fit the three segment thermal state modeling under natural conditions.

2) $\omega_1 \neq 0$ and we may have three different cases

i. $\omega_2^2 - 4\omega_1\omega_3 < 0$

Equation (4.103) has no solution, it means that the extreme value does not lie in the middle part of the simulation site.

ii. $\omega_2^2 - 4\omega_1\omega_3 = 0$

There is a only point of extreme value,

$$x = -\frac{\omega_3}{2\omega_1} \qquad (4.105)$$

It could be the maximum or minimum depth of the thawing front along the profile

iii. $\omega_2^2 - 4\omega_1\omega_3 > 0$

There are two solutions which are extreme values on a thawing front

$$x = \frac{-\omega_2 \pm \sqrt{\omega_2^2 - 4\omega_1\omega_3}}{2\omega_1} \qquad (4.106)$$

We have to select one solution which fits for the thawing front profile as a maximum or a minimum value according to its physical meaning.

One consideration is that the x value calculated above still is a function of thawing depth h. It is necessary to put the x value back to the original equation (4.95) for calculating the thawing depth h. After that we put the calculated h value into equation (4.97) recalculate the distance x_0 again. Using this recalculated x_0 value which is the x-coordinate of the extreme value of a thawing front

profile, we get the maximum or minimum thawing depth h_{max} or h_{min} from equation (4.95). We then have

$$0 = \begin{cases} a_i \left[\frac{\pi}{2} - arctg \frac{a + x_0}{h_{max}} \right] + \\ a_{ii} \left[arctg \frac{a - x_0}{h_{max}} + arctg \frac{a + x_0}{h_{max}} \right] + \\ a_{iii} \left[\frac{\pi}{2} - arctg \frac{a - x_0}{h_{max}} \right] \end{cases} \qquad (4.107)$$

Mathematically, equation (4.95) has no derivative at the points x = -a and x = a, and we could not use the above method to find the extreme value of thawing depth at these two points. Thus, we have to calculate them individually, and compare them with the extreme values computed with above procedure. Eventually, we may get the maximum or minimum thawing depth of the entire simulation profile which would match their physical meaning and geographical conditions.

4.4 Model Testing

The model was applied to a transect in the continuous permafrost area near Resolute, N.W.T. (74°43'N, 94°59'W). The 34 m transect consisted of a gravel segment and a segment

with peaty soil cover, and their stratigraphy has been given in Figure 2.13.

This site was chosen because of the availability of frost and water table measurements for seven summers (Woo and Steer 1983). Two water table wells, one in the gravel and the other in peaty materials, provided inputs for moisture profile estimation. Air temperatures from the nearby Resolute weather station allowed estimations of ground temperatures using equation (4.86) in the model testing. In addition, frost tables were monitored at five points along the transect to allow verification of model results.

4.4.1 Modeling Procedures

Mean ground surface temperature and mean thickness of the saturated zone for both soil types were calculated over periods of 15, 35 and 55 days from the beginning of thaw in 1988 and 1989. The initial ice contents were estimated from the water table positions for the end of the previous summers. The thawing depths (h) along the transect (x) for the test periods of various durations were obtained by an optimization method such that the right-hand-side of equations (4.89) and (4.90) could satisfy the condition of $T(x,h) = 0$.

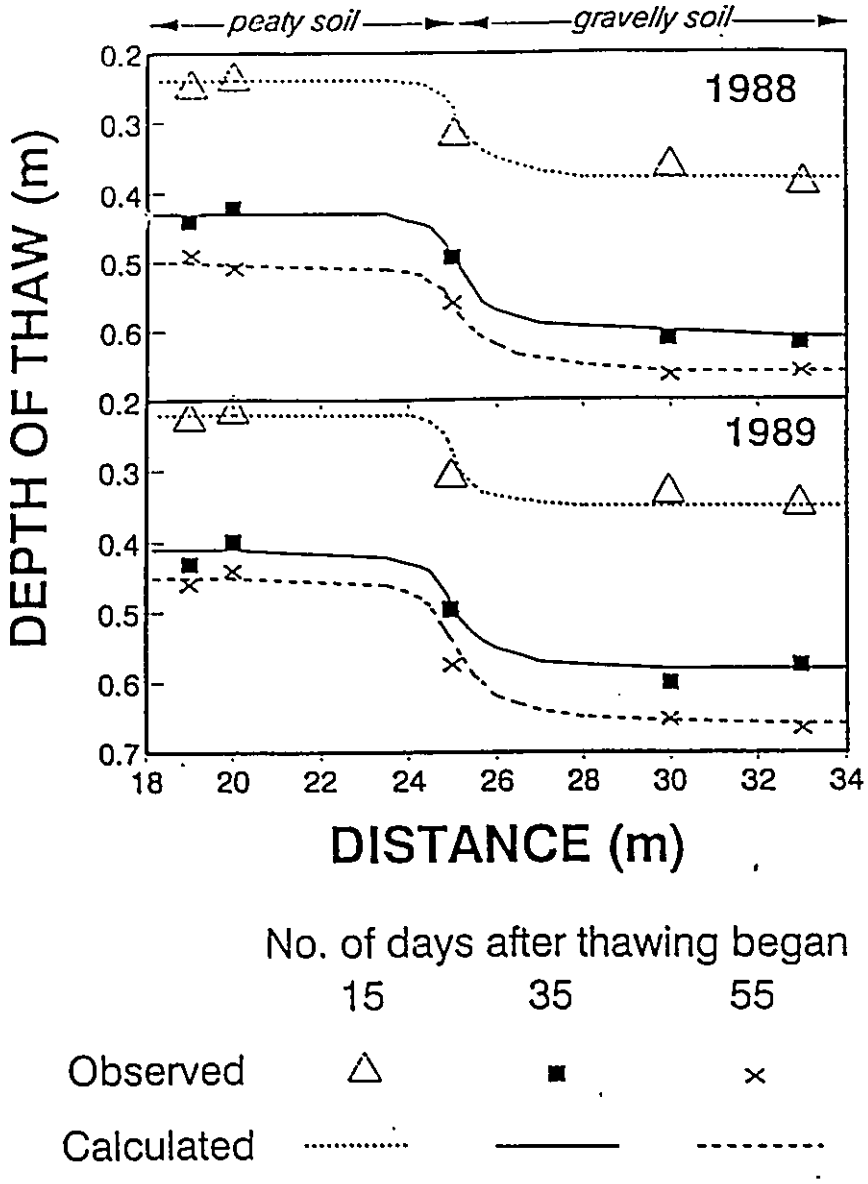

Figure 4.7 Calculated and Measured Frost Table Positions along the Transect, Resolute, 1988 and 1989.

4.4.2 Modelling Results

Figure (4.7) showed the part of the transect adjacent to the border between the gravel and the peaty soils. Comparison of the calculated frost table positions (which appear as lines in Fig. 4.7) with the observed values (symbols in Fig. 4.7) suggests that the model results were close to the field data for the three time periods during the two years of model testing. The root-mean square error estimation method

$$RMSE = [\, N^{-1} \sum_{i=1}^{N} (P_i - O_i)^2 \,]^{0.5} \qquad (3.26)$$

was employed to the model testing. The calculated root-mean square error from all the points was 0.014 m in 1988 and 0.017 m in 1989.

Experiments were performed to determine the sensitivity of active layer thaw to varying degrees of soil saturation, ice content and air temperature conditions.

Maximum, mean and minimum values were extracted from water level records obtained over seven years at the Resolute experimental site to estimate the saturated moisture content and the ice content for the wettest, average and driest

summers. These variables were combined with the warmest, the average and the coolest summers (55 days of the thawed season) reported by the Resolute weather stations to estimate the thawing responses. Table (4.3) shows the input variables of the modeled sensitivity of ground thaw to temperature, moisture and ice contents. Table (4.4) and (4.5) are the output of the modeled active layer thaw to varying degrees of soil saturation, ice content and air temperature conditions.

The calculated model results show that while thaw depth is controlled by temperatures, it is also significantly

Table 4.3 The input variables of Modeled Sensitivity

Soil Type	Summer Temperature (^{0}C)	Saturated Zone Thickness (m)	Ice-rich Zone Thickness (m)
Gravelly Soil			
Maximum	6.62	0.40	0.39
Average	4.35	0.22	0.23
Minimum	2.24	0.04	0.04
Peaty Soil			
Maximum	6.88	0.43	0.42
Average	4.53	0.26	0.29
Minimum	2.35	0.10	0.09

Table 4.4 The Output Variables in Gravelly Soil Segment (thawed depth in m)

Temperature	Max.	Avg.	Min.
Saturated Zone: Max.	0.81	0.67	0.49
Avg.	0.76	0.62	0.45
Min.	0.71	0.57	0.40
Ice-rich Zone: Max.	0.72	0.58	0.42
Avg.	0.76	0.62	0.45
Nub,	0.81	0.67	0.49

Table 4.5 The Output Variables in Peaty Soil Segment (thawed depth in m)

Temperature	Max.	Avg.	Min.
Saturated Zone: Max.	0.59	0.46	0.35
Avg.	0.55	0.42	0.32
Min.	0.48	0.39	0.27
Ice-rich Zone: Max.	0.50	0.39	0.26
Avg.	0.55	0.42	0.32
Nub,	0.62	0.51	0.37

affected by the thickness of the saturated zone and by the thickness of the zone saturated with ice.

Given similar summer temperature, a thick saturated zone will enhance thawing due to higher thermal conductivity value relative to the dry soil; but a large ice content in the soil will retard frost table descent as more heat is needed in ice melt. Theses experiments demonstrated the hydrological influence on ground thaw.

Figure (4.8) and (4.9) showed the patterns of the frost table change caused by the sensitivity of ground thaw to temperature, moisture and ground ice contents.

The above experiments showed that the frost table position within the active layer is highly sensitive to both the temperature conditions and the hydrological status of the soils. Thus, in terms of permafrost responses to climate warming, it is necessary to consider the wetting or drying scenarios that accompany temperature changes.

4.5 Theoretical Analysis of Model Application

The Xia model can be applied to both scientific and engineering problems. In scientific research, it could be used in modeling the effects of climate warming and

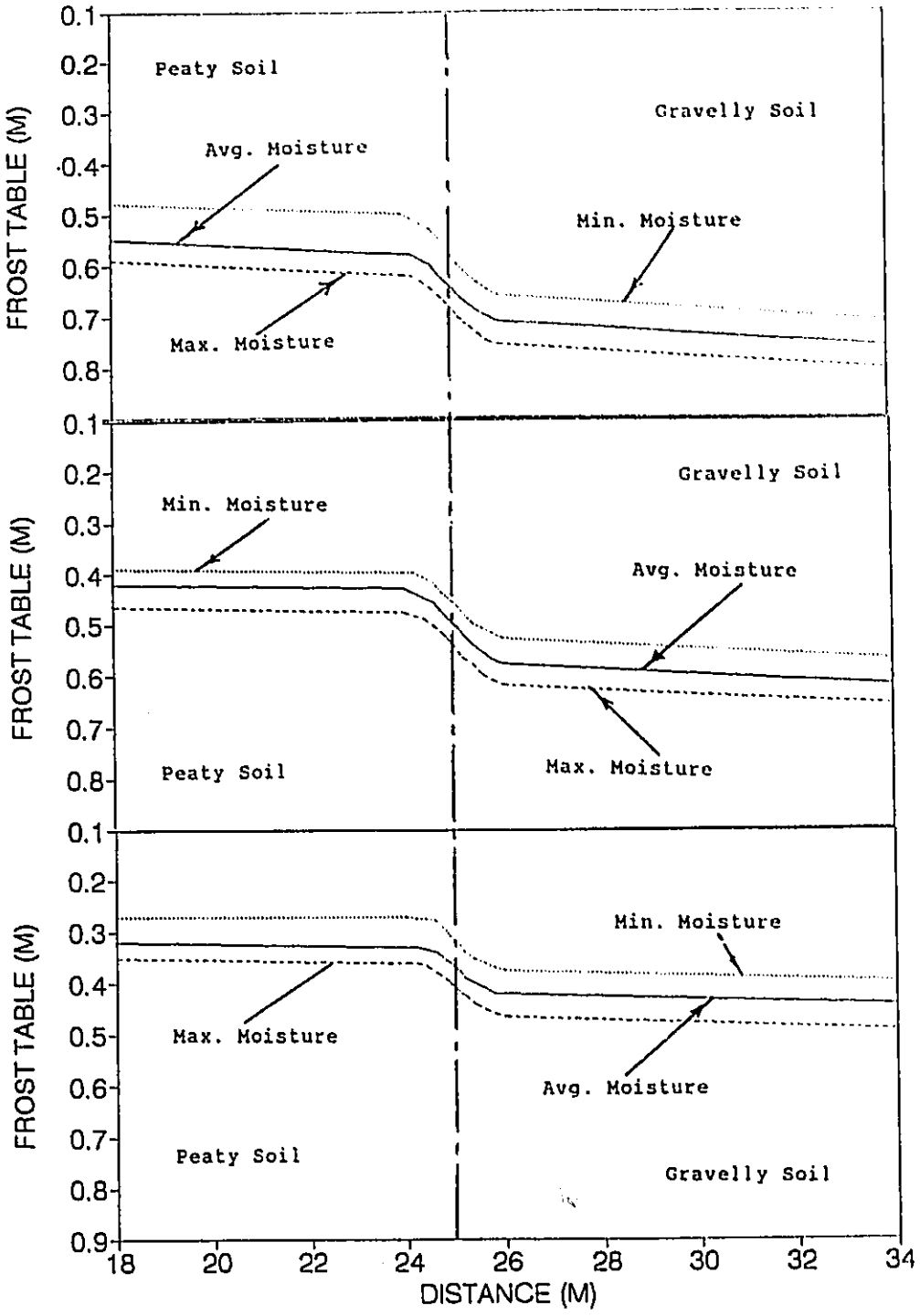

Figure 4.8 The Sensitivity of Ground Thaw to Temperature and Soil Moisture, Above is Modeled with Max. T., Meadle with Avg. T. and Below with Min. T.

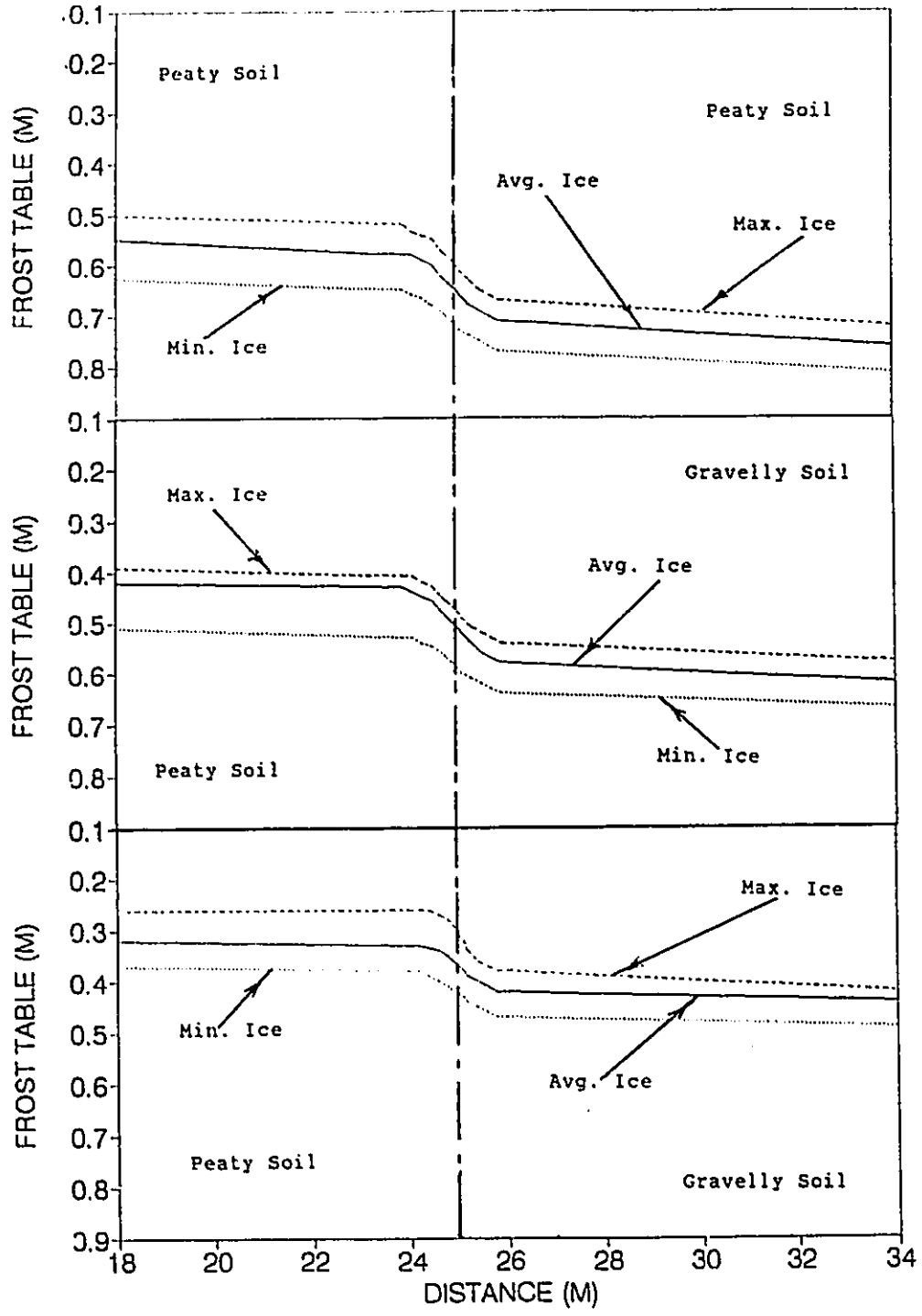

Figure 4.9 The Sensitivity of Ground Thaw to Temperature and Ice Content, Above is Modeled with Max. T., Meadle with Avg. T. and Below with Min. T.

environment change, as is exemplified by the above sensitivity experiment for the Resolute site. In engineering, it could be applied to various fields of civil engineering, hydraulic engineering and agricultural engineering. Examples of such applications are given below.

4.5.1 Thawing Depth at Geometrical Characteristic Points

In many civil engineering applications, it is not necessary to know the whole profile of the thawing front. For

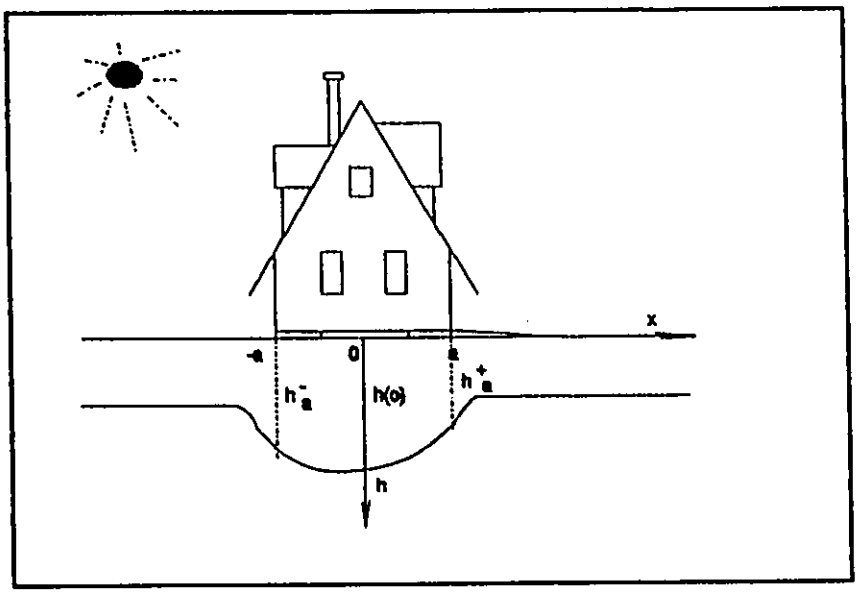

Figure 4.10 Thawing Depth at Building Characteristic Points

example, in designing a house or a road in the continuous permafrost environment, four basic points are enough for considering the permafrost thawing effects, including the maximum thawing depth under the structure, thawing depth in the middle of the house or road, and thawing depths on both edges of the house or the road. These points are identified in Figure (4.10) in relation to the structure above ground.

The computation of the maximum or minimum thawing depth has already been discussed. Now we focus on the computation of the other three points.

All these three characteristic points are located in the middle segment, with one at the center, other two at the each ends of the segment. We assume that the thermal conductivity $k_{(x,t)}$ is equal to $k_{(b,t)}$. Then these thawing depths could be computed by equation (4.108) with $T_{(x,t)} = 0$. We may have

$$0 = \begin{cases} \dfrac{T_a^*}{\pi\, k(b,t)}\, k(a,t)\ \left[\ \dfrac{\pi}{2} - arctg\ \dfrac{a+x}{h}\ \right] + \\ \dfrac{T_b^*}{\pi}\ \left[\ arctg\ \dfrac{a-x}{h} + arctg\ \dfrac{a+x}{h}\ \right] + \\ \dfrac{T_c^*}{\pi\, k(b,t)}\, k(c,t)\ \left[\ \dfrac{\pi}{2} - arctg\ \dfrac{a-x}{h}\ \right] \end{cases} \tag{4.108}$$

The thawing depth at the center of the middle soil segment is h(0), with x = 0, and we have

$$h_{(0)} = a\ Ctg\ [\ \frac{\pi}{2}\ \frac{T_a^* \frac{k_{(a,t)}}{k_{(b,t)}} + T_c^* \frac{k_{(c,t)}}{k_{(b,t)}}}{T_a^* \frac{k_{(a,t)}}{k_{(b,t)}} + T_c^* \frac{k_{(c,t)}}{k_{(b,t)}} - 2T_b^*}\ ] \qquad (4.109)$$

The thawing depths at either side of the middle soil segment, will be

$$h_{(-a)} = 2a\ Ctg\ [\ \frac{\pi}{2}\ \frac{T_a^* \frac{k_{(a,t)}}{k_{(b,t)}} + T_c^* \frac{k_{(c,t)}}{k_{(b,t)}}}{T_c^* \frac{k_{(c,t)}}{k_{(b,t)}} - T_b^*}\ ] \qquad (4.110)$$

for the left edge with x = - a, and

$$h_{(a)} = 2a\ Ctg\ [\ \frac{\pi}{2}\ \frac{T_a^* \frac{k_{(a,t)}}{k_{(b,t)}} + T_c^* \frac{k_{(c,t)}}{k_{(b,t)}}}{T_a^* \frac{k_{(c,t)}}{k_{(b,t)}} - T_b^*}\ ] \qquad (4.111)$$

for the right edge with x = a.

In some of cases, especially for house and road construction, the two sides of the soil segments may have

similar soil characteristics, and even their soil moisture and hydrological conditions may be same. Thus,

$$k_{(a,t)} = K_{(c,t)} = k_{(t)} \tag{4.112}$$

For this special case, equations (4.109), (4.110) and (4.111) can be simplified to

$$h_{(0)} = a\ Ctg\ \left[\ \frac{\pi}{2}\ \frac{\frac{T_a^* + T_c^*}{2}}{\frac{T_a^* + T_c^*}{2} - T_b^*\ \frac{k_{(b,t)}}{k_{(t)}}}\ \right] \tag{4.113}$$

for the geometric center,

$$h_{(-a)} = a\ Ctg\ \left[\ \frac{\pi}{2}\ \frac{T_a^* + T_c^*}{T_c^* - \frac{k_{(b,t)}}{k_{(t)}}\ T_b^*}\ \right] \tag{4.114}$$

for the left hand side and for right side it is

$$h_{(a)} = a\ Ctg\ \left[\ \frac{\pi}{2}\ \frac{T_a^* + T_c^*}{T_a^* - \frac{k_{(b,t)}}{k_{(t)}}\ T_b^*}\ \right] \tag{4.115}$$

4.5.2 Thawing Front Profile under the Middle Soil Segment

Another example is to consider the depth of thaw beneath a sluice gate built in permafrost area. The engineers have to consider both the thawing front profile and the maximum thawing depth under the middle soil segment as they strongly affect the sluice gate stability and its seepage control.

The governing equation for the sluice foundation stability is

$$\begin{cases} \sum F(x) = 0 \\ \sum F(z) = 0 \\ \sum M(y) = 0 \end{cases} \tag{4.116}$$

and for the seepage control, we consider

$$Q_w = A_{min}\, k_H \frac{\Delta H}{\Delta L} \tag{4.117}$$

Here $\Sigma F(x)$ is the sum of forces along x axial direction

$\Sigma F(z)$ is the sum of forces along z axial direction

$\Sigma M(y)$ is the sum of momentums in xz plane

Q_w is minimum seepage water under a sluice gate

A_{min} is the minimum seepage section area

k_w is hydraulic conductivity

$\Delta H / \Delta L$ is slope of the seepage flow under sluice gate.

It is important to determine the thawing front profile and the maximum or minimum thawing depth under the middle soil segment. Let us assume that the following curve could fit the thawing front profile under the middle soil segment.

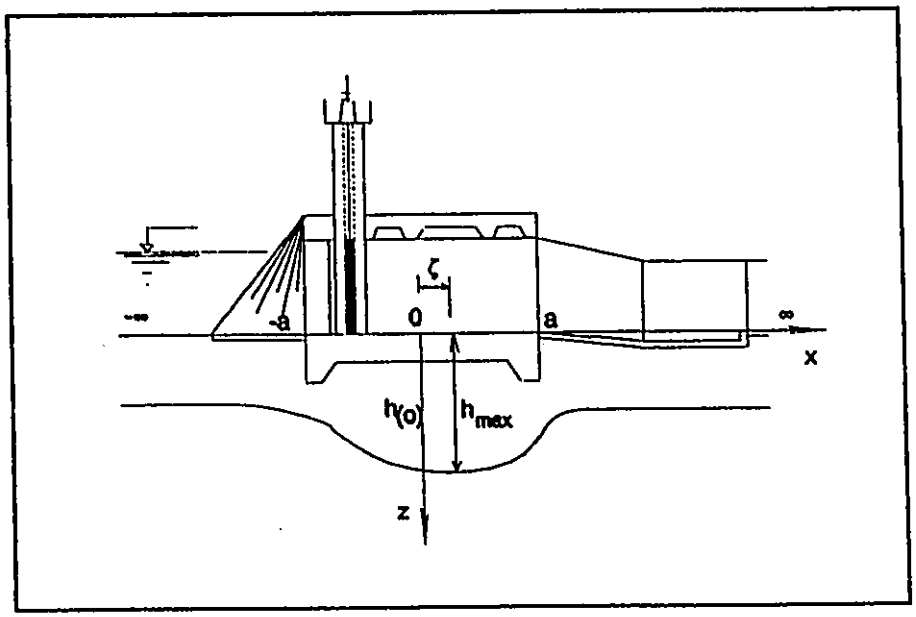

Figure 4.11 Thawing Front Profile and its Maximum Thawing Depth

$$h_{(x)} = Ax^2 + Bx + C \qquad (4.118)$$

with the boundary conditions

$$h_{(x)} = \begin{cases} h_{(0)} & x = 0 \\ h_{(-a)} & x = -a \\ h_{(a)} & x = a \end{cases} \qquad (4.119)$$

solve equation (4.118) we have

$$A = \frac{1}{2a^2}[\, h_{(a)} + h_{(-a)} - 2h_{(0)}] \qquad (4.120)$$

$$B = \frac{h_{(a)} - h_{(-a)}}{2a} \qquad (4.121)$$

$$C = h_{(0)} \qquad (4.122)$$

Put A, B and C into equation (4.118), we have

$$h_{(x)} = \frac{h_{(a)} + h_{(-a)} - 2h_{(0)}}{2a^2}x^2 + \frac{h_{(a)} - h_{(-a)}}{2a}x + h_{(0)} \qquad (4.123)$$

for the thawing front profile under the middle soil segment. We then have

$$h_{max} = A\zeta^2 + B\zeta + C \qquad (4.124)$$

where ζ is the x coordinate of the maximum or minimum thawing depth, with

$$\zeta = \frac{a(h_{(a)} - h_{(-a)})}{2(h_{(a)} + h_{(-a)} - 2h_{(0)})} \qquad (4.125)$$

It is quite clear that in equation (4.125) that if $h_{(a)} = h_{(-a)}$ the x-coordinate of the maximum or minimum thawing depth ζ = 0 too. Then we may find that the maximum or minimum thawing depth is the one in the geometric center of the middle soil segment.

4.5.3 Thawing beneath Trenches

With increasing development in permafrost areas, many trenches are dug for water drainage and other purposes. Some of them may fill with water in summer time and others may not.

4.5.3.1 Open Trench

The thermal state beneath the trenches can be calculated by Xia's model. Here, we need to consider heat conduction in both horizontal and vertical directions. Let us set up a coordinate system that consist of five segments as shown in Figure (4.12):

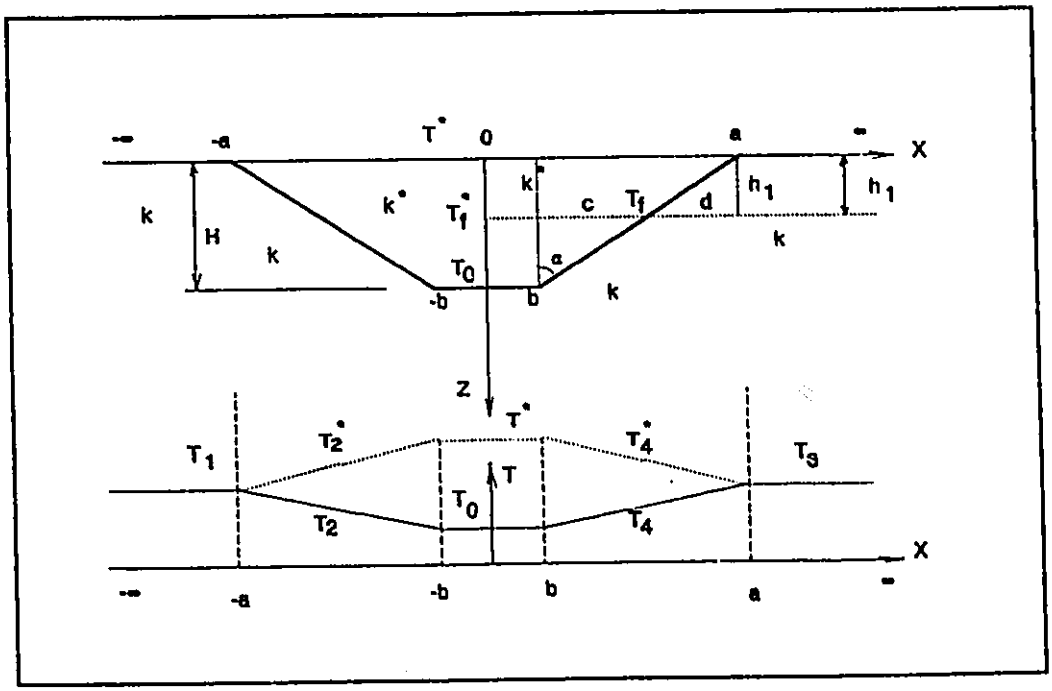

Figure 4.12 The Coordinate System and the Assumed Temperature Distribution

The known surface temperature as input is

$$T_0(x) = \begin{cases} T_1 & -\infty < x < -a \\ T_0 & -b < x < b \\ T_3 & a < x < \infty \end{cases} \qquad (4.126)$$

We assume the temperatures, T_2, T_4 at the slope surface on both sides of the trench to vary linearly with distance from the trench edges (Fig. 4.12):

$$T_2 = \frac{T_0 - T_1}{-b + a} (x + a) + T_1 \qquad (4.127)$$

for $-a < x < -b$,

$$T_4 = \frac{T_3 - T_0}{a - b} (x - b) + T_0 \qquad (4.128)$$

for $b < x < a$.

Further assumptions are made to simplify the problem. First, we assume that the trench which has no water is located in a flat area; both sides of the trench have the same soil material with similer temperature and hydrologic conditions, and their soil thermal conductivity is k. Then,

we assume that the trench was filled with a different soil material, which has a known thermal conductivity k^*, and this occupies the middle parts of the five soil segments. We further suppose that energy transfer in the filled trench is only through thermal conduction.

The apparent temperature acting on the central part of the top surface ($-b < x < b$) is T^*. According to the law of energy conservation, we may have

$$\frac{T^* - T_f^*}{h_1} = \frac{T^* - T_0}{H} \tag{4.129}$$

in vertical direction, and

$$k^* \frac{T_f^* - T_f}{c} = k \frac{T_f - 0}{d} \tag{4.130}$$

in the horizontal direction. T_f^* is the apparent temperature of the full filled trench at depth h_1:

$$c = (H - h_1)\ tg\ \alpha \tag{4.131}$$

$$d = h_1\ tg\ \alpha \tag{4.132}$$

where h_l is the thawing depth in the soil of the natural state under the right hand segment, i.e. $a < x < \infty$. H is the trench depth. α is the angle between the trench slope with the vertical line. T_f is slope surface temperature at depth h_l. T_f could be calculated by equation (4.128), with $c = x - b$:

$$T_f = \frac{T_3 - T_0}{a - b} c + T_0 \qquad (4.133)$$

Solving equations 4.129 to 4.133 we can find the apparent temperature T^*. Then we can obtain the apparent temperature at the fully filled trench surface

$$T_2^* = \frac{T^* - T_1}{-b + a} (x + a) + T_1 \qquad (4.134)$$

on the left hand side of the trench transect ($-a < x < -b$); and

$$T_4^* = \frac{T_3 - T^*}{a - b} (x - b) + T^* \qquad (4.135)$$

on the right hand side ($b < x < a$).

Now, we could use equation (4.66) to model the thermal

state of the trench with different thermal conductivities in different segments.

As thermal conductivity is also a function of time, the weighted average thermal conductivity in the thawed zone k(x,h,t) is k(x,t). For the trench transect, therefore, we have

$$k(x,h,t) = \begin{cases} k_1(t) & -\infty < x < -a \\ k_2(t) & -a < x < -b \\ k_0(t) & -b < x < b \\ k_4(t) & b < x < a \\ k_3(t) & b < x < \infty \end{cases} \qquad (4.136)$$

Since both sides of the trench have the same soil material, similar hydrological conditions and the same surface temperature, we may use its symmetrical property to simplify the computation. The axis of symmetry is along Z, and quantitatively, $T_1 = T_3$, $k_1(t) = k_3(t)$.

The thawing front profile at different time period can be modeled with equation (4.137). In permafrost ares where different slope orientations receive different amounts of energy (e.g. north and south slopes), the symmetry assumption will not hold, and the model applied to the trench problem may have to consider five full segments instead.

$$T_{(x,h)} = \frac{1}{\pi\, k(x,t)} \left\{ \begin{array}{c} [\, \int_{-\infty}^{-a} \frac{k_1(t)\ T_1\ h}{(x-\xi)^2 + h^2}\, d\xi + \int_{-a}^{-b} \frac{k_2(t)\ T_2^*\ h}{(x-\xi)^2 + h^2}\, d\xi + \\ \int_{-b}^{b} \frac{k_0(t)\ T^*\ h}{(x-\xi)^2 + h^2}\, d\xi + \\ \int_{b}^{a} \frac{k_4(t)\ T_4^*\ h}{(x-\xi)^2 + h^2}\, d\xi + \int_{a}^{\infty} \frac{k_3(t)\ T_3\ h}{(x-\xi)^2 + h^2}\, d\xi\,] \end{array} \right. \qquad (4.137)$$

4.5.3.2 Trench with water

Most trenches are used for water transfer or for drainage. In modelling the problem of a trench without water, it is assumed to be filled with soil with known thermal conductivity. But in the modelling of a trench with water, we may assume it to be filled with water in order to calculate its apparent temperature. Special attention has to be paid to soil moisture change and the effects of the wetted perimeter and the extent of seepage into the earth materials. Those effects may complicate the thermal conductivity computation. The coordinate system is shown in Fig. (4.13).

Let us assume that, before we filled up the trench, the temperature at the water surface is T_0, and at bottom of the trench is T_{b0}. Assume further the water in the trench is stagnant or has laminar flow with linear temperature

distribution along with its depth. We may have

$$T^* = \frac{T_0 - T_{b0}}{H - h_0} H + T_{b0} \qquad (4.138)$$

here T_0 is the water surface temperature, T_{b0} is the temperature at trench bottom, and it is assumed that the

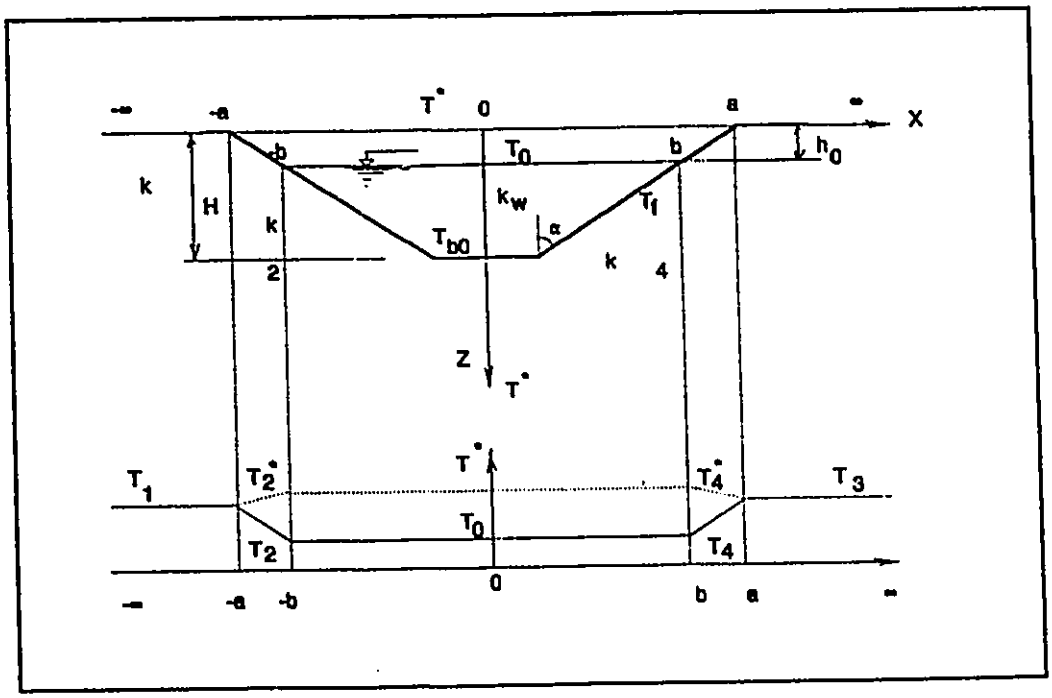

Figure 4.13 The Coordinate System and the Assumed Temperatures Distribution for the Problem of Trench with water

temperature at trench bottom, and it is assumed that the water and the soil at the trench bottom have equal temperature. In the same manner as we treated the problem of trench without water we could have

$$T_2^* = \frac{T^* - T_1}{-b + a} (x + a) + T_1 \qquad (4.139)$$

and

$$T_4^* = \frac{T_3 - T^*}{a - b} (x - b) + T^* \qquad (4.140)$$

Then, the thawing front of the trench could be modeled with equation (4.137).

4.6 Joint Application of WAD and Xia Models

The one dimensional model described in chapter 3, and the two dimensional model presented above can be linked, so that only a limited amount of climatic data is needed as input variables to both hydrologic models. To demonstrate how this is applicable to a relatively warm (1977) and a relatively cold year (1978), two sets of simulation were

performed.

4.6.1 Joint Application

The vertical soil profiles used for testing the linked models are the same as those used in the previous two dimensional model (Fig. 2.13). For the one-dimensional simulation, surface temperature, frost and water table positions for both year were calculated for the gravel and the peaty soil sites, using air temperature, global radiation, and precipitation data as inputs. Outputs from this model were used in the Xia model to simulate frost tables along a transect, for a period of 30, 50 and 70 days after the initiation of thaw. The average thicknesses of the saturated zone were calculated as the difference between the frost table and water table depths. The initial ice conditions at the sites were obtained from one-dimensional calculation of the saturated zone thickness at the end of the 1976 and 1977 summer seasons (Table 4.6). The final simulated results using the joined models are shown in Fig. 4.13.

Compared with former field observations, results of the combined models, are close to the measured data for their three time periods during the two years of simulation. The root-mean-square errors for the simulation of frost tables along the transect were 0.018 m in 1977 and 0.021 m in 1978.

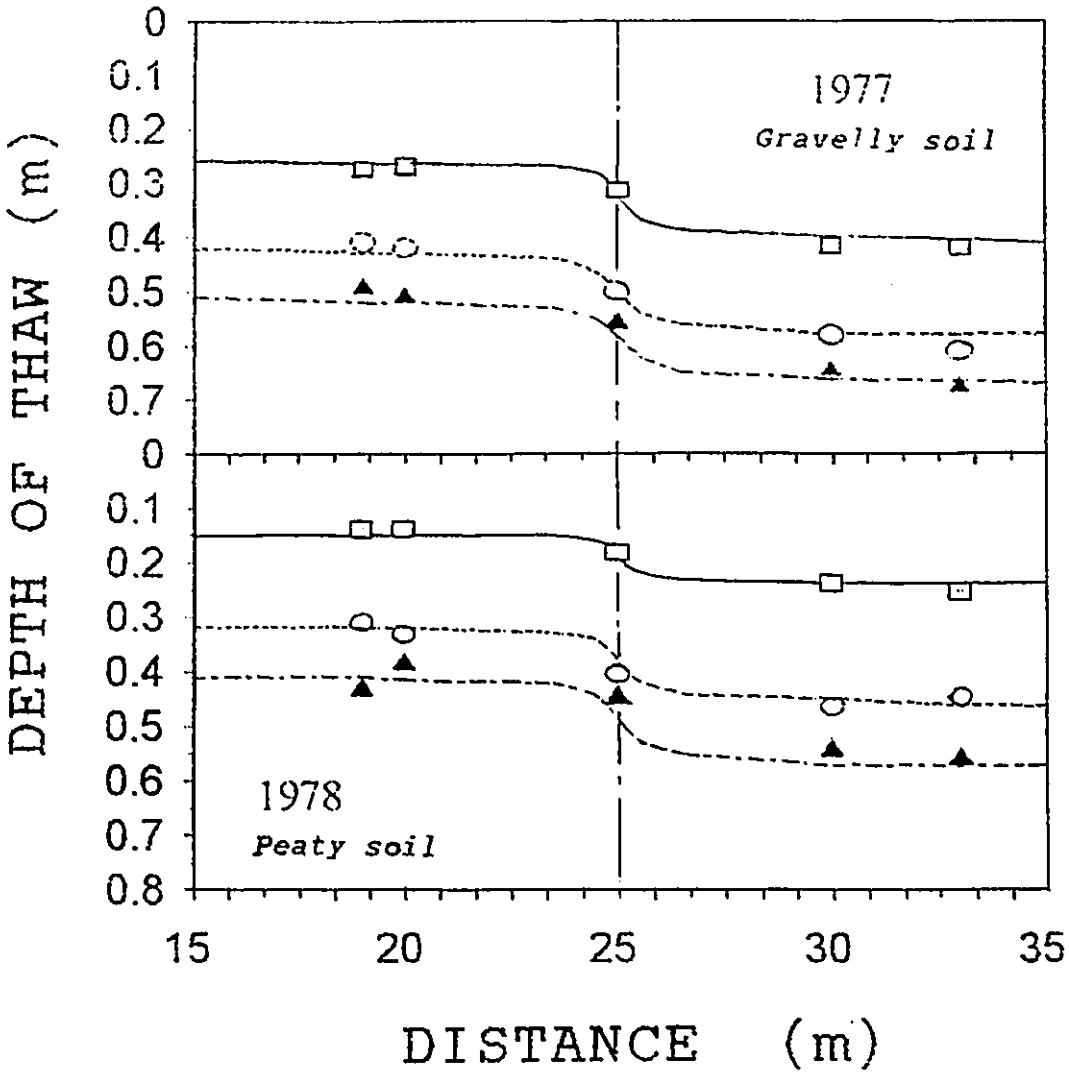

Fig. 4.14 Simulated Frost Table Position using a Combination of WAD model outputs and the Xia Model, Compared with Measured Frost Table Position along the Transect near Resolute, 1977 and 1978.

Table 4.6 The inputs and parameters used in two-dimensional model, supplied from the one-dimensional model.

Julian Day	Surface Temperature (^{0}c)	Water Layer Thickness (cm)	Ice Layer Thickness (cm)
1977			
Gravel			
160 - 190	4.52	6.70	16.0
160 - 210	6.02	8.38	38.0
160 - 230	7.22	9.00	42.0
Peaty			
160 - 190	4.94	7.60	26.0
160 - 210	6.29	13.55	46.0
160 - 230	7.37	18.90	51.0
1978			
Gravel			
160 - 190	3.04	3.01	0.0
160 - 210	4.99	8.49	1.4
160 - 230	5.84	14.90	12.0
Peaty			
160 - 190	3.22	3.25	8.0
160 - 210	5.31	11.76	25.3
160 - 230	6.21	20.10	34.0

4.6.2 Discussion

The Woo and Drake model is a one dimensional comprehensive hydrologic model for a continuous permafrost environment. The model computes the hydrologic and thermal conditions on a daily basis for a particular site.

The Xia model is a two dimensional analytical mathematical model solving heat transfer problem in continuous permafrost. It also needs hydrological information, such as mean thickness of the saturated zone and the depth of the ice rich zone in order to obtain thermal conductivity and for latent heat effect calculations. If we have those information from field measurements, it should be good enough to run this model. If not, the Woo and Drake model can be used to derive thermal and hydrological values for single soil columns. Then, the frost table profile linking these two adjacent columns can be calculated using the two dimensional Xia model presented in this chapter.

CHAPTER 5

CONCLUSIONS

The WAD model is a one-dimensional physical based deterministic model proposed by Woo and Drake (1988) to simulate the daily hydrological and thermal conditions of a vertical column of the active layer. In order to extend the frost table modeling of the WAD model, from one dimension to two, the Xia model was developed. These two models were calibrated and tested with Resolute data in a High Arctic permafrost environment. Several conclusions can be drawn from the results of this study.

1. The WAD model can be calibrated easily for application to a continuous permafrost site. Once calibrated this model can reproduce local, seasonal, annual and multi-annual hydrological patterns of the active layer. It can be used to simulate snow accumulation and melt processes, water table fluctuation, daily mean evaporation variation, thawing front development and freezing front penetration.

2. The WAD model uses simple daily inputs, including precipitation, global solar radiation and air temperature,

which are easily transferred from and readily obtainable at nearby weather station. As it is built on physical basis, the model does not require many alternative inputs and empirical parameters.

3. The WAD model was applied to the historical data processes from 1976 to 1981, and it yielded outputs that compare well with observations collected during former field investigations.

4. Freeze-thaw processes have potential significance in permafrost hydrology modeling. The WAD model incorporates their regimens into a water balance model such that frost depths, thaw depth, soil moisture and water table were calculated and updated, based on the interdependency of soil hydrologic and thermal precesses.

5. The model is sensitive to snow and surface cover, soil column profile and composition. The initial conditions of the soil moisture have a significant effect on the simulations. It is suggested that two years of start-up run is enough to ensure that the simulation is not affected by the initial conditions set up at the beginning of the run.

6. Heat and water interaction with soil composition produce special variations of frost table development. Given the surface temperature, site specification and soil moisture profile, the Xia model was developed to calculate frost table variation in two dimensional profile.

7. This is a physically based, deterministic model, which incorporates the effect of ground ice content and soil moisture status. The modeled results compares well with observed frost table data collected in the continuous permafrost area, along a line that traversed a peaty and a gravelly soil segment.

8. Sensitivity experiments with the Xia model using different moisture and ice contents and subjected to various temperature conditions demonstrated that the hydrological status of the soils is important in modifying the rate of summer thaw. Thus, in terms of permafrost responses to climate warming, it is necessary to consider the wetting or drying scenarios that accompany temperature changes.

9. Using the hydrological output of the WAD model as input to the Xia model to specify hydrological conditions, we can extend the frost table modelling from one dimension to two very easily. The joint application performed well with field measurements in continuous permafrost environment.

Both of these models have been used for a High Arctic environment with satisfactory simulation results. They can also be used for the study of the hydrological response of climate change and environmental disturbance in continuous permafrost areas. Future work is needed to extend these models to the discontinuous permafrost area. Theoretically, physically based models incorporate most hydrological

processes, but this demands a considerable variety of input data. Practically, a certain degree of empiricism has to be built into the model to overcome limited data. Future model development may consider a two-dimensional finite element model adapted to the cold regions. This will allow the modelling of slope hydrology for permafrost terrain. Finally, to study climate change or land use impacts, a better understanding of how macroclimate is translated into mesoclimate and microclimate is needed; specifically, how surface temperature is related to measured air temperature and how will the snow and ice climate be altered. All these suggested areas of improvement will allow better prediction of the hydrology of permafrost areas.

REFERENCES

Ad Hoc Study Group on Ice Segregation and Frost Heaving, 1984. *Ice Segregation and Frost Heaving*. National Academy Press, Washington, D.C., 72p.

Anderson, D.M. and A.R. Tice, 1973. The Unfrozen Interfacial Phase in Frozen Soil Water Systems. *Analysis and Synthesis*. Ecological Studies, Vol. 4, Editors, A. Nodos et al., New York: Springer-Verlag. P. 107-124.

Bergström, S., 1976. *Development and Application of a Conceptual Runoff Model for Scandinavian Catchments*. Swedish Meteorological and Hydrological Institute, Norrkoping, Sweden, Report No RHO7.

Black, R.F., 1974. Ice-wedge Polygons of Northern Alaska. *Glacial Geomorphology*, Annual Geomorphology Series, 5th, Proceedings, Binghamton, New York, State University, New York. 398p.

Bonan, G.B., 1989. A Computer Model of the Solar Radiation, Soil Moisture, and Soil Thermal Regimes in Boreal Forests, *Ecological Modelling.*, P. 275-306.

Bonan, G.B., 1991. A Biophysical Surface Energy Budget Analysis of Soil Temperature in the Boreal Forests of Interior Alaska. *Water Resources Research*, 27, P. 767-781.

Bondarev, P.D., 1959. A General Engineering-geocryological Survey on the Permafrost Regions of USSR and Methods of Construction in Permafrost Areas. *Problems of the North*. 3, P. 23-27.

Bostock, H.L., 1972. *Physiographic Subdivisions of Canada*. In Douglas, R.J.W. (ed.), Geology and Economic Minerals of Canada, Geological Survey of Canada.

Economic Report 1, Department of Energy, Mines and Resources, Ottawa, P. 10-30.

Brown, R.J.E., 1956. Permafrost investigations in the Mackenzie Delta. *Canadian Geographer*, 7, P. 21-26.

Brown, R.J.E., 1962. A Review of Permafrost Investigations in Canada. *Canadian Geographer*, 6, P. 162-165.

Brown, R.J.E., 1970. *Permafrost in Canada - its influence on northern development*. University of Toronto Press, Toronto, Ontario, 234p.

Brown, R.J.E., 1978. *Influence of Climate and Terrain on Ground Temperatures in the Continuous Permafrost Zone of Northern Manitoba and Keewatin District, Canada*. NRCC-17085. Research Paper No. 809, Div. Build. Res. Ottawa, 6p.

Campbell, G.S., 1977. *An Introduction to Environmental Biophysics*. Springer-Verlag, New York, 159 p.

Carslaw, H.S., and J.C., Jaeger, 1947. *Conduction of Heat in Solids*: Oxford, England, Clarendon Press, 1953.

Colbeck, S.C., 1976. An Analysis of Water Flow in Dry Snow. *Water Resources Research*, 12, P. 523-527.

Cook, F.A., 1958. Temperatures in Permafrost at Resolute, N.W.T. *Geogr. Bull.*, 12, P. 5-18.

Cruickshank, J.G., 1971. Soils and Terrain Units Around Resolute, Cornwallis Island. *Arctic*, 224, P. 195-209.

Dilley, A.C., 1968. On the Computer Calculation of Vapor Pressure and Specific Humidity Gradients from Psychrometric Data. *Journal of Applied Meteorology*, 7, P. 717-719.

Dilley, J.F., 1978. *Heat Transfer Analysis of Nearshore Ice Formation, Growth and Decay Utilizing a Numerical Simulation Model*. Ph.D. Thesis, University of Pennsylvania, 245p.

Drake, J.J., 1979. Some Observations on the Constancy of α in the Equilibrium Model for Evapotranspiration *Climatological Bulletin*, 26, P. 11-17.

Energy, Mines and Resources, 1974. *National Atlas of Canada*. MacMillan of Canada, Toronto, 254p.

Farouki, O.T., 1981. *Thermal Properties of Soils*. U.S. Army CRREL Monograph, 81-1, 136p.

Finizio, N. and G. Ladas, 1982. *An Introduction to Differential Equations*. University of Rhode Island. Wadsworth Publishing Company, Belmont, California.

Fox, J.D., 1992. Incorporating Freeze-thaw Calculations into a Water Balance Model. *Water Resources Research*. 28, P. 2229-2243.

French, H.M., 1976. *The Periglacial Environment*, London, Longman Group Limited, New York, Longman Inc., 309p.

Goering, D.J. and J.P. Zarling, 1985. Geotechnical Thermal Analysis with a Microcomputer. *Proc. Civil Engineering in the Arctic Offshore*. Am. Soc. Civ. Eng., P. 604-616.

Granger, R.J., D.M. Gray and G.E. Dyck, 1984. Snowmelt Infiltration to Frozen Prairie Soils, *Canadian Journal of Earth Sciences*, 21, P. 669-677.

Heron, R., 1979. *Computation of Snowmelt at a High Arctic Site*. M.Sc. Thesis, McMaster University, 89p.

Heginbottom, J.A. (Compiler), 1989. A Survey of Geomorphic Processes in Canada. *Chapter 9 in- Quaternary Geology of Canada and Greenland*, R.J. Fulton (Editor), Geology of Canada No.1, Geological Survey of Canada, Ottawa, Ontario, and Vol. K-1, Geology of North America, Decade of North American Geology, Geological Society of America, P. 573-644.

Heron, R., 1985. *Decay of a High Arctic Lake Ice Cover*. Ph.D. Thesis, McMaster University, 189.

Hinzman, L.D., D.L. Kane, R.E. Gieck and K.R. Everett, 1990. Hydrologic and Thermal Properties of the Active Layer in the Alaskan Arctic. *Cold Regions Science and Technology*, 19, P. 95-110.

John, F., 1982. *Partial Differential Equations*. Springer-Verlag, New York., 249p.

Johnston, G.H. 1981. *Permafrost: Engineering Design and Construction*. Associate Committee on Geotechnical Research, National Research Council of Canada, John Wiley and Sons Canada Ltd., Toronto, 540p.

Jumikis, A.R., *Thermal Soil Mechanics*, Rutgers University Press, New Brunswick, N.J. 267p.

Kane, D.L. and J. Stein, 1983. Water Movement into Seasonally Frozen Soils. *Water Resources Research*, 19, P. 1547-1557.

Kane, D.L., L.D. Hinzman, C.S. Benson and G.E. Liston, 1991. Snow Hydrology of a Headwater Arctic Basin, 1, Physical Measurements and Process Studies), *Water Resources Research*, 27, P. 1099-1109.

Kane, D.L., L.D. Hinzman and J.P. Zarling, 1991. Thermal Response of the Active Layer to Climatic Warming in a Permafrost Environment. *Cold Regions Science and Technology*, 19, P. 111-122.

Kersten, M.S., 1949. *Laboratory Research for the Determination of the Thermal Properties of Soils*. Final Report to U.S. Army Corps of Engineers, St Paul District. University of Minnesota, Engineering Experiment Station. 225p.

Lachenbruch, A.H., 1957. Thermal Effects of the Ocean on Permafrost. *Bulletin of the Geological Society of America*, 68, P. 1515-1530.

Lachenbruch, A.H., 1966. Contraction Theory of Ice Wedge Polygons: A Qualitative Discussion; 63-71 in *Permafrost International Conference (Lafayette, Ind., 11-15 Nov. 1963) Proc.*: Ntl. Acad. Sci-Ntl. Research Council Pub. 1287. (563p.)

Lachenbruch, A.H., J.H. Sass, L.A. Lawver, M.C. Brewer and T.H. Moses, 1982. *Depth and Temperature of Permafrost on the Alaskan Arctic Slope*. Preliminary Results. U.S. Geological Survey. Open-file Report, No.82-1, 30p.

Latimer, J.R., 1971. Radiation Measurement. *Technical Manual Series* 2, International Field Year for the Great Lakes, 53p.

Lewkowicz, G.G., 1981. *A Study of Slopewash Processes in*

the Continuous Permafrost Zone, Banks Island, Western Canadian Arctic. Ph.D. Theses, University of Ottawa, 293p.

Lewkowicz, A.G. and H.M. French 1982. The Hydrology of Small Runoff Plots in an Area of Continuous Permafrost, Banks Island, N.W.T. *The Roger J.E. Brown Memorial Volume, Proceedings Fourth Canadian Permafrost Conference, 2-6 March 1981, Calgary, Alberta*, Associate Committee on Geotechnical Research, National Research Council of Canada, P. 151-162.

Lunardini, V.J., 1981. *Heat Transfer in Cold Climates*. U.S. Army Cold Regions Research and Engineering Laboratory, Hanover, N.H.. Van Nostrand Reinhold Company. 731p.

Luthin, J.N., 1966. *Drainage Engineering*. John Wiley and Sons Inc., New York, 250p.

Mackay, J.R., 1973. A Frost Tube for the Determination of Freezing in the Active Layer above Permafrost. *Canadian Geotech Journal*, 10, P. 392-396.

Marsh, P., 1978. *Water Balance of a Small High Arctic Basin*. M.Sc. Thesis, McMaster University, 108p.

Marsh, P., W.R. Rouse and M.K. Woo, 1981. Evaporation at a High Arctic Site, *Journal of Applied Meteorology*, 20, P. 714-716.

Marsh, P. and M.K. Woo, 1984. Wetting Front Advance and Freezing of Meltwater within a Snow Cover, 1. Observations in the Canadian Arctic, *Water Resources Research*, 16, P. 1853-1864.

Marsh, P. and M.K. Woo, 1993. Infiltration of Meltwater into Frozen Soils in a Continuous Permafrost Environment. Accepted by *the 6th International Conference on Permafrost, Beijing, China*.

Maxwell, J.B., 1980. The Climate of the Canadian Arctic Islands and Adjacent Waters. *Climatological Studies*, 30, Atmospheric Environment Service, Environment Canada, Ottawa. 1120p.

McCann, S.B. and J.G. Cogleg. 1972. Hydrologic Observations on a Small Arctic Catchment, Devon Island. *Canada*

Journal Earth Science. 9, P. 361-365.

McCann, S.B., J.G. Cogley, S.P. Blachut, C.K. Ballantyne and B.G. Bennett, 1975. *Hydrology and Sediments of the "Sverdrup" and "Schei" Rivers with Particular Reference to Ice Marginal Drainage Conditions.* Hydrological Studies, South Central Ellesmere Island, Contract Report DSS 01SU-KL398-4-0331, Section A of a Report on Investigations Undertaken in the Vendom Fiord Area in 1974, McMaster University, Hamilton, Ontario for Glaciology Division, Inland Waters Branch, Department of the Environment, Ottawa, Ontario, May, 283p.

McMillan, B.C. 1983. *Active Layer Heat Fluxes: Central Keewatin, N.W.T.* M.Sc. Thesis - McMaster University, 117p.

Meisner, A.D., 1955. Heat Flow and Depth of Permafrost at Resolute Bay, Cornwllis Island, N.W.T., Canada. *Trans. Am. Geophys. Union* 36, P. 1055-1066.

Meinzer, O.E., 1923. The Occurrence of Groundwater in the United States, with a Discussion of Principles. *U.S.G.S. Water Supply Paper,* No. 489, 321p.

Muller, S.W. 1945. *Permafrost or Perennially Frozen Ground and Related Engineering Problems.* U.S.G.S. Special Report, Strategic Engineering Study, 62, 231p.

Nakano, Y. and J. Brown, 1972. Mathematical Modeling and Validation of the Thermal Regimes in Tundra Soils, Barrow, Alaska. *Arctic and Alpine Research,* 4, P. 19-38.

Outcalt, S.I. and J. Brown, 1975. Computer modelling of terrain modifications in the arctic and subarctic. *Selected Papers and Summaries, Symposium K-29, Geography of Polar Countries, J. Brown (Editor), 23rd International Geographical Congress,* 22-26 July 1976, Leningrad, U.S.S.R., CRREL Special Report No.77-6, Cold Regions Research and Engineering Laboratory, U.S. Army Corps of Engineers, Hanover, New Hampshire, 24-32.

Outcalt, S.I., C. Goodwin, G. Weller and J. Brown, 1975. Computer Simulation of the Snowmelt and Soil Thermal Regime at Barrow, Alaska. *Water Resources Research,* 11, P. 709-715.

Pollard, W.H. and H.M. French, 1983. Seasonal Frost Mound Occurrence, North Fork Pass, Oglvie Mountains, Northern Yukon, Canada, *Proceedings, 4th International Conference on Permafrost*, Fairbanks, Alaska, P. 1000-1008.

Price, A.J. and Dunne, T., 1976. Energy Balance Computations on Snowmelt in a Subarctic Area, *Water Resources Research*, 12, P. 686-694.

Priestley, C.G.B. and R.J. Taylor, 1972. On the Assessment of Surface Heat Flux and Evaporation Using Large Scale Parameters. *Monthly Weather Review*, 100, P. 81-92.

Roulet, N.T. and M.K. Woo, 1986. Low Arctic Wetland Hydrology. *Canadian Water Resources Journal*, 11, P. 69-75.

Roulet, N.T. and M.K. Woo, 1986. Hydrology of Wetland in the Continuous Permafrost Region. *Journal of Hydrology*, 89, P. 73-91.

Rouse, W.R., P.F. Milles and R.B. Stewart, 1977. Evaporation in High Latitudes, *Water Resources Research*, 13, P. 909-914.

Sheppard, M.I., B.D.Kay and J.P.G. Loch, 1978. Development and Testing of a Computer Model for Heat and Mass Flow in Freezing Soil. *Proceedings, Third International Conference on Permafrost, 10-13 July 1978, Edmonton, Alberta*, Vol.1, National Research Council of Canada, Ottawa, Ontario, P. 75-81.

Smith, M.W., 1977. *Computer simulation of microclimate and ground thermal regimes: test results and program description*. ALUR Report No. 73-76-72, Department of Indian Affairs and Northern Development, Ottawa, Ontario, 74p.

Steer, P., 1982. *Hydrology of a Slope in the High Arctic*. M.Sc. Thesis, McMaster University, 89p.

Thorsteinsson, R., 1958. Cornwallis and Little Cornwllis Islands, District of Franklin, Northwest Territories. *Geological Survey of Canada Memoir* 294, 134p.

Tsytovich, N.A., 1975. *The Mechanics of Frozen Ground*.

Scripta Book Company, Washington, D.C., 426p.

Van Everdingen, R.O., 1982. Management of Groundwater Discharge for the Solution of Icing Problems in the Yukon. *Proceedings 4th Canadian Permafrost Conference, Calgary, Alberta*. National Research Council of Canada, P. 212-226.

Van Everdingen, R.O., 1987. The Importance of Permafrost in the Hydrological Regime. *Chapter 9 in Canadian Aquatic Resources*, M.C. Healey and R.R. Wallace (Editors), Canadian Bulletin of Fisheries and Aquatic Sciences No.215,243-276.

Wang, H.F. and M.P. Anderson, 1982. *Introduction to Groundwater Modelling*. W.H. Freeman, San Fracisco. 237p.

Washburn, A.L., 1979. *Geocryology, A Survey of Periglacial Processes and Environments*. Edward Arnold Ltd., Printed in Great Britain by Fletcher & Sons Ltd, Norwich. 406p.

Washburn, A.L. and M. Stuiver, 1985. Radiocarbon Dates from Cornwallis Island Area, Arctic Canada - an Interim Report. *Canadian Journal of Earth Science*, 22, P. 630-637.

Williams, P.J., 1982. *The Surface of the Earth*. Longman's, New York. 212p.

Woo, M.K., 1976. Evaporation and Water Level in the Active Layer. *Arctic Alpine Research*. 8, P. 213-217.

Woo, M.K., 1986. Permafrost Hydrology in Northern Canada. *Proceedings, 5th International Conference on Permafrost*, K. Senneset (Editor), 2-5 August 1988, Trondheim, Norway, Tapir Publishers, Vol. 1, P. 644-649.

Woo, M.K., 1990. Permafrost Hydrology. *Northern Hydrology, Canadian Perspectives*, T.D. Prowse and C.S.L. Ommanney (Editors), 11 June 1990, NHRI Science Report No.1, P. 63-76.

Woo, M.K., 1992. Arctic Streamflow. *Proceedings, Symposium of Arctic Environment: Past, Present & Future*, M.K. Woo (Editor), Nov. 14-15, 1991, McMaster University, Hamilton, Ontario. P. 105-111.

Woo, M.K. and P. Steer, 1979. Measurement of Trace Rinfall at a High Arctic Site. *Arctic*, 32, P. 80-84.

Woo, M.K. and R. Heron, 1981. Occurrence of Ice Layers at the Base of High Arctic Snowpacks, *Arctic and Alpine Research*, 13, P. 225-230.

Woo, M.K. and P. Steer, 1982. Occurrence of Surface Flow on Arctic Slopes, Southwestern Cornwallis Island. *Canadian Journal of Earth Science*, 20, P. 2368-2377.

Woo, M.K. and P. Steer, 1983. Slope Hydrology as Influenced by Thawing of the Active Layer, Resolute, N.W.T., *Canadian Journal of Earth Sciences*. 20, P. 978-986.

Woo, M.K., R. Heron, P. Marsh and P. Steer, 1984. Comparison of Weather Station Snowfall with Winter Snow Accumulation in High Arctic Basins. *Atmosphere-Ocean*, 21, P. 312-325.

Woo, M.K. and J.J. Drake, 1988. *A Study to model the effects of Uranium Mine Tailings on a Permafrost Environment*. Environmental Studies No.53, northern Affairs Program, Indian and Northern Affairs Canada, Ottawa, Ontario, March, 41p.

Woo, M.K. and P. Marsh, 1990. Response of Soil Moisture Change to Hydrological Processes in a Continuous Permafrost Environment. *Nordic Hydrology*, 21, P. 235-252.

Xia, Z.J., 1983. A Study of Thermal Cracks in Frozen Ground, *4th International Conference on Permafrost, Fairbanks, Alaska, July 17-22, 1983. Proceedings*. Washington, DC. National Academy Press, P. 1418-1422.

Xia, Z.J. and M.K. Woo, 1992. Theoretical Analysis of Snow-dam Decay. *Journal of Glaciology*, 38, P. 191-199.

Xia, Z.J. and M.K. Woo, 1993. Active Layer Thaw Calculation using Simplified Thermal and Hydrological Parameters. Accepted by *the 6th International Conference on Permafrost*, Beijing, China.